# Lecture 2-3

Formation and redox properties of hydrous oxide thin film modified electrodes in aqueous solution.
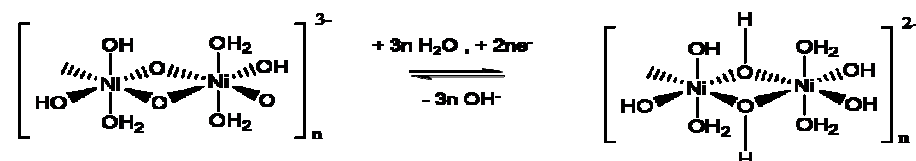
Introduction.

Metal surfaces in contact with aqueous electrolytic solution are always oxidized and coated with some type of metal oxide when polarised at Oxidizing potentials as is the case in oxygen evolution. Some types of metal oxide are also quite stable and may exist in significantly cathodic potential regions .

Mechanism of oxide growth at both noble and non noble metal electrodes in aqueous solution is a well established aspect of surface electrochemistry.

Of particular interest from viewpoint of energy conversion/storage applications are noble metals such **as Pt, Au, Ir, Rh** and non noble metals such as **Fe, Ni, Co** and **Mn**.

Metal oxide films formed on metal surfaces via the thermally induced decomposition of simple inorganic salt precursors or using sol/gel methods are also technologically important.

It is established that an oxide film present on the transition metal affects the mechanism & kinetics of various anodic and cathodic redox reactions which occur at the electrode/solution interface such as molecular oxygen electro-reduction or water electro-oxidation to form molecular oxygen .

The oxide layer can (and usually does):
- affect the thermodynamics and kinetics (very important) of the interfacial reaction
- change the electronic properties of the metal surface
- impose a barrier to charge transfer across the surface oxide film
- influence the adsorption behaviour of reaction intermediates and/or products at the catalytic surface
- the properties (electronic, magnetic, crystallographic) of the surface oxide species may differ from that of the bulk phase equivalent

BE Conway,
Electrochemical oxide film formation
At noble metals as a surface chemical
Process.
Prog. Surf. Sci., 49(4), 1995, 331-452.

L. D. Burke, M.E.G. Lyons,
Electrochemistry of hydrous oxide films.
Modern Aspects Electrochemistry, 18 (1986)169-248.

200 µm   5.00 kV   Zone Mag = 69 X   SE2   Time :11:30:42   4 Dec 2012
WD = 7.5 mm   File Name = Fe_120cy_01.tif
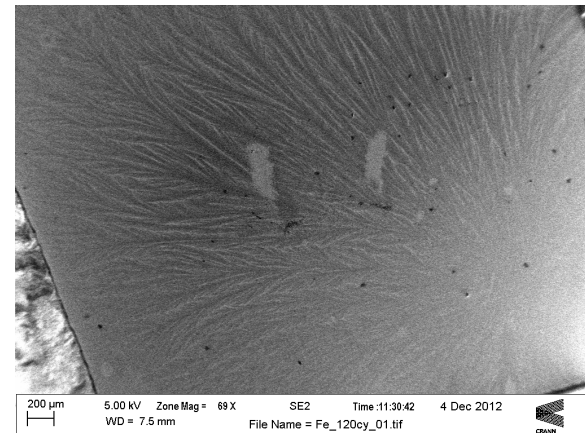
Low magnification SEM image
Of hydrous Fe oxide film.

Transition Metal Oxides : Compact and hydrous.

- 2 types:

- **Compact anhydrous oxides**, e.g. rutile, perovskite, spinel.

  - Oxygen present only as bridging species between two metal cations and ideal crystals constitute tightly packed giant molecules.

  - Prepared via thermal techniques, e.g decomposition of unstable salt

titanium(IV) oxide
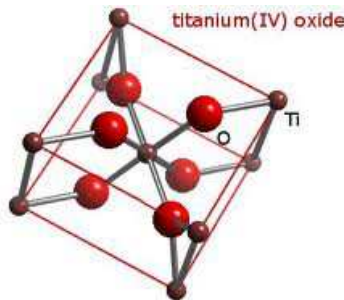
Geothite   FeOOH

- **Micro-dispersed hydrous oxides**

  - Oxygen is present not just as a bridging species between metal ions, but also as O^-, OH and OH_2 species in coordinated terminal group form.

  - Hydrous oxides in contact with aqueous media contain large quantities of loosely bound and trapped water plus electrolyte species.

  - Prepared via base precipitation, electrochemical techniques.

  - Materials are prepared in kinetically most accessible rather than thermodynamically most stable form.

  - Are often amorphous or only poorly crystalline and prone to rearrangement.

L. D. Burke, M.E.G. Lyons,
Modern Aspects Electrochemistry, 18 (1986)169-248.

Note on reference Electrode Scales.

The Standard Hydrogen Electrode (SHE) scale is the well-known, internationally recognized, primary reference based on the following electrode, $Pt/H_2(a = 1)/H^+(a = 1)$, arbitrarily assigned a potential value of zero. As such an electrode is virtually impossible to construct, it is convenient in practice to use the Reversible Hydrogen Electrode (RHE) scale in which the zero point is taken as that of a hydrogen electrode in the cell electrolyte (hydrogen ion activity $= a_{H^+}$), i.e., the electrode system $Pt/H_2(a = 1)/H^+(a_{H^+})$. The two scales coincide for solutions of pH = 0; while the potential of the SHE is pH independent, that of the RHE drops (relative to the SHE) by a factor of $2.303 RT/F$ volts per unit increase in solution pH.

$$E_{SHE} = E_{RHE} - 0.059pH$$

Experimentally one uses other reference electrodes such as Hg/HgO for base
And Ag/AgCl or SCE for less alkaline media.

Many papers use RHE scale in discussions. Best
To convert experimentally measured potentials
To RHE scale.
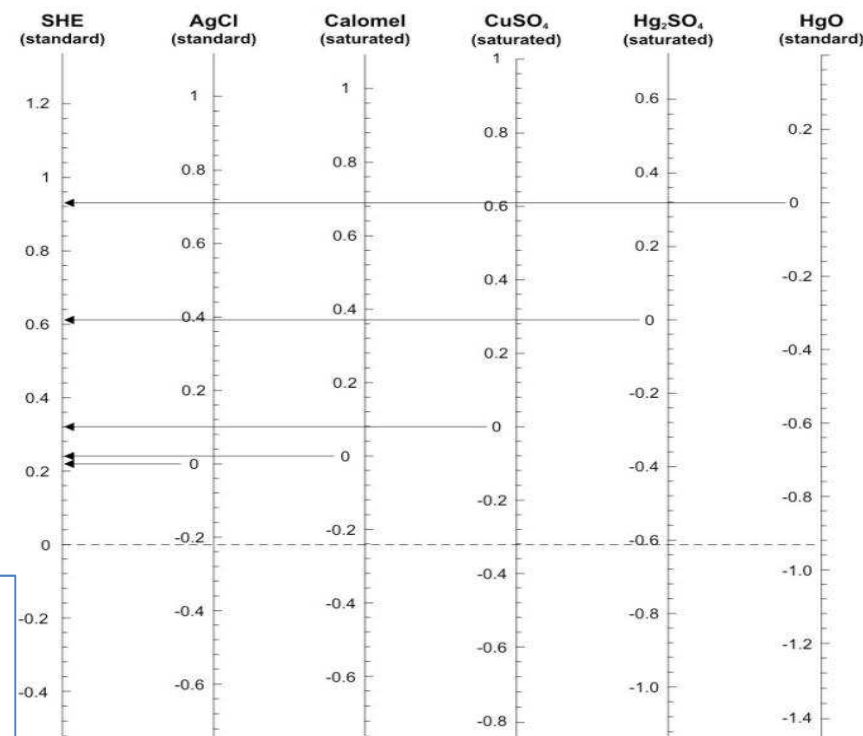
Metal oxide thin film modified electrodes.

Preparation via Controlled Potential Multicycling.

Hydrous thin films are conveniently grown on parent metal (either noble Or non-noble) via an electrochemical potential cycling technique in aqueous acid or base solution.

Basic idea is to apply an oxidative/reductive triangular or square wave potential waveform to the metal electrode at a fixed frequency/sweep rate for a given length of time. Distinct lower (reductive) and upper (oxidative) potential limits are utilized to optimize the growth of the metal oxide layer. The LPL and UPL used depend on the solution pH and on the chemical nature of the metal.

The type of oxide growth cycle used –sinusoidal, square, or triangular Wave – apparently makes little difference. The triangular wave is most Convenient as changes in the current/voltage response, i.e. Cyclic Voltammetry (CV), can, be used employed during the oxide growth reaction to monitor, in real time, changes in redox behaviour associated with the latter. In particular, the charge passed under characteristic Voltammetric redox peaks can be measured and plotted as a function of time/number of oxide growth cycles in order to quantify the oxide Formation kinetics.

CPM has been largely applied to noble metals such as Ir and Rh, and to non noble metals such as Fe, Ni, Co, Mn in a very effective manner.

Mechanism of CPM oxide growth has been established in recent years and is now reasonably well understood.

Efficiency of oxide growth depends on a number of variables other than the UPL and LPL such as electrolyte concentration, solution pH and solution temperature and sweep rate/pulse frequency.

Preparation via direct anodization.

Transition metal oxide films may also be prepared by direct anodization of the metal in a suitable electrolyte using galvanostatic (constant current) or potentiostatic (constant potential) techniques.

The mechanism is regarded here is regarded in terms of a dissolution/precipitation process. In this case the charge passed is monitored as a function of time to quantify the growth kinetics. This technique has proved to be effective for noble metals such as Pt and Au , but not for Ir.

For most metals, but especially Au, Pt, Ir and Rh, extension of oxide growth beyond the monolayer level under conventional galvanostatic or potentiostatic conditions is usually quite slow. This is due to the presence of an initial compact oxide product layer which acts as a barrier to further oxide growth.

Preparation via direct cathodic/anodic electro-precipitation.

Cathodic electro-precipitation is a technique used commercially to prepare Nickel hydroxide deposits for battery applications. In this case a nickel salt is present in solution at low pH (ca. 3) and hydrogen gas evolution around the cathode causes a local increase in pH resulting in the precipitation of an adherent layer of nickel hydroxide $Ni(OH)_2$ at the metal surface. Similarly anodic electro-precipitation is used commercially to produce layers of another highly active battery material γ-MnO_2.
In this procedure the support electrode need not be of the parent metal but is typically a relatively inert material such as Au or GC.
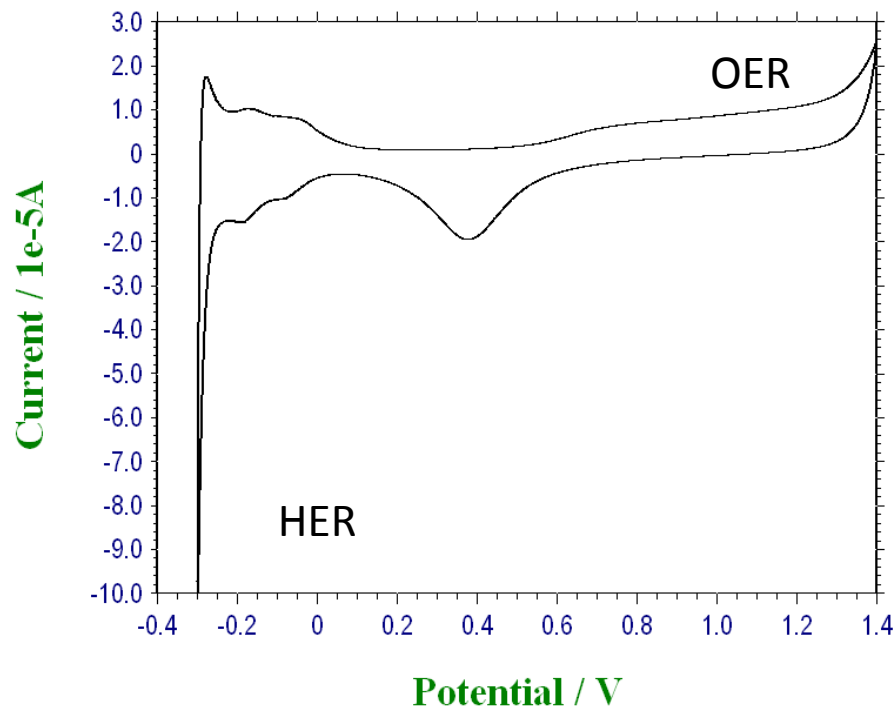
Polycrystalline Pt electrode, 100 mV/s 0.5 M H_2SO_4. Ian Godwin 2013.
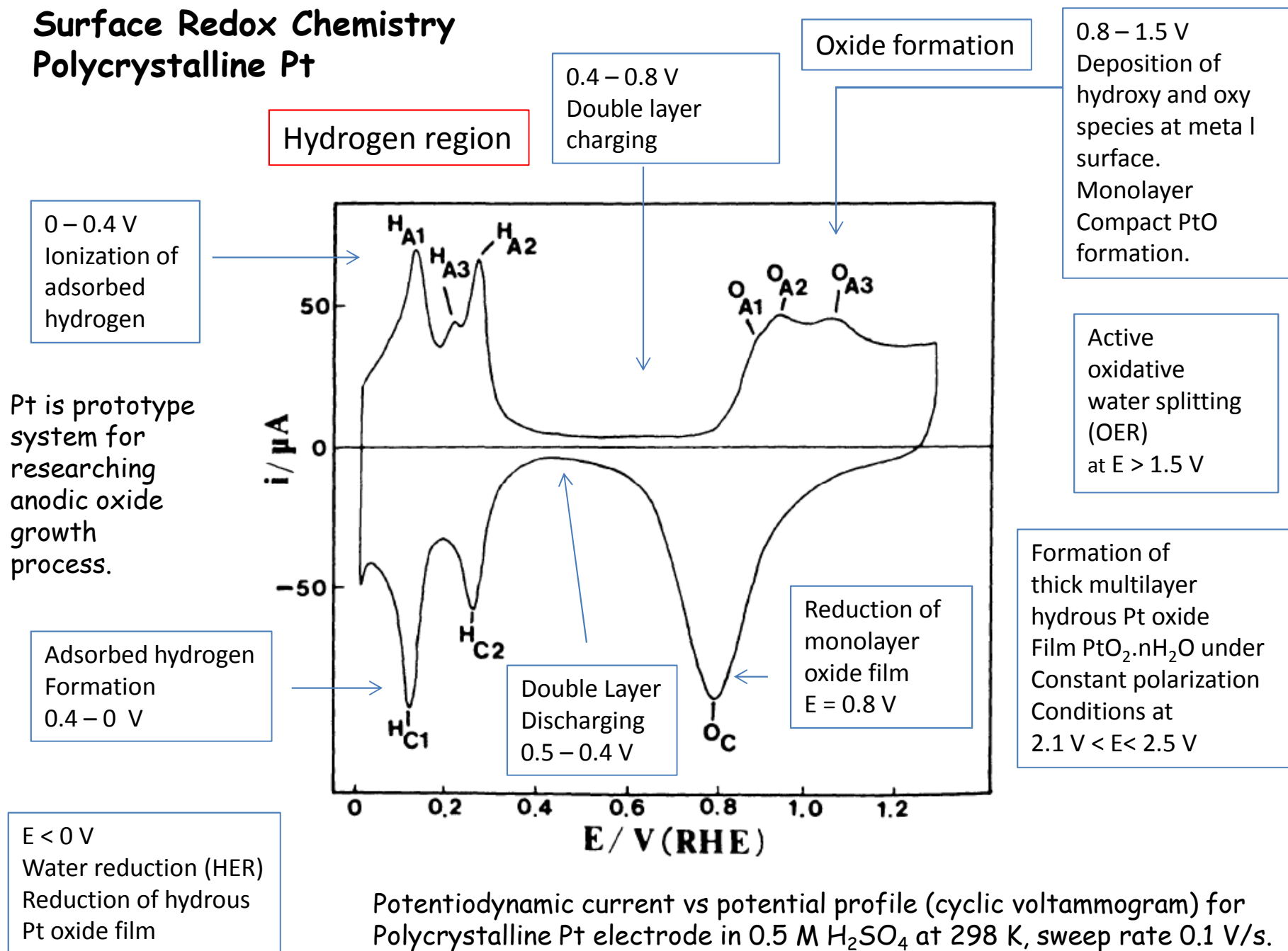
Potentials quoted vs SCE (3M KCl).

Polycrystalline Pt electrode, 100 mV/s 1.0 M NaOH. Ian Godwin 2013.

CV response of polycrystalline Pt electrode In aqueous solution very characteristic.
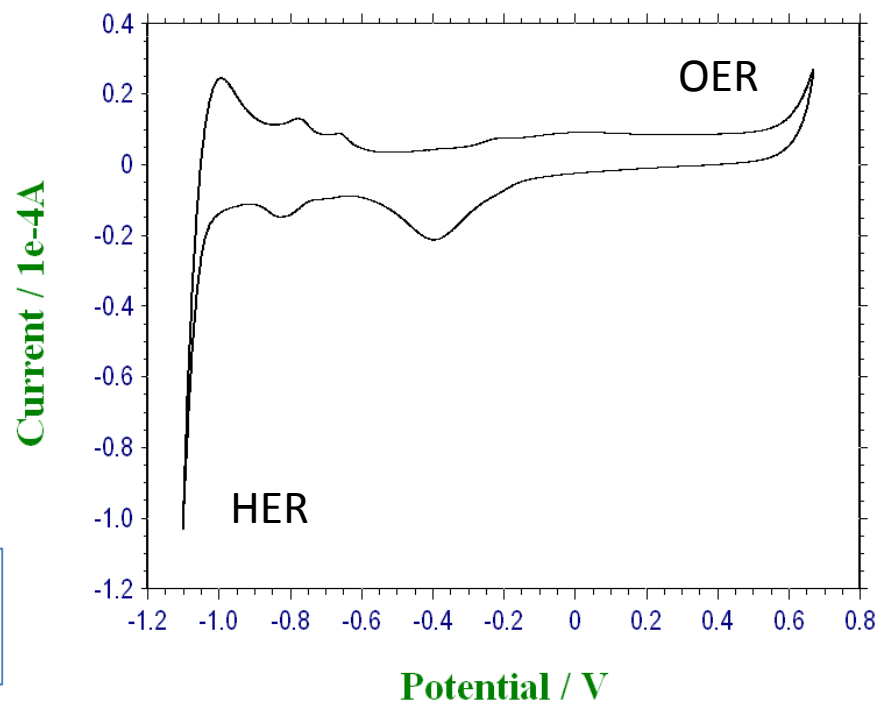
# Surface Redox Chemistry Polycrystalline Pt

Oxide formation

0.4 – 0.8 V
Double layer charging

0.8 – 1.5 V
Deposition of hydroxy and oxy species at meta l surface.
Monolayer Compact PtO formation.

Hydrogen region

0 – 0.4 V
Ionization of adsorbed hydrogen

Pt is prototype system for researching anodic oxide growth process.

Active oxidative water splitting (OER)
at E > 1.5 V

Adsorbed hydrogen Formation
0.4 – 0 V

Double Layer Discharging
0.5 – 0.4 V

Reduction of monolayer oxide film
E = 0.8 V

Formation of thick multilayer hydrous Pt oxide Film $PtO_2.nH_2O$ under Constant polarization Conditions at 2.1 V < E < 2.5 V

E < 0 V
Water reduction (HER)
Reduction of hydrous Pt oxide film

Potentiodynamic current vs potential profile (cyclic voltammogram) for Polycrystalline Pt electrode in 0.5 M H_2SO_4 at 298 K, sweep rate 0.1 V/s.

Traditional interpretation of Pt metal oxidation (Conway et al)

1. Formation of adsorbed hydroxyl species via water oxidation.
2. Interfacial place exchange.
3. Oxidation of OH_{ads} to form PtO.

$$Pt + H_2O \rightarrow Pt\text{-}OH_{ads} + H^+ + e^-; \quad 0.85\text{-}1.10\,V \qquad (1)$$

$$Pt\text{-}OH_{ads} \xrightarrow{\text{place exchange}} (OH\text{-}Pt)_{\text{quasi-3D lattice}} \qquad (2)$$

$$(OH\text{-}Pt)_{\text{quasi-3D lattice}} \rightarrow (Pt\text{-}O)_{\text{quasi-3Dlattice}} + H^+ + e^-;$$
$$1.10\text{-}1.40\,V \qquad (3)$$

Initially adsorbed OH species is generated via water oxidation. The Adsorbed oxygen species deposited on the anodic sweep beyond the PtOH stage is considered to rearrange rapidly to a OHPt species via a 'place exchange mechanism PtOH → OHPt where the chemisorbed OH species and a Pt atom change places resulting in the OH species being located in an inverted position below the surface. Finally a further step is envisaged involving oxidation of the rearranged film to form a phase oxide layer of monolayer dimensions.

Initial film formation 0.8 – 1.1 V is more or less Reversible, above 1.1 V the oxidation becomes irreversible.
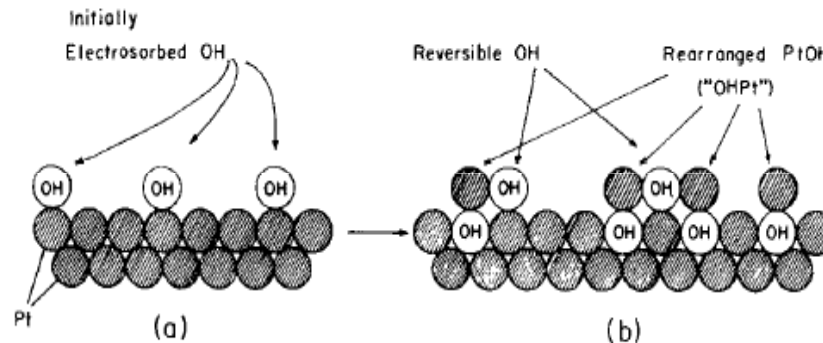
Schematic diagrams of increasing extent of deposition of OH or O species on a Pt or Au electrode with progressive transformation of an initially 2-d electrosorbed state to a quasi-3-d, place-exchanged state.

Beyond E = 1.1 V, in CV anodic sweep a broad plateau current practically independent of potential is observed leading finally to the oxygen evolution region. The current plateau corresponds to an increasing extent of surface oxidation beyond the monolayer limit.

The three overlapping peaks O_{A1}, O_{A2}, O_{A3} are believed to be due to successive overlay structures of OH species on the Pt lattice which can be represented as 'Pt$_4$OH', 'Pt$_2$OH'. PtOH corresponding to progressive filling of surface lattice sites in regular arrays determined by (i) the underlying substrate lattice geometry and (ii) repulsive forces between initially formed Pt-OH dipoles on each occupied site.

$$Pt_4 + H_2O \rightarrow Pt_4OH + H^+ + e^-$$
$$Pt_4OH + H_2O \rightarrow 2Pt_2OH + H^+ + e^-$$
$$Pt_2OH + H_2O \rightarrow 2PtOH + H^+ + e^-$$
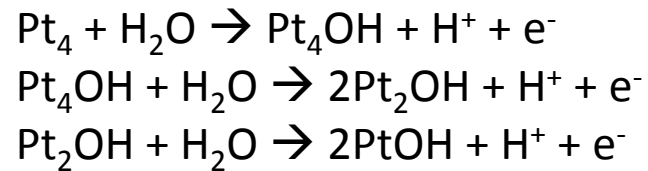
These designations do not represent stoichiometric compounds but rather the lattice occupancy ratio by OH to Pt atoms
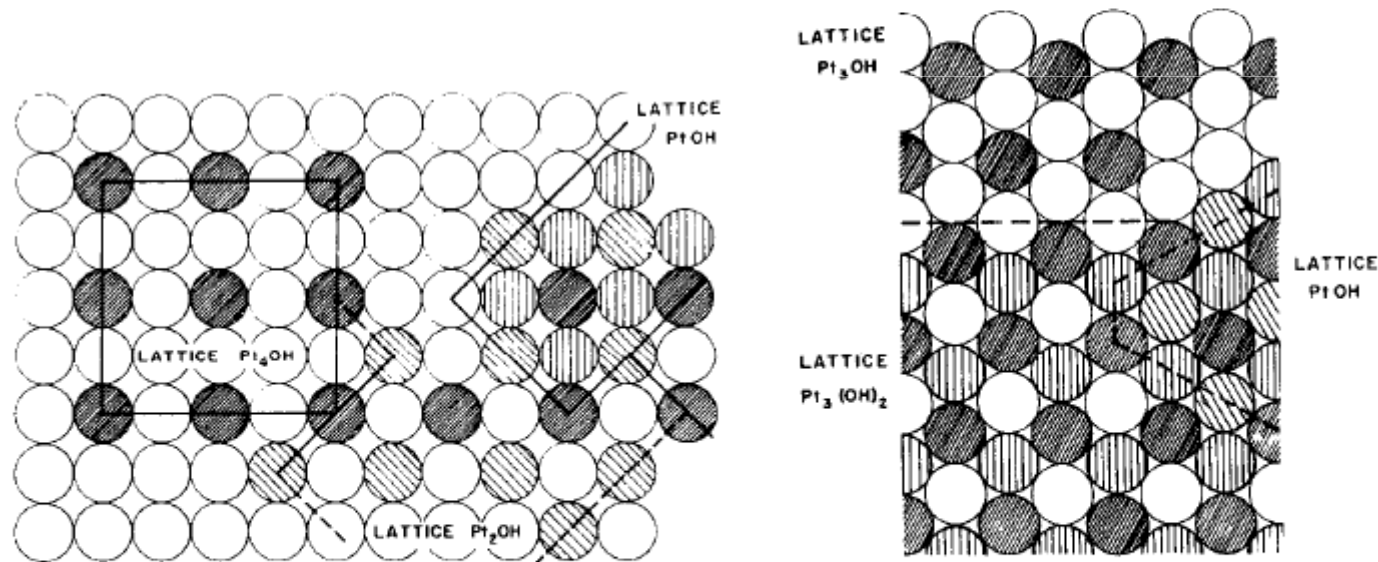
Fig. 5 Succession of lattice arrays of electrosorbed OH or O species on (100) or (111) substrate single-crystal surfaces (from ref. 55).

Useful practical Note

CV of noble metal electrodes can be used to evaluate real surface area. A useful feature of the hydrogen region of the Pt CV is that the charge associated with the adsorption or desorption of a monolayer of hydrogen ca. 210 mC/cm^2 can be used to evaluate the real area or
roughness factor of the electrode surface.
By comparing the charge required for oxide formation or reduction Q_O with the charge got monolayer hydrogen conversion Q_H, the degree of surface oxidation can be assessed.
It is generally assumed that each Pt atom at the surface can chemisorb One hydrogen or oxygen atom, and that the condition $Q_O/Q_H = 2$ corresponds to monolayer oxide coverage.
Hence oxide surface coverage $\theta = Q_O/2Q_H$.

Nernstian & Super Nernstian potential/pH shifts

Many redox processes involve the transfer both of electrons and protons.
Provided the proton coupled electron transfer (PCET) process is <u>electrochemically reversible</u> the Nernst equation may be constructed.
Hence a plot of the characteristic redox potential for the reaction (which can either Occur on a surface or in solution) as a function of solution pH should be linear with A characteristic slope S.
The numerical magnitude of the slope will depend on the ratio of protons to electrons and hence on the stoichiometry of the redox reaction.

$$A + ne^- + mH^+ \rightleftharpoons B$$
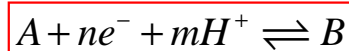
$$E = E^0 - \frac{2.303RT}{F}\left(\frac{m}{n}\right)pH + \frac{2.303RT}{nF}\log\left(\frac{c_A}{c_B}\right)$$

$$S = \frac{dE}{dpH} = -2.303\frac{RT}{F}\left(\frac{m}{n}\right)$$

When m = n, equal numbers of electrons and protons are transferred the slope is Termed Nernstian since S = -2.303(RT/F) = -0.059 V/dec at 298 K. Hence the redox Potential decreases by ca. 60 mV per unit increase in solution pH.

E

S = - 2.303(RT/F)

pH
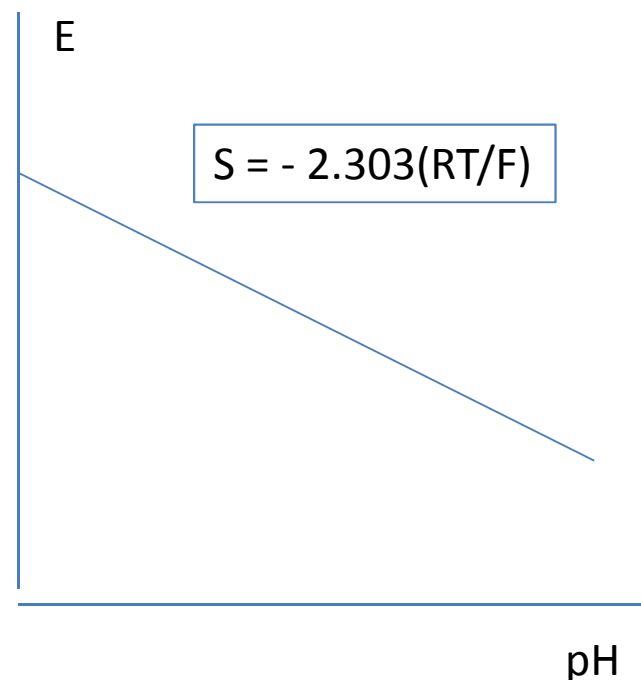
Surface Q/QH₂ functionalities on SWCNT exhibit redox behaviour
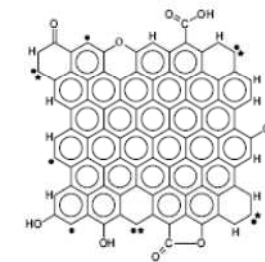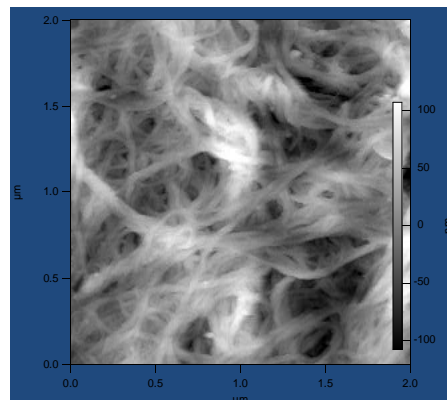
Fig. 1 Schematic representation of a graphene layer including the oxygen containing functional groups at the edges. Dot and dot+* mean unpaired σ, electron and in-plain σ pair (where * is a localized π electron), respectively

Lyons & Keeley 2006

$$\frac{dE_p}{dpH} = -61.5 \, mV/dec$$

$$Q(ads) + 2e^- + 2H^+ \rightleftarrows H_2Q(ads)$$
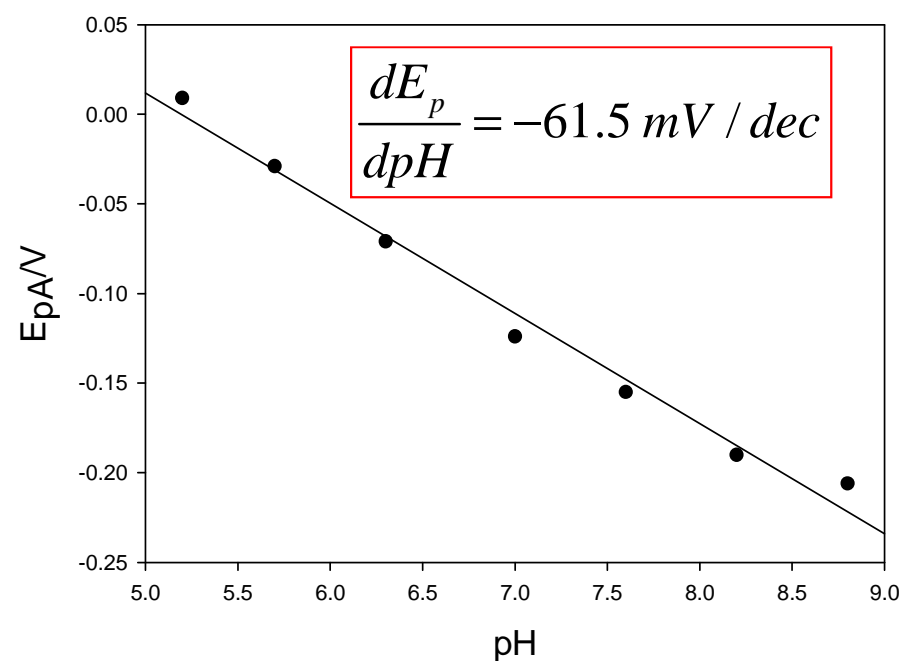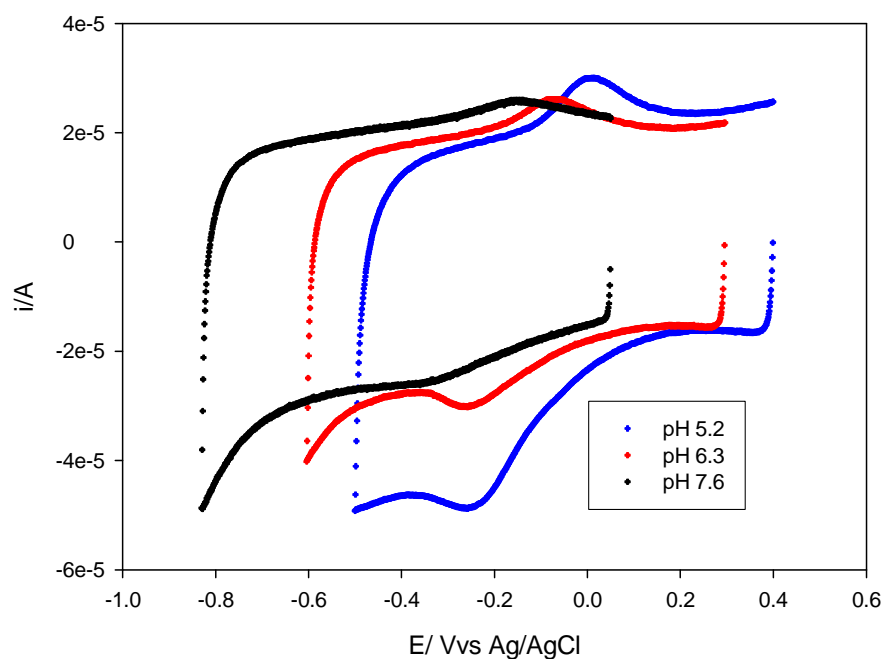
Equal number of protons and electrons transferred in redox reaction involving SWCNT surface groups. Typically m = n = 2.

pH shifts in metal oxide electrodes.
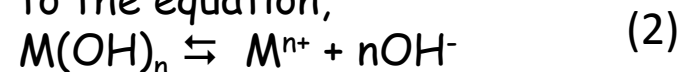
From a thermodynamic viewpoint, oxide electrodes are frequently regarded as metal/insoluble salt electrodes in which the activity of the metal ion is modified by interaction with the ligands, which in this case are the OH^- ions. The use of oxide electrodes such as Hg/HgO to measure pH is a well established electroanalytical technique. Any metal/metal oxide system is suitable for such an application provided its oxide and hydroxide (in this area the two are usually assumed to be in equilibrium according to the reaction $MO_{n/2}$ + n $H_2O \leftrightarrows M(OH)_n$) are fairly insoluble and the metal itself is not attacked by the solution whose pH is being measured . It is well established that the potential for an ideal oxide electrode system in aqueous solution at 25°C, decreases with increasing pH by ca. 59 mV/pH unit, with respect to a pH independent reference electrode such as the NHE or the saturated calomel electrode (SCE).

Regular Nernstian pH shift

We consider a metal oxide/hydroxide electrode system described by the general equation:

$$MO_n + nH_2O + 2ne^- \leftrightarrows M + 2nOH^- \quad (1)$$
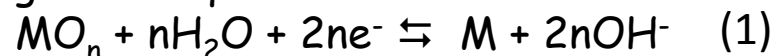
The solubility constant, K_S, for the hydroxide is defined by reference to the equation,

$$M(OH)_n \leftrightarrows M^{n+} + nOH^- \quad (2)$$

and is given by:

$$K_S = a_{M^{n+}} a_{OH-}^n \quad (3)$$

Rearranging for the metal ion activity achieves,

$$a_{M^{n+}} = \frac{K_S}{a_{OH-}^n} = \frac{K_S a_{H_3O+}^n}{K_w^n} \quad (4)$$

where, K_w is the ionic product of water. The Nernst equation for the redox process, $M^{n+} + ne^- \leftrightarrows M$, can be written as:

$$E = E^0 - \frac{RT}{nF} \ln \frac{a_M}{a_{M^{n+}}} \quad (5)$$

Substituting for $a_{M^{n+}}$ from equation (4) and following the usual convention that $a_M = 1$ yields the following expression:

$$E = E^0 + \frac{RT}{nF} \ln \frac{K_S . a_{H_3O+}^n}{K_w^n} \qquad (6)$$

Equation 6 can be re-written as:

$$E = E^0 + \frac{RT}{nF} \ln \frac{K_S}{K_w^n} - \frac{2.303RT}{F} pH \qquad (7)$$

The potential variation with pH, for the redox transition $M^{n+} + ne^- \leftrightarrows M$, at 25°C is then given by:

$$\frac{\partial E}{\partial pH} = -\frac{2.303RT}{F} = -0.059 \qquad (8)$$

According to equation 8, the potential for an ideal oxide electrode system in aqueous solution at 25°C, decreases with increasing pH by ca. 59 mV/pH unit, with respect to a pH independent reference electrode such as the NHE or the saturated calomel electrode (SCE). Such a shift in potential with pH, is referred to as a *Nernstian shift,* since it is predicted by the Nernst equation. It should be noted that if the reference electrode is pH dependent, such as the reversible hydrogen electrode (RHE) or the Hg/HgO electrode, no potential pH shift will be observed, since the potential of this type of electrode also alters by ca. 59 mV per unit change in pH at 25°C.

Pt oxidation : Hydrolysis complications. Burke et al.

Burke et al suggested that examination of potential vs pH response of surface redox
Transformations should provide information on stoichiometry of process (proton/electron
Ratio).

For the oxidation process $Pt + H_2O \rightarrow PtOH + H^+ + e^-$ the redox potential should decrease
By a factor of – 0.059 V per unit change in pH (potential measured wrt a pH independent
reference electrode).
Burke & Roche showed that the oxidation onset potential decreases with increasing pH
By an amount – 0.088 V per unit pH change i.e. – 3/2(2.303RT/F) V/pH unit.
This result is indicative that the ratio of protons to electrons involved in oxidation
reaction is 3/2.
To rationalize this result it was proposed that the <u>discharge</u> step was linked with a
<u>hydrolysis</u> step which would result in an anionic Pt surface species.
The hydrolysis step can be written in a number of ways.
$2\ PtOH \rightarrow [Pt_2O.OH]^- + H^+$
$2\ PtOH + OH^- \rightarrow [Pt_2O.OH.H_2O]^-$
$2\ PtOH + H_2O \rightarrow [Pt_2O.OH.H_2O]^- + H^+$
The surface species may well be a mixture of partially hydrated Pt(I) species such as PtO^-
And PtOH, in either monomeric, dimeric or two dimensional polymeric form presumably
With counterbalancing H^+ or M^+ ion located in the Helmholtz layer.
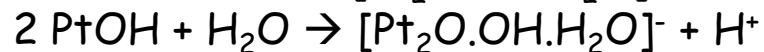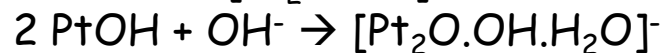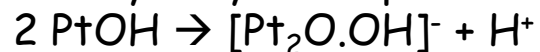
Hence the **Super-Nernstian** potential pH
shift is ascribed to:
$2 \, Pt + 2H_2O \rightarrow [Pt_2O.OH]^- + 3H^+ + 2e^-$.
The surface oxidation step could also involve
OH^- ions
especially at higher pH,
$2Pt + 3OH^- \rightarrow [Pt_2O.OH]^- + H_2O + 2e^-$. Hence
an anionic
Pt(I) surface complex is proposed.
One can envisage the oxidation product as an
oxygen bridged surface dimer of one
of the possible types illustrated across.
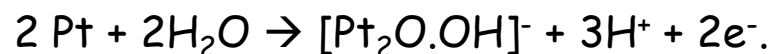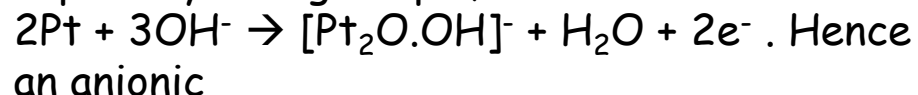
$$O \text{———} H \longleftrightarrow O^-$$

Pt   Pt

(diagram: O bridging two Pt atoms with H, and O below)

Pt   H   Pt

O
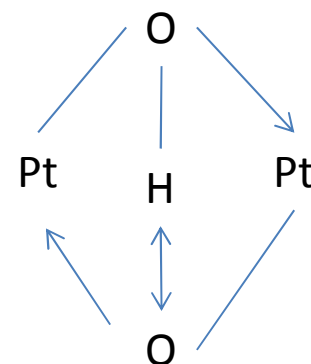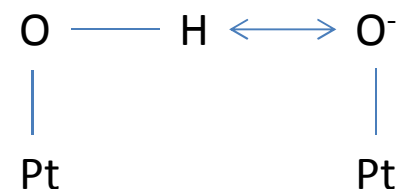
Note that the value of oxide reduction peak potential observed on the reverse sweep
varied less radically (and in a non linear manner) with changes in solution pH.
This was attributed to the occurrence of the following process
$PtO^-.PtOH.xH_2O + Pt_s \rightarrow Pt_s \text{—}O\text{—}Pt + PtOH.xH_2O$
Hence due to the occurrence of subsequent place exchange reactions during the anodic
Sweep the anodic film is gradually converted to a more neutral, considerably less
protonated layer. The non linearity could be due to a lack of complete equilibration in
the freshly grown oxide film in which layer rearrangement could cause potential drift.

Conjoint EQCM/CV measurement.

Fig. 1. CV (————) and associated frequency change (- - - - - -) of a Pt-coated quartz crystal in 0.1 M H₂SO₄: scanning rate, 50 mV/s.
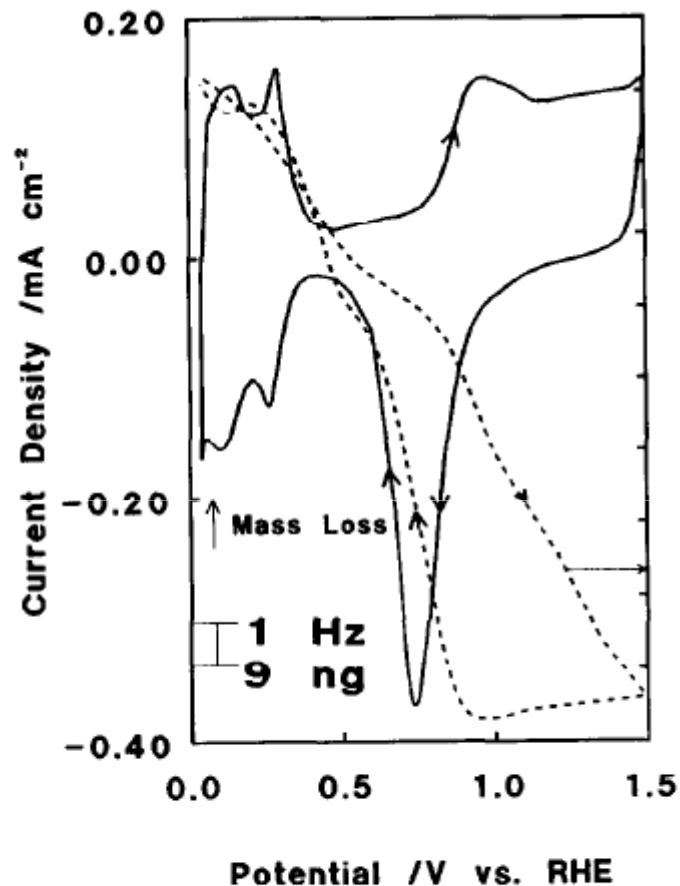
Mass increase seen during Pt oxide Formation, while oxide reduction is Accompanied by mass loss.

Experimental data from potential Range of oxide reduction peak Suggests that a-Pt oxide is anhydrous.

$$Pt + H_2O \rightarrow PtO + 2H^+ + 2e^-$$

EQCN Technique

- Complete description of redox switching requires a consideration of concomitant changes in ion and solvent populations.
- This can be achieved using the EQCN method.
- The quartz crystal nano/microbalance is a piezoelectric device capable of monolayer mass sensitivity. The method involves sandwiching a quartz crystal between two electrodes, one of which is used as the working electrode of an electrochemical cell. These electrodes are used to impose a radio frequency RF electric field across the crystal at a resonant frequency determined by the crystals dimensions and mass loading.
- A change in the mass of the working electrode causes a change in the resonant frequency of the device which can then be used to determine the quantity of added mass.
- This effect is quantified via the Sauerbrey equation which relates the change in resonant frequency Δf from its value f at the start of the experiment, and the mass change ΔM per unit area of the electrode.
- Sauerbrey equation valid if polymer is a rigid layer, if Δf << f, and if the layer is thin.

Resonant frequency

$$\Delta f = -\frac{2}{\rho \upsilon} f^2 \Delta M$$

Density of crystal

Velocity of acoustic Shear wave in polymer film

$$\Delta f \downarrow$$

$$\Delta M \uparrow$$
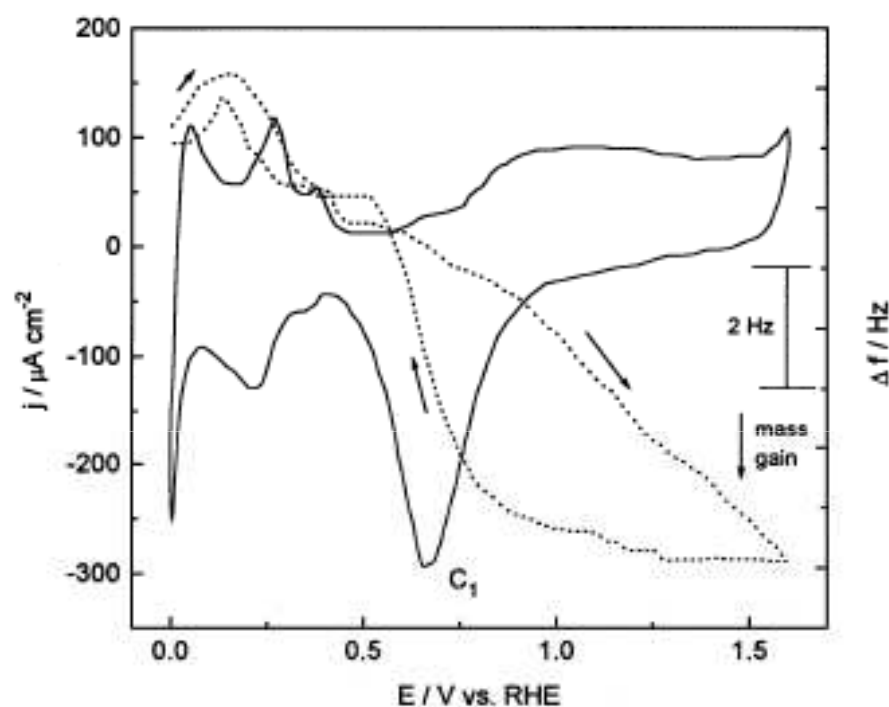
Fig. 1. CV (solid line) and associated frequency change (dotted line) of a Pt-coated quartz crystal in 0.1 M NaOH between 0 and 1.6 V at 50 mV/s.
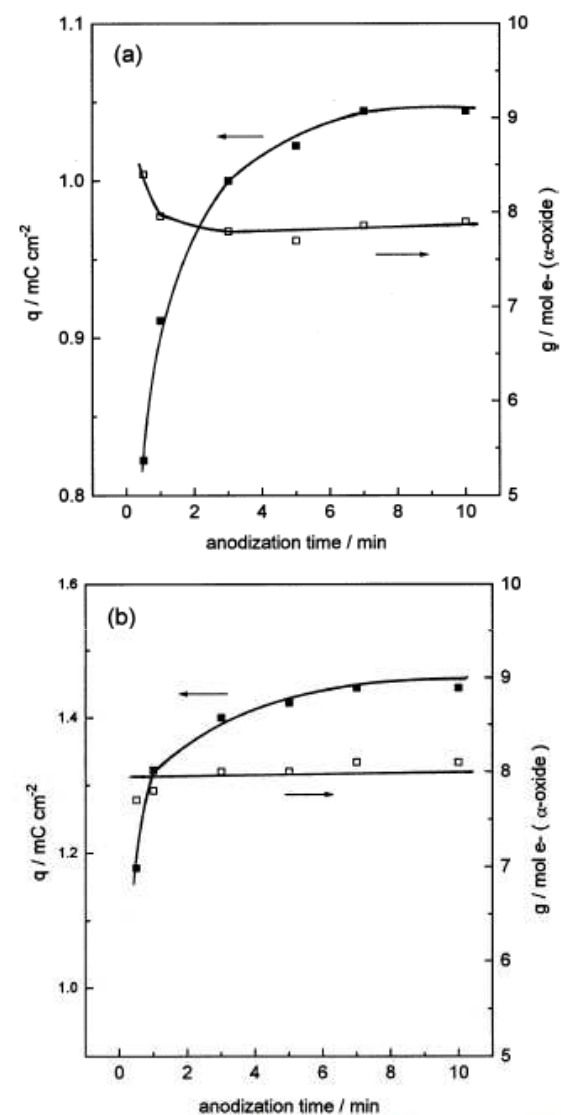

Fig. 2. α-Oxide reduction charge density (solid symbols) 10 mV/s and its g/mol e$^-$ ratio (open symbols) as a function of anodization time of Pt-coated quartz crystal at (a) 1.3 V and (b) 1.6 V in 0.1 M NaOH.

More modern interpretation of Pt metal oxidation

CV and mass response (EQCM) profiles recorded on same Pt coated quartz crystal.

Traditional mechanism considered too simple. Conjoint CV/EQCN/AES (Jerkiewicz et al Electrochim. Acta 49(2004) 1451-1459.
experiments suggest a more complex mechanism.

$$M = \frac{\delta \, \Delta m n F}{\Delta q}$$

n = 2

Potential zero total charge

PZTC
(Pt,H_2SO_4) =
0.27V

$0.85 < E < 1.40$ V
$\Delta q = 372$ mC/cm^2
$\delta \Delta m = 23.8$ ng/cm^2
M = 12.3 g/mol
$0.27 < E < 1.40$ V
$\delta \Delta m = 30.5$ ng/cm^2
M = 15.8 g/mol

1 ML O : PtO : M = 16 g/mol
1 ML monohydrated PtO (PtO.H2O) : M = 34 g/mol
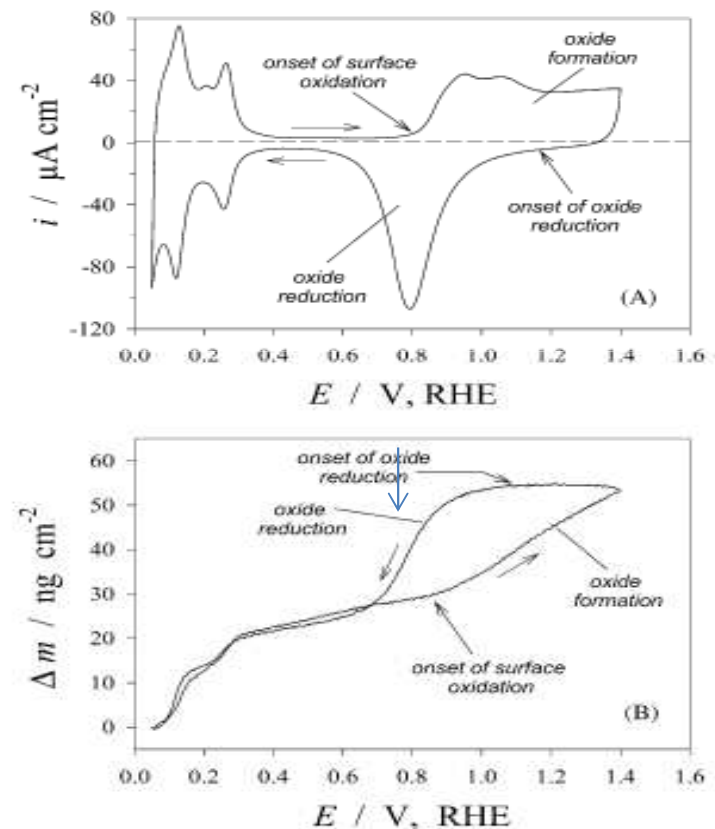
Fig. 1. Cyclic-voltammetry (i vs. E) profile (A) and mass-response (Δm vs. E) profile (B) for a Pt electrode in 0.5 M aqueous H_2SO_4 solution recorded at $s = 50$ mVs^{-1} and $T = 298$ K.

1. The electrochemical quartz-crystal nanobalance when combined with other experimental methodologies is a powerful tool in research on electro-oxidation of noble-metal electrodes and provides an insight into the interfacial mass balance.
2. The experimentally determined molecular weight of the Pt surface oxide is $15.8\,g\,mol^{-1}$, thus pointing to the addition of O to the surface and PtO as the oxide species formed. The surface oxide is an anhydrous species.
3. Platinum electro-oxidation does not involve OH_{ads} as an intermediate; the process proceeds with the initial discharge of half a monolayer of H_2O leading to the formation of half-monolayer of O_{chem} that resides on-top of the Pt surface without any place exchange.
4. Discharge of the second half-monolayer of H_2O molecules and development of the second half-monolayer of O_{chem} trigger the interfacial place exchange between O_{chem} adatoms and the top-most Pt surface atoms. The process occurs in the 1.10–1.20 V potential range.
5. The interfacial place exchange leads to the development of a quasi-3D surface lattice comprising Pt^{2+} cations and O^{2-} Anions.

$$Pt + H_2O \xrightarrow{\text{strong physisorption}} Pt^{\delta+}-O^{\delta-}H_2;$$

$$pztc = 0.27\text{–}0.85\,V \tag{5}$$

$$(Pt-Pt)-H_2O \xrightarrow{\text{discharge}} (Pt-Pt)^{\delta+}-O_{chem}{}^{\delta-} + 2H^+ + 2e^-;$$

$$0.85\text{–}1.15\,V \tag{6}$$

$$Pt-O_{chem} + H_2O \xrightarrow{\text{discharge, place exchange, completion of charge transfer}}$$

$$(Pt^{2+}-O^{2-})_{\text{quasi-3D lattice}} + 2H^+ + 2e^-; \sim 1.15\text{–}1.40\,V \tag{7}$$
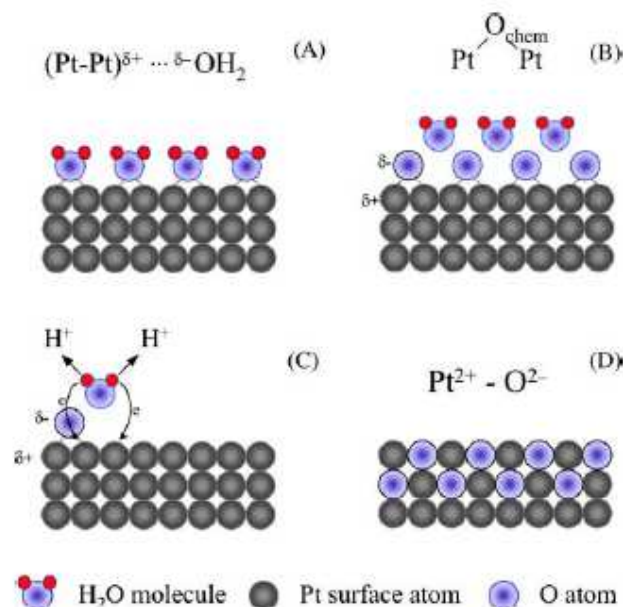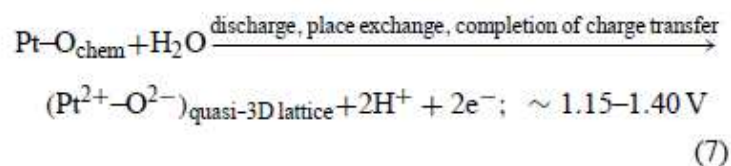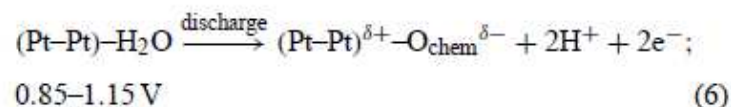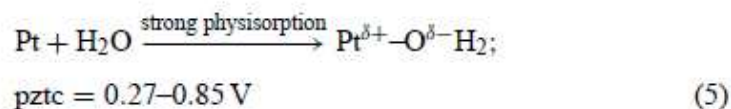

Fig. 7. Visual representation of the platinum-oxide growth mechanism: (A) interaction of H_2O molecules with the Pt electrode that occurs in the $0.27 \le E \le 0.85$ V range; (B) discharge of half a monolayer of H_2O molecules and formation of $\sim0.5\,ML$ of chemisorbed oxygen (O_{chem}); (C) discharge of the second half-monolayer of H_2O molecules; the process is accompanied by the development of repulsive interactions between $(Pt-Pt)^{\delta+}-O_{chem}{}^{\delta-}$ surface species that stimulate an interfacial place exchange of O_{chem} and Pt surface atoms and (D) quasi-3D surface PtO lattice comprising Pt^{2+} and O^{2-} moieties that forms through the place-exchange process.

Recent DFT studies have shed further light on PtO formation energetics & mechanism.
EF Holby, J Greeley, D Morgan, J.Phys. Chem.C., 116 (2012) 9942-9946.

We conclude that redox chemistry of noble metal surface oxidation is very complex and subject to controversy.

Pt : Multilayer Oxide Formation

Vigorous direct fixed potential anodization of Pt electrodes in acid solution in potential range 2.1 – 2.5 V for extended periods of time results in formation of yellow multilayer oxide termed the β-layer. Oxide thicknesses may extend up to ca. 6 nm without showing any limiting values.

Cathodic linear potential sweep voltammograms obtained for heavily anodized Pt electrodes yield two main peaks, the first at ca. 0.6 V relates to reduction of compact Film of monolayer dimensions (designated the a-layer) which is located at the interface Between bulk Pt and bulk Pt oxide. The second peak observed at ca. 0.2V corresponds to the quantitative reduction of the β-layer to Pt metal, a process which is accompanied by a substantial increase in surface area of Pt electrode, the area increasing with increasing surface area of β-layer initially present.

Note that β–oxide Growth is most readily observed with electrodes whose surface is abraided prior to Polarization. The important role of residual stress due to mechanical pretreatment Of the electrode is suggestive that a nucleation process may play an important role in the Formation of the b-oxide layer. Spectroscopic investigations have shown that the b-oxide layer has the general structure $PtO_2.xH_2O$.

Burke & co-workers have shown that a multilayer oxide film can be grown on Pt under potential cycling conditions. Multicycling between optimum sweep limits of ca. 0.5 – 2.8 V at a given scan rate results in the development of a relatively thick layer after ca. 6000 cycles.

The initial layer formed on the Pt metal surface under these conditions is assumed to be a relatively inert, compact monolayer of oxide or hydroxide.

However when the layer is subjected to conditions of vigorous oxygen evolution at the upper limit of the anodic potential sweep, changes both in the oxidation state and oxygen coordination number occur which result in the transformation of the relatively inert, largely anhydrous monolayer to a hydrated material, in which the majority of cations are assumed to be in the Pt(IV) state, and hence the composition of the hydrated

Film is assumed to be $PtO_2.xH_2O$.

In contrast to potentiostatically grown films it is possible to grow a thick multilayer film on Pt under potential cycling conditions without the need to generate mechanical stress on the electrode surface.

This can be attributed to the fact that the formation and subsequent reduction of the monolayer film leaves the metal atoms at the surface in a disturbed state. On subsequent re-oxidation the compact oxide layer is regenerated by oxidation of the underlying bulk metal lattice while the dispersed Pt atoms are more fully oxidized and reduced at the compact oxide/hydrous oxide interface to the hydrous state.

VI Birss, M.Chang, J. Segal, J. Electroanal. Chem., 355 (1993) 181-191.
LD Burke, MBC Roche, J. Electroanal. Chem. 159 (1983) 89-99

Duplex peaks observed
For both a and b Pt oxide
Reduction.
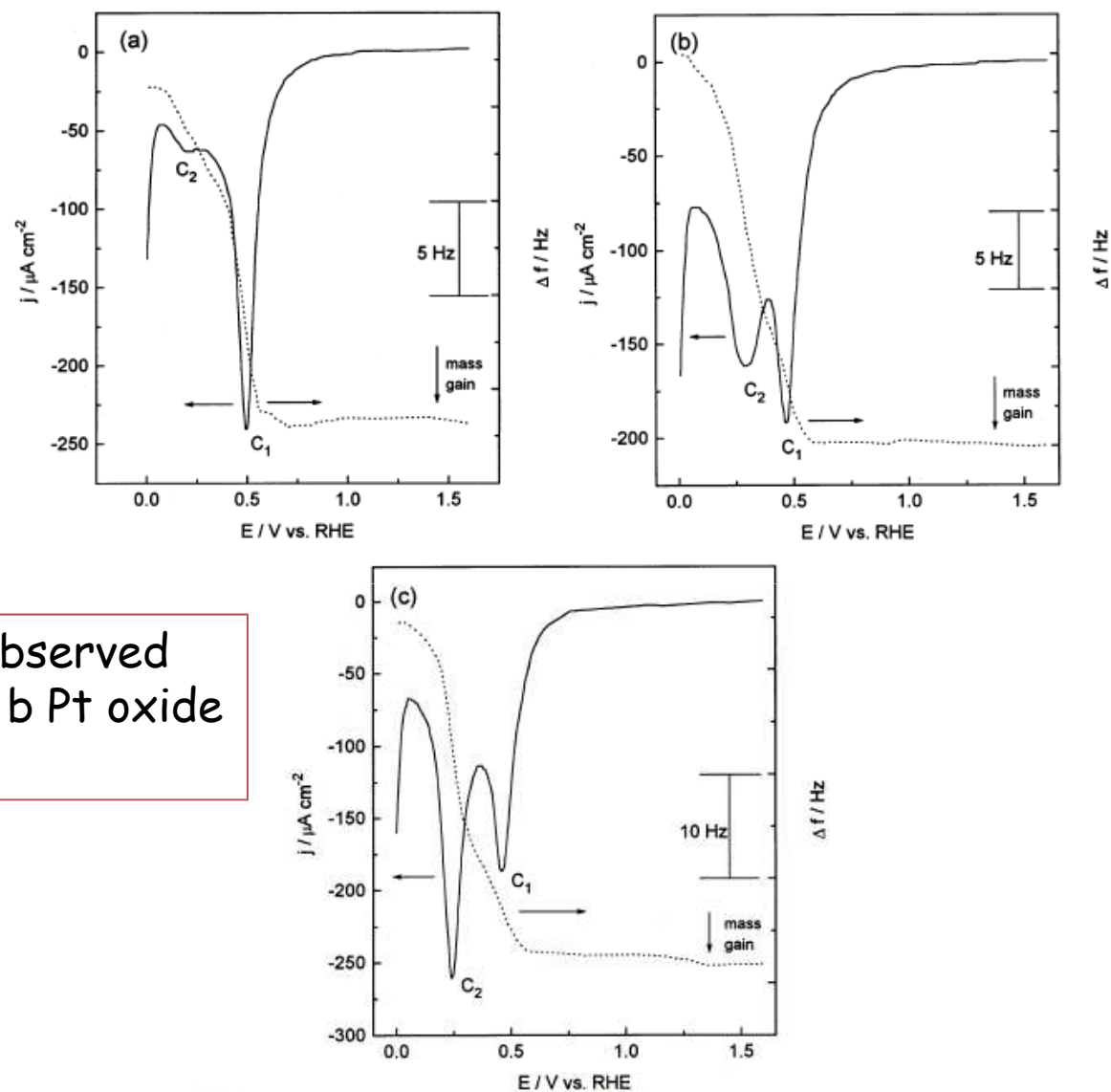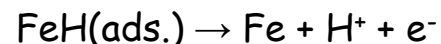
Fig. 4. Typical i/E (solid line) and f/E (dotted line) profiles during Pt oxide film reduction at 10 mV/s and associated frequency change after oxide growth on Pt-coated quartz crystal, by cycling for (a) 30 s, (b) 3 min and (c) 5 min between 0.5 and 2.82 V at 2 V/s, in 0.1 M NaOH.
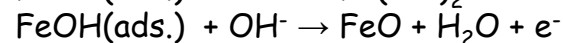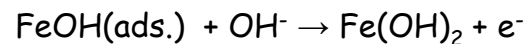
# Surface redox chemistry: Bright Fe electrode

A₁

$Fe + OH^- \rightarrow FeOH(ads.) + 2e^-$

$FeH(ads.) \rightarrow Fe + H^+ + e^-$

A₂

$FeOH(ads.) + OH^- \rightarrow Fe(OH)_2 + e^-$

$FeOH(ads.) + OH^- \rightarrow FeO + H_2O + e^-$

A₄

$3Fe(OH)_2 + 2OH^- \rightarrow Fe_3O_4 + 4H_2O + 2e^-$

$3FeO + 2OH^- \rightarrow Fe_3O_4 + H_2O + 2e^-$
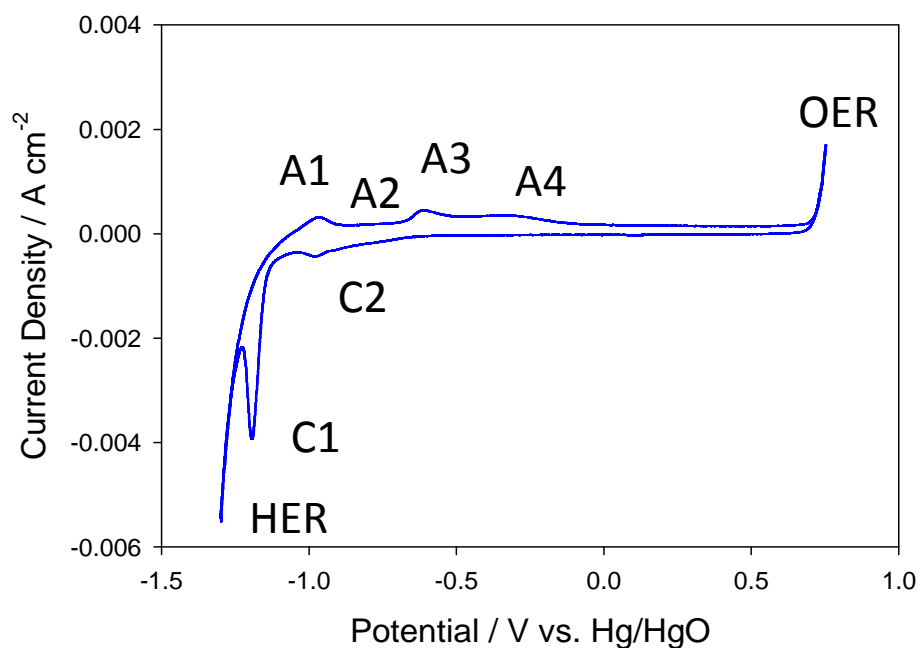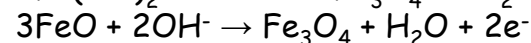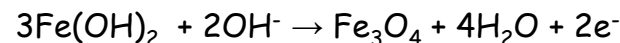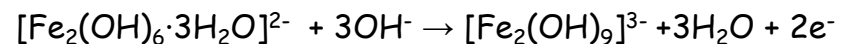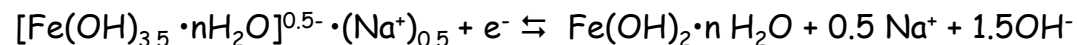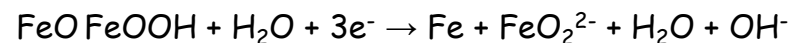
In situ Raman
EQCM
RRDE

Greater fine structure observed at low sweep rate.

A₃/C₂

$[Fe_2(OH)_6 \cdot 3H_2O]^{2-} + 3OH^- \rightarrow [Fe_2(OH)_9]^{3-} + 3H_2O + 2e^-$

$[Fe(OH)_{3.5} \cdot nH_2O]^{0.5-} \cdot (Na^+)_{0.5} + e^- \leftrightarrows Fe(OH)_2 \cdot n\,H_2O + 0.5\,Na^+ + 1.5OH^-$

C₁

$FeO \cdot FeOOH + H_2O + 3e^- \rightarrow Fe + FeO_2^{2-} + H_2O + OH^-$
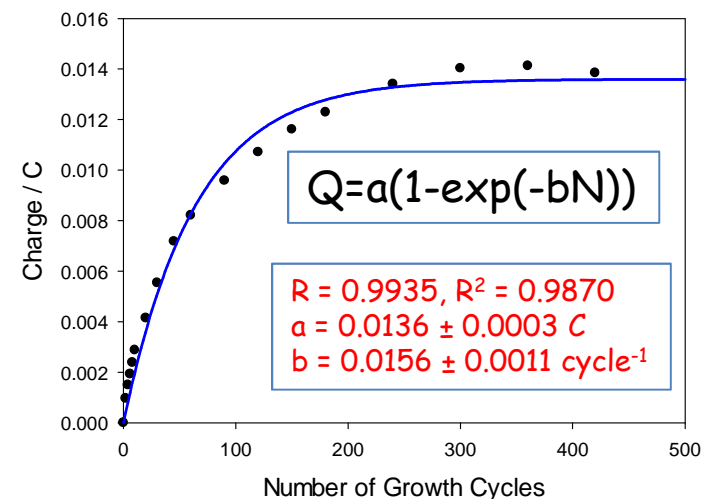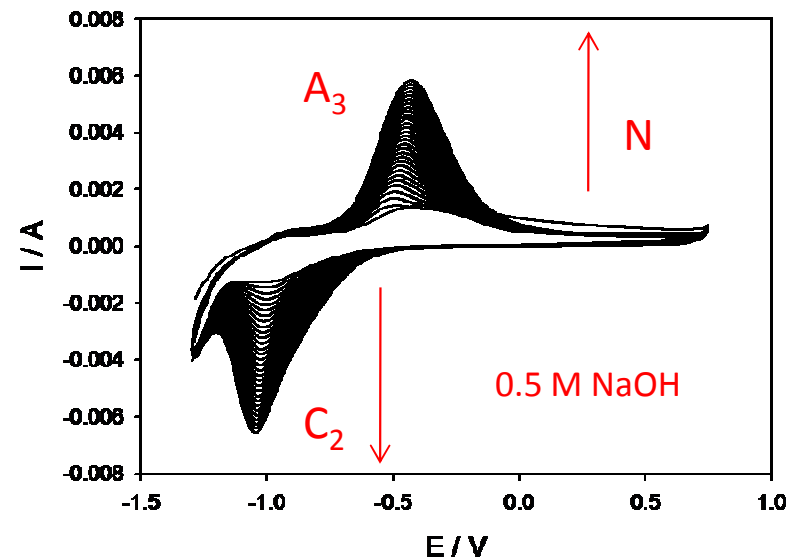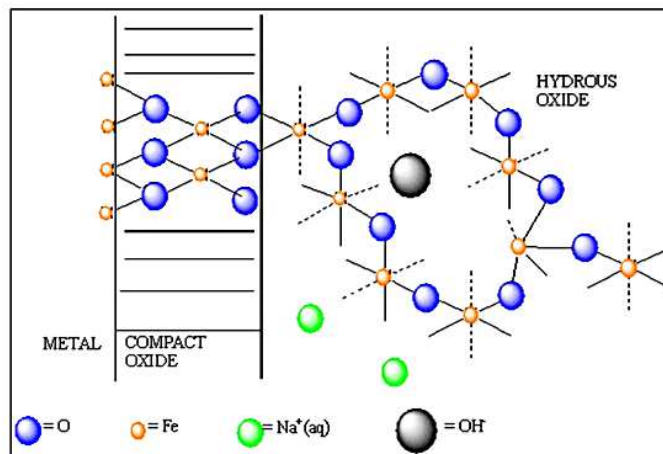
Hydrous Oxide Growth via Cyclic Potential Multicycling (CPM) Procedure of Fe electrode in aqueous alkaline solution.

Layer growth parameters:
- Upper, lower potential sweep limits.
- Solution temperature.
- Solution pH.
- Potential sweep rate.
- Base concentration.

CPM methodology is scalable.
Hydrous oxide growth process does not depend on electrode size.
Important for commercial viability.

Hydrous oxide film regarded as a surface bonded polynuclear species. Metal cations in polymeric network held together by sequence of oxy and hydroxy bridges.
Mixed conduction (electronic, ionic) behaviour similar to that exhibited by Polymer Modified Electrodes.
Can regard microdispersed hydrous oxide layer as open porous mesh of interconnected surfaquo metal oxy groups.

0.5 M NaOH

A_3

N

C_2

I / A

E / V

HYDROUS OXIDE

METAL | COMPACT OXIDE

= O   = Fe   = Na⁺(aq)   = OH

$$Q=a(1-\exp(-bN))$$

R = 0.9935, R² = 0.9870
a = 0.0136 ± 0.0003 C
b = 0.0156 ± 0.0011 cycle⁻¹

Charge / C

Number of Growth Cycles
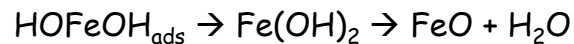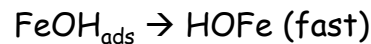
Mechanism of duplex layer film growth.

- Initial oxidation process involves formation of OH and O radical species which reversibly adsorb on metal surface:

  $Fe + OH^- \rightarrow FeOH_{ads} + e^-$
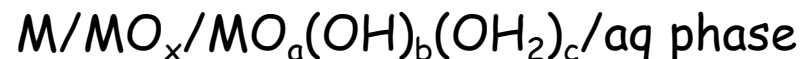
- With increasing degree of surface coverage the adsorption takes on a more irreversible character. A thin largely anhydrous passivating phase oxide is formed via a place exchange mechanism:

  $FeOH_{ads} \rightarrow HOFe$ (fast)

  $HOFe + OH^- \rightarrow HOFeOH_{ads} + e^-$ (rds)

  $HOFeOH_{ads} \rightarrow Fe(OH)_2 \rightarrow FeO + H_2O$

  In the anhydrous film ions are held in a rigid manner in an extended network of polar covalent bonds which drastically reduce ion transport through (and consequently extension of) the surface layer.

- The film thickening reaction (the hydration process) is slow since it involves rupture of primary coordination M-O bonds. The dependence of film growth on the lower potential sweep limit E_{LL} implies that partial reduction of anhydrous layer is important in generation of thick microdispersed hydrous deposit.

- On subsequent re-oxidation the compact layer is restored but the outer region of the film is present in a more dispersed form. On further reduction this latter material is incorporated into the dispersed hydrated outer layer.

- The hydrated layer formed in this way exhibits an open, zeolite type structure.

- The optimum upper limit E_{UL} corresponds to a potential which represents the best compromise between two opposing effects – the compact layer must attain a reasonable thickness (hence the requirement of a high anodic potential) but application of too high an upper limit results in a very unreactive layer

$M/MO_x/MO_a(OH)_b(OH_2)_c/aq\ phase$

Hydrous oxide film regarded as a surface bonded polynuclear species. Metal cations in polymeric network held together by sequence of oxy and hydroxy bridges.
Mixed conduction (electronic, ionic) behaviour similar to that exhibited by Polymer Modified Electrodes.
Can regard microdispersed hydrous oxide layer as open porous mesh of interconnected surfaquo metal oxy groups.

Lyons, Burke, J. Electroanal. Chem., 170 (1984) 377-381

Lyons, Burke, J. Electroanal. Chem., 198 (1986) 347-368

Lyons, Brandon Phys. Chem. Chem. Phys., 11 (2009) 2203-2217

SOLUTION
$2H_2O \rightarrow OH\cdots O^- + 3H^+ + 2e^-$

METAL LATTICE

1. INITIAL DISCHARGE

2. PLACE-EXCHANGED MONOLAYER

3. REDUCTION TO FORM DISRUPTED OUTER LAYER

4. INITIATION OF HYDROUS FILM GROWTH ON 2nd SWEEP

DISPERSED OXIDE

COMPACT OXIDE
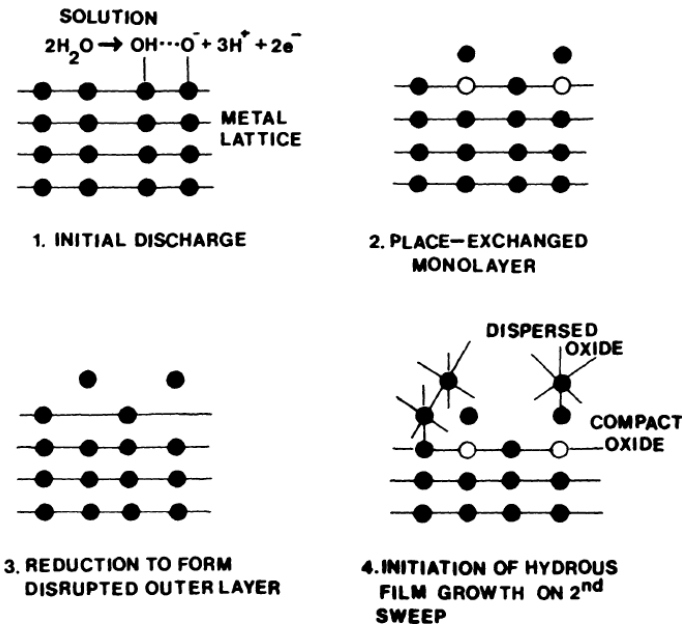
Figure 1. Schematic outline of the processes involved in hydrous oxide growth under potential cycling conditions.

OUTER HYDROUS OXIDE

METAL ELECTRODE   INNER COMPACT OXIDE

$\bigcirc = O$ $\bigcirc = Fe$ $\bigcirc = Na^+(aq)$ $\bigcirc = OH^-$

Fig. 3 Schematic representation of the $M/MO_x/MO_a(OH)_b(OH_2)_c/$ electrolyte interface region. M = metal ion, in this case Fe.
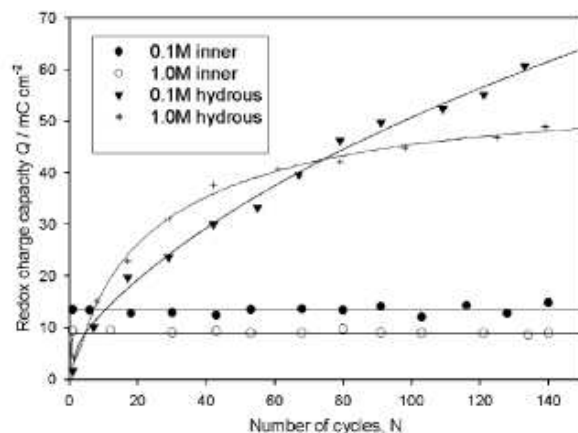
Fig. 4 Variation of the charge capacity Q associated with the outer hydrated oxide film (evaluated by integration of the A3 peak) and the inner compact oxide film (based on integration of the C1 peak) with increasing number of cycles, N, as a function of OH^- ion concentration at 25 °C. The oxide films were grown by repetitive potential cycling between -1.425 and 0.325 V at a sweep rate of 0.35 V s^{-1}.
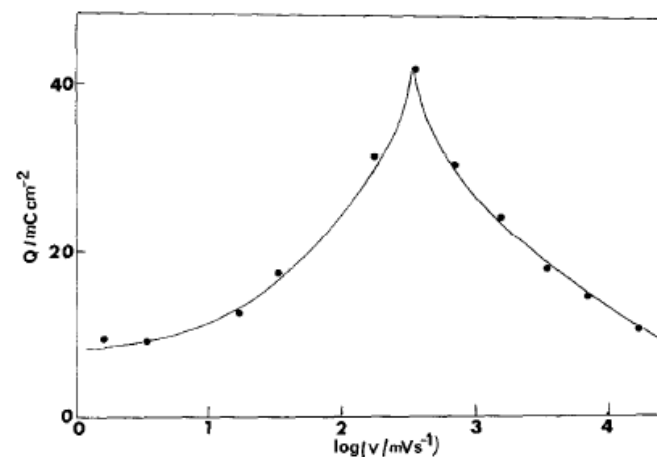
Fig. 3. Effect of sweep rate (v) on the oxide charge capacity (Q) developed after 30 cycles for an iron electrode in N$_2$-stirred 1.0 mol dm^{-3} NaOH at 25°C. Oxide growth sweep limits, -0.5 to 1.25 V; analytical conditions, -0.35 to 1.65 V, 40 mV s^{-1}.
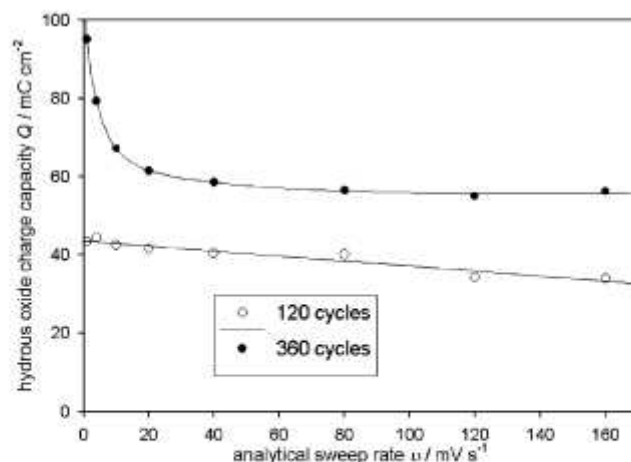
Fig. 6 Variation of charge capacity Q (evaluated by integration of the A3 voltammetric peak) with analytical sweep rate for iron oxide films grown under potential cycling conditions (-1.425 to 0.325 V, 0.35 V s^{-1}) for either 120 or 360 cycles in 1 M NaOH at 25 °C.
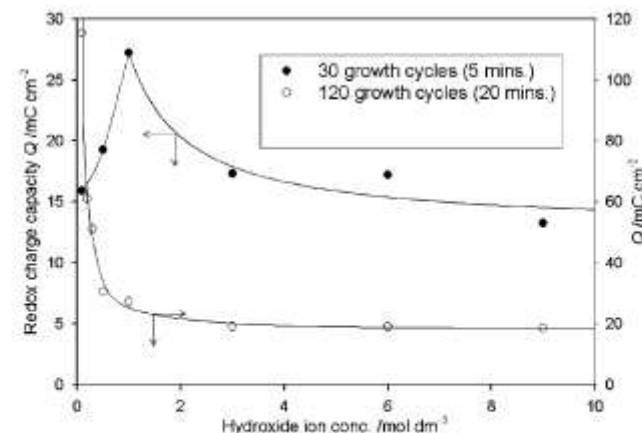
Fig. 5 Variation of multi-layer oxide growth with hydroxide ion concentration for multi-cycled iron electrodes (-1.425 to 0.325 V, 0.35 V s^{-1} at 25 °C) with different growth times. Q was evaluated by integration of the A3 voltammetric peak.

Hydration process promoted by increasing adsorption of OH⁻ ions as pH increases. Hence adsorbed OH⁻ species repel each other and attract hydrated positive counter ions into oxide matrix hence encouraging hydroxylation processes.

Increased instability of hydrous layer and more effective passivation as solution temperature increases.
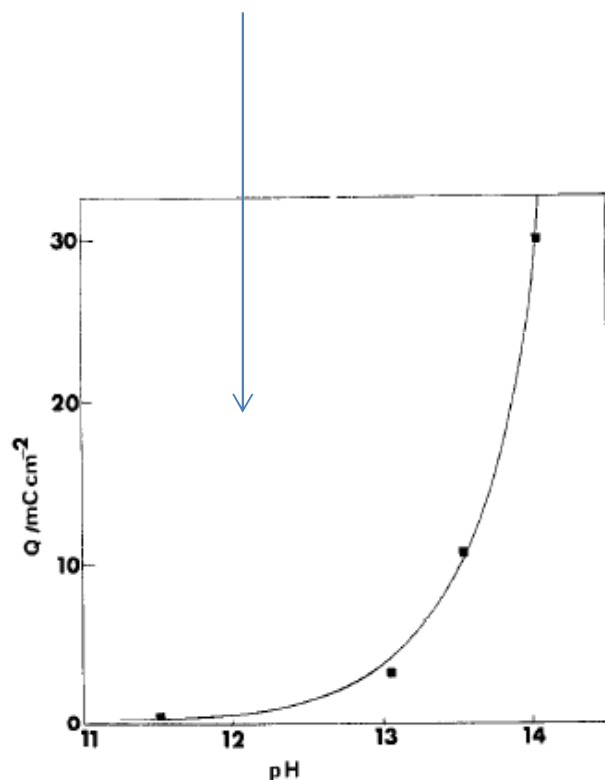

Fig. 7. Effect of solution pH on the extent of multilayer oxide growth (measured as oxide charge capacity, Q) for an iron electrode in buffer solution of various pH values. Oxide growth was carried out between -0.5 and 1.25 V at a sweep rate of 0.35 V s^{-1} for 30 cycles.
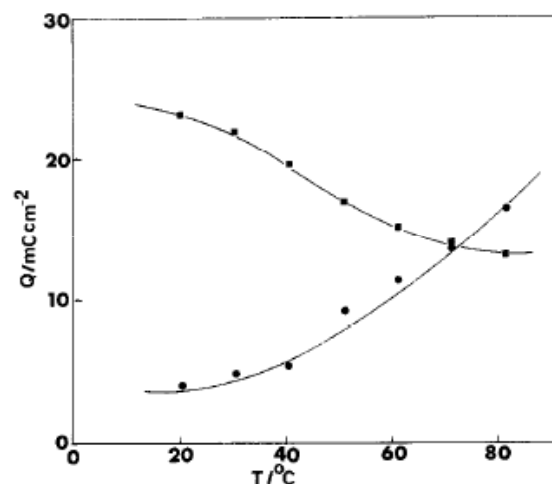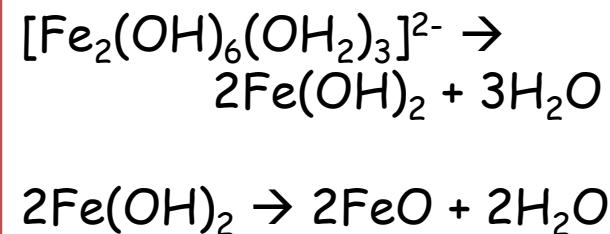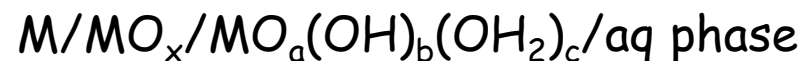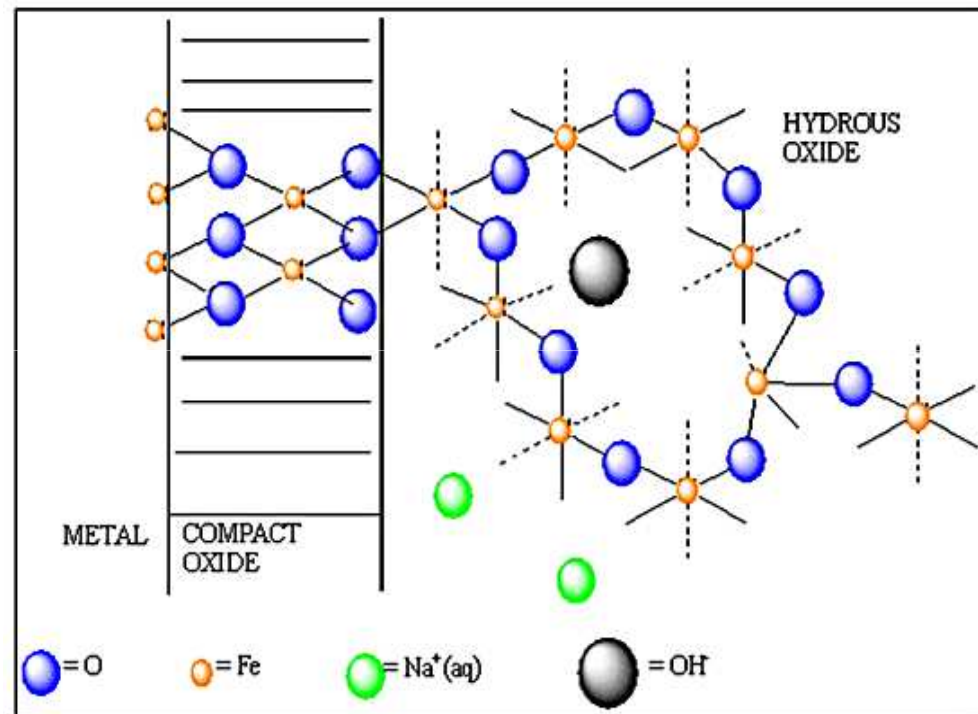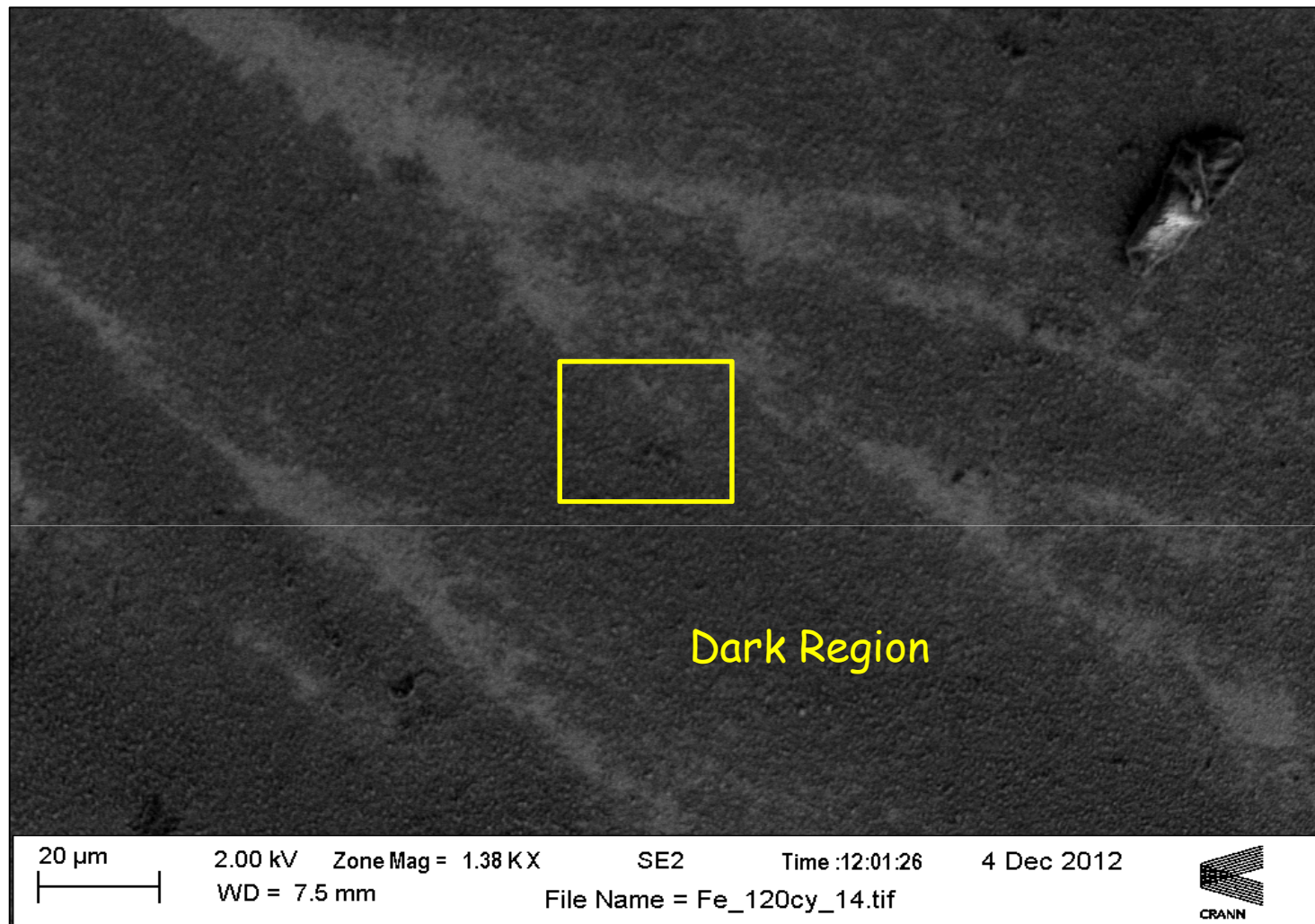
Fig. 9. Variation of oxide charge capacity (Q) with solution temperature (T) for a multicycled iron electrode (-0.5 to 1.25 V, 0.35 V s^{-1}, 30 cycles) in 1.0 mol dm^{-3} NaOH. (■) peak C_2; (●) C_1.

$$[Fe_2(OH)_6(OH_2)_3]^{2-} \rightarrow 2Fe(OH)_2 + 3H_2O$$

$$2Fe(OH)_2 \rightarrow 2FeO + 2H_2O$$

Duplex Layer Model of Metal oxide/solution interface region.
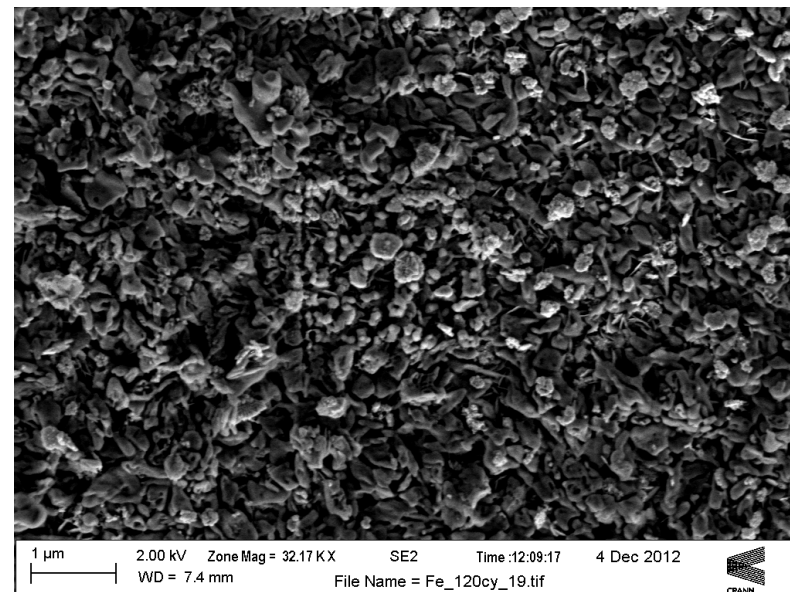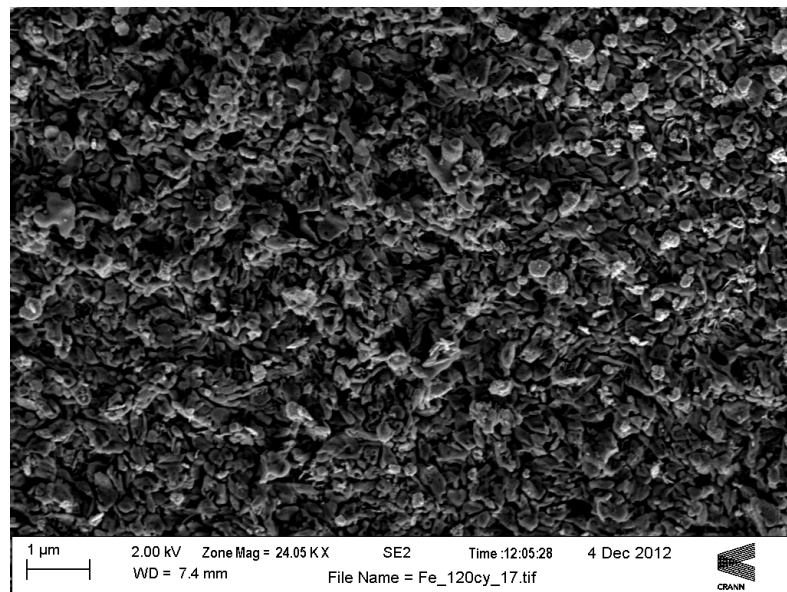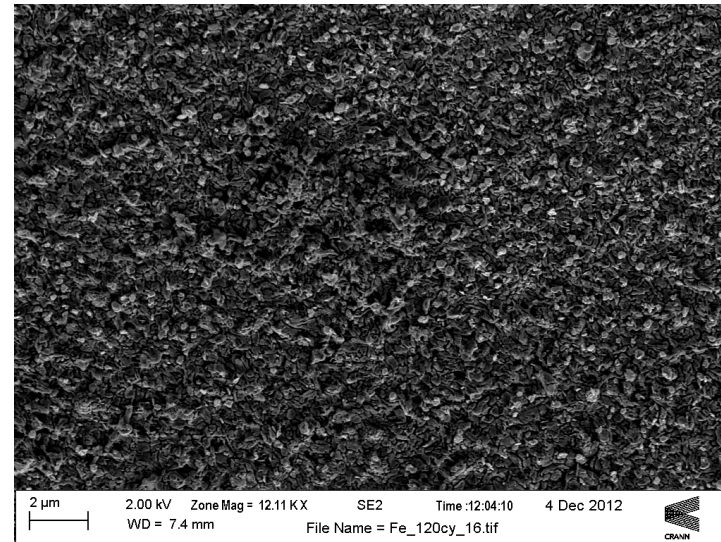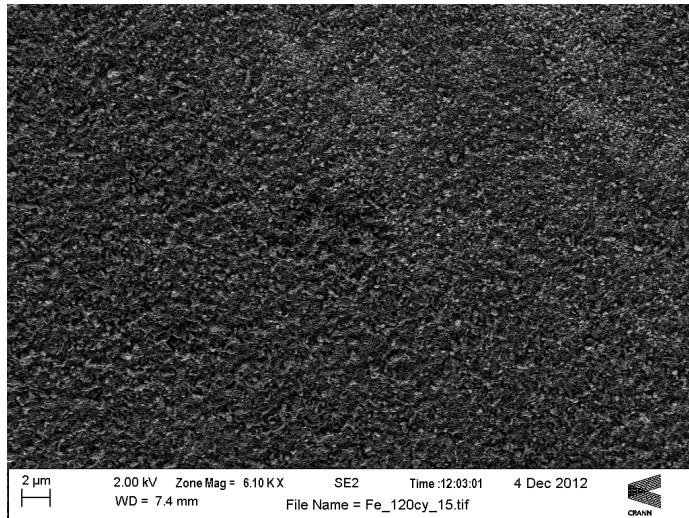
Hydrous oxide film regarded as a surface bonded polynuclear species. Metal cations in polymeric network held together by sequence of oxy and hydroxy bridges.
Mixed conduction (electronic, ionic) behaviour similar to that exhibited by Polymer Modified Electrodes.
Can regard microdispersed hydrous oxide layer as open porous mesh of interconnected **surfaquo** metal oxy groups.


HYDROUS OXIDE

METAL | COMPACT OXIDE

$\bullet$ = O $\circ$ = Fe $\circ$ = Na$^+$(aq) $\bullet$ = OH

$M/MO_x/MO_a(OH)_b(OH_2)_c/aq$ phase
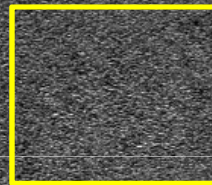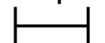
Higher magnification SEM image of the hydrous iron oxide coated electrode surface (N = 120 cycles, 1.0 M NaOH) illustrating characteristic '2 tone' feature.

Sequential magnification of the dark region
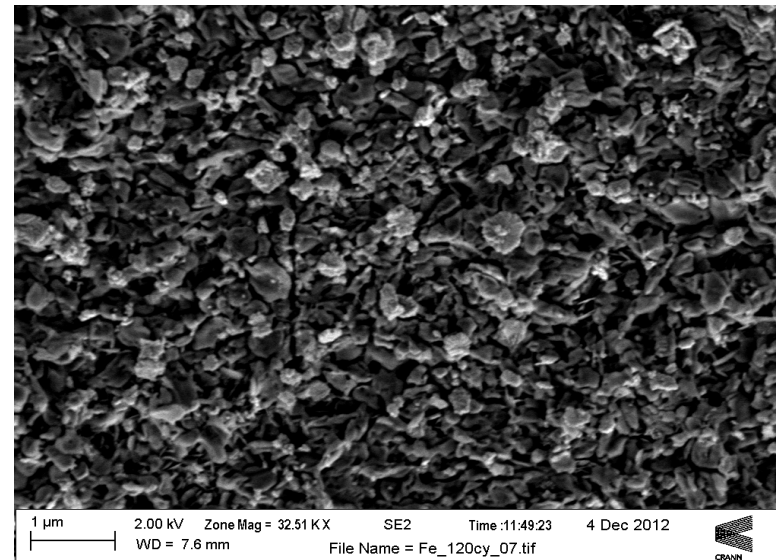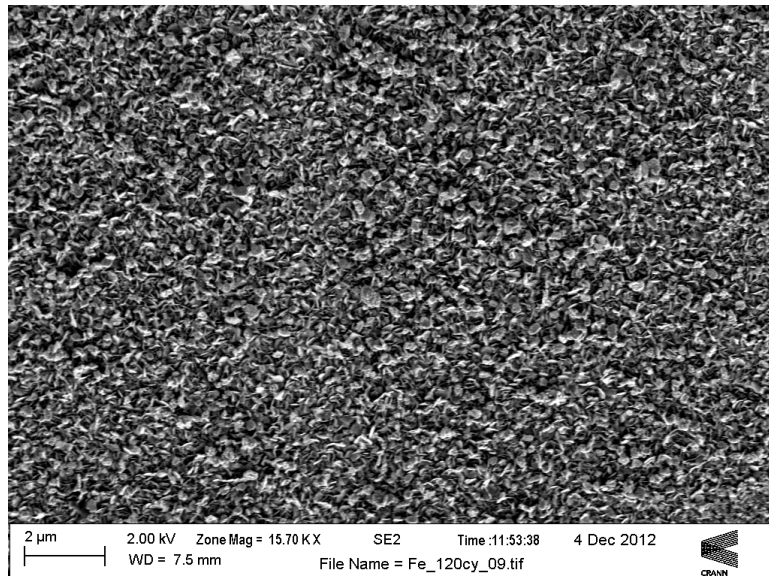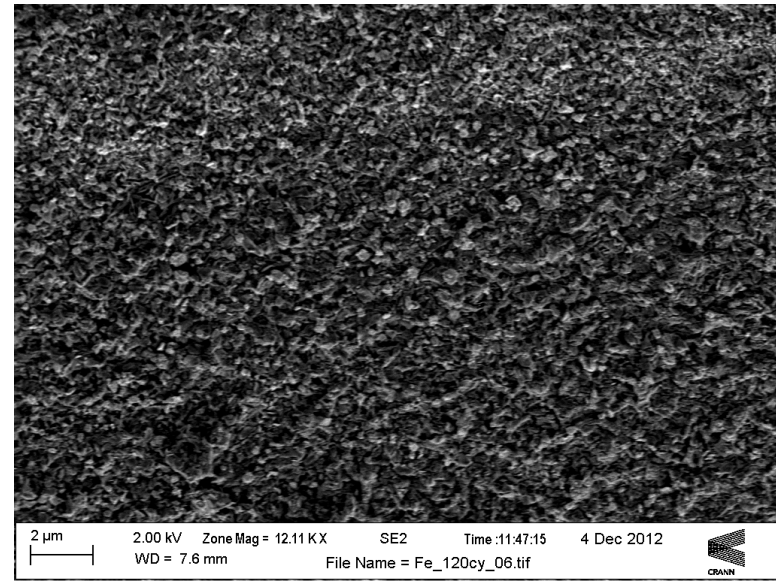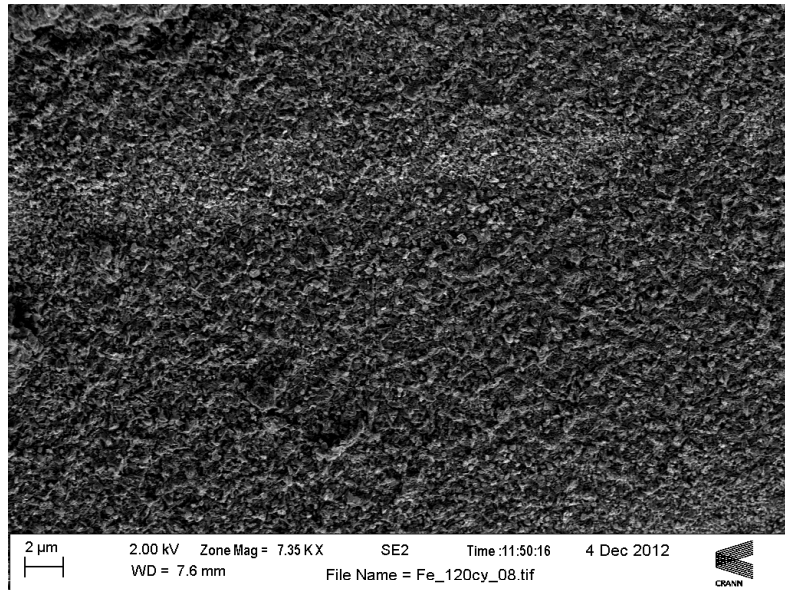
# Sequential magnification of the light region

2 µm 2.00 kV Zone Mag = 7.35 K X SE2 Time :11:50:16 4 Dec 2012
WD = 7.6 mm File Name = Fe_120cy_08.tif

2 µm 2.00 kV Zone Mag = 12.11 K X SE2 Time :11:47:15 4 Dec 2012
WD = 7.6 mm File Name = Fe_120cy_06.tif

2 µm 2.00 kV Zone Mag = 15.70 K X SE2 Time :11:53:38 4 Dec 2012
WD = 7.5 mm File Name = Fe_120cy_09.tif

1 µm 2.00 kV Zone Mag = 32.51 K X SE2 Time :11:49:23 4 Dec 2012
WD = 7.6 mm File Name = Fe_120cy_07.tif

40⁻

Preliminary note

INFLUENCE OF HYDROLYSIS ON THE REDOX BEHAVIOUR OF HYDROUS OXIDE FILMS

L.D. BURKE, M.E. LYONS, E.J.M. O'SULLIVAN and D.P. WHELAN

Chemistry Department, University College, Cork (Ireland)

First paper to demonstrate and explain Super-Nernstian pH shift.
Also MEGL's first real scientific publication !
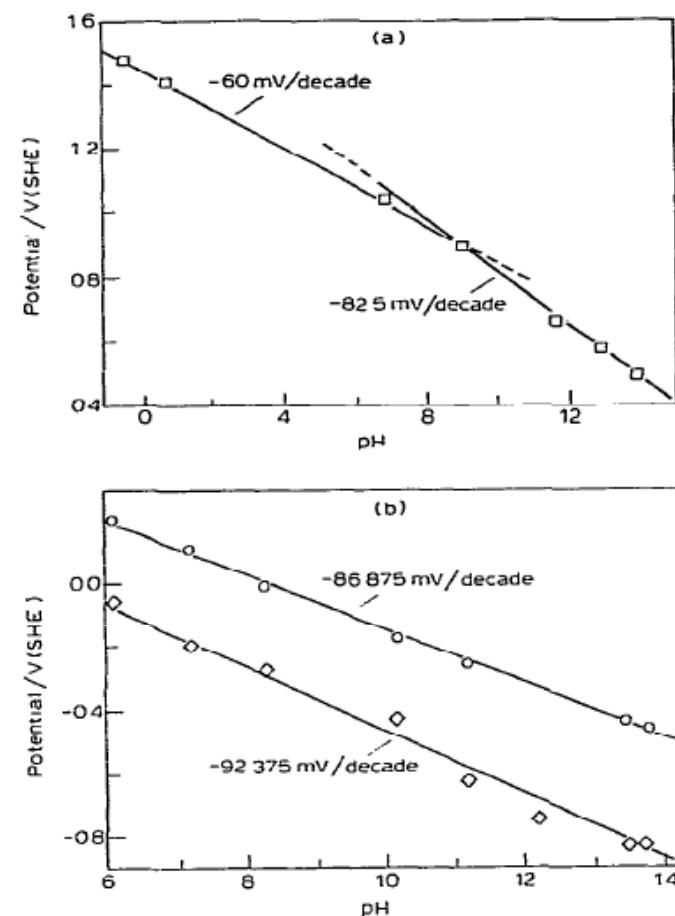
Fig. 1. (a) Effect of pH on the maximum of the cathodic peak (□) in the charge storage region for a hydrous rhodium oxide film grown originally in base (0—1.50 V, 5 Hz for 10 min). Solutions (1.0 mol dm⁻³): pH = 0—2, H_2SO_4 (+ NaOH); pH = 6—12, H_3PO_4 (+ NaOH); pH = 12—14, NaOH; T = 25°C. (b) Effect of pH on the anodic (○) and cathodic (◇) peak potentials in the charge storage region for a hydrous iron oxide film grown initially in 1.0 mol dm⁻³ NaOH (−0.51 to 1.26 V, 0.1 Hz, 30 cycles). Solutions. pH = 6—12, 0.3 mol dm⁻³ H_3PO_4 (+ NaOH); pH = 12—14, 1.0 mol dm⁻³ NaOH. The electrode was allowed to equilibrate for 1 h in each solution before the analytical scan (0.1 Hz, 40.7 mV s⁻¹) T = 25°C.

SN shift = -88.5 mV/dec wrt pH
independent reference electrode,
S = -3/2{2.303RT/F}
m/n = 3/2

THICK OXIDE GROWTH ON GOLD IN BASE

LAURENCE D. BURKE and MARY McRANN

Chemistry Department, University College, Cork (Ireland)

Fig. 5. Variation of the potential of the oxide reduction maxima with solution pH at 25°C:
(○) first oxide reduction peak: (△) second oxide reduction peak. Oxide grown at 2.2 V for

389

Compact oxide

S = -6.5 mV/unit pH

S = - 26.5 mV/unit pH

Hydrous oxide

(a)

(b)

Anodic
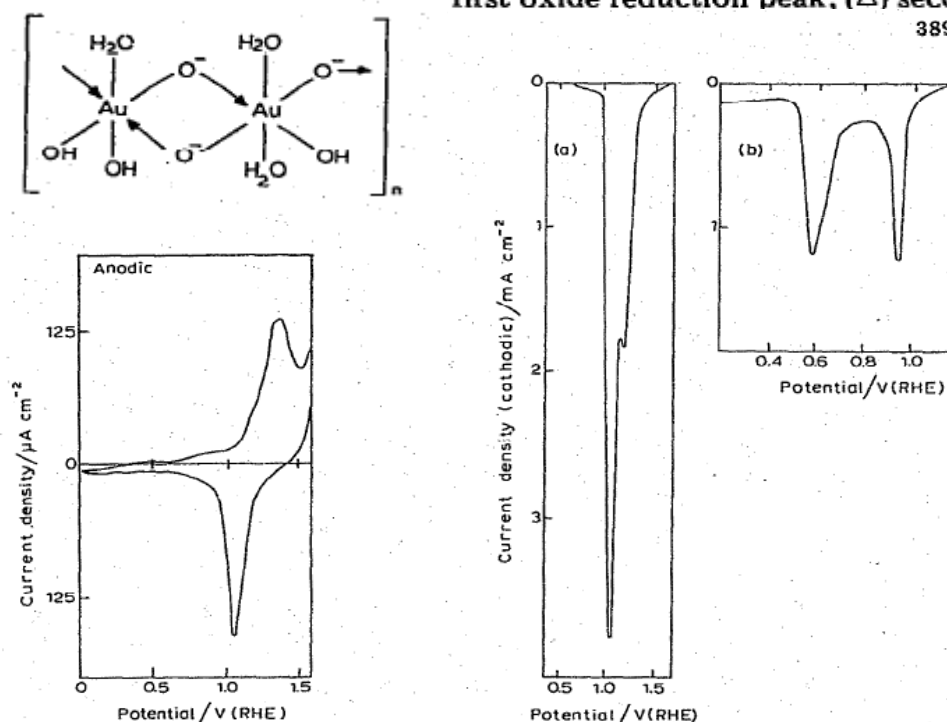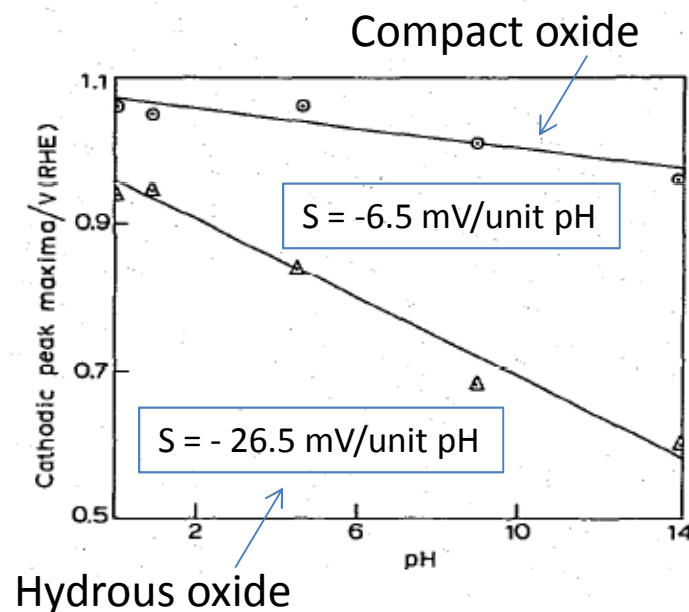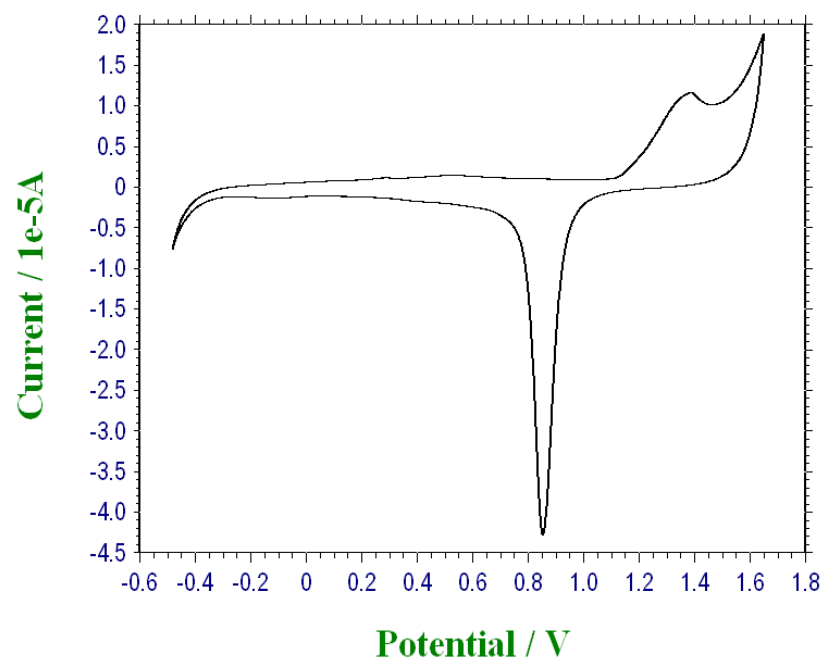
Fig. 1. Cyclic voltammogram (40 mV s⁻¹) for gold in nitrogen-stirred 1.0 mol dm⁻³ NaOH at 25°C.

Fig. 2. Peak splitting during the course of oxide reduction (cathodic sweep speed = 50 mV s⁻¹) in: (a) 1 mol dm⁻³ H_2SO_4 where the film was grown at 2.2 V for 10 s; (b) 1.0 mol dm⁻³ NaOH where the film was grown at 2.4 V for 10 s. T = 25°C.
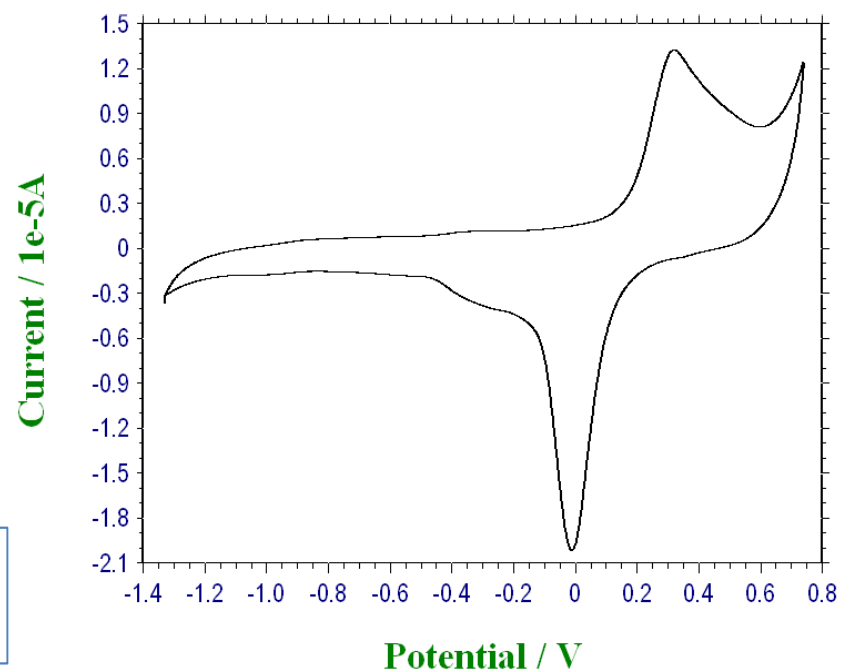
SN shift = 30 mV/dec (wrt RHE)
N shift = zero shift (wrt RHE)

Polycrystalline Au electrode, 100 mV/s 0.5 M H_2SO_4. Ian Godwin 2013.

Polycrystalline Au electrode, 100 mV/s 1.0 M NaOH. Ian Godwin 2013.

CV response of polycrystalline Au electrode in aqueous solution very characteristic.

Super-Nernstian potential vs pH shift : Au

We initially consider the reduction of the hydrous oxide layer on gold, a reaction which exhibits a potential vs pH response (- 88.5 mV/pH). The observed response can be rationalized if it is assumed that the cations in the film can co-ordinate to a given number q of hydroxide ions. This concept is in close analogy with polarography where the reduction potential of a cation may be decreased by addition of a complexing agent. The complex formation reaction in the hydrous film may be represented in this case by the following expression:

$$Au^{3+} + q\ OH^- \leftrightarrows Au(OH)_q^{(q-3)-} \quad (1)$$

The stability constant K for the latter reaction is given by the equation:

$$K = \frac{a_{Au(OH)_q}^{(q-3)-}}{a_{Au^{3+}} a_{OH^-}^q} \quad (2)$$

The electrode reaction is given by:

$$Au^{3+} + 3e^- \rightarrow Au \quad (3)$$

It is assumed to behave in a reversible manner so the Nernst equation pertains.

$$E = E^0 + \frac{RT}{3F} \ln a_{Au^{3+}} \quad (4)$$

An expression for a_{Au}^{3+} may be obtained from eqn. 2 and substituting into eqn. 4 yields

$$E = E^0 + \frac{RT}{3F} \ln \frac{a_{Au(OH)_q}^{(q-3)-}}{K_W^q K^q} - \frac{2.303RT}{F}\left(\frac{q}{3}\right) pH \quad (5)$$

Hence the sensitivity of the potential to changes in pH is given by

$$\frac{dE}{dpH} = -\frac{2.303RT}{F}\left\{\frac{q}{3}\right\} = -0.059\left\{\frac{q}{3}\right\} V \quad (6)$$

According to the observed experimental data dE/d pH = - 0.0885 V . Comparing with the result derived in eqn. 6 we can assign q = 4.5. Thus it is assumed that the complex present in the hydrated oxide layer on gold is or . The latter composition corresponds to the molecular formula $[Au_2O_3(OH)_3(OH_2)_3]^{3-}$.

# INFLUENCE OF pH ON THE REDUCTION OF THICK ANODIC OXIDE FILMS ON GOLD
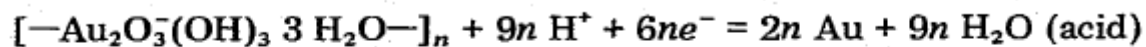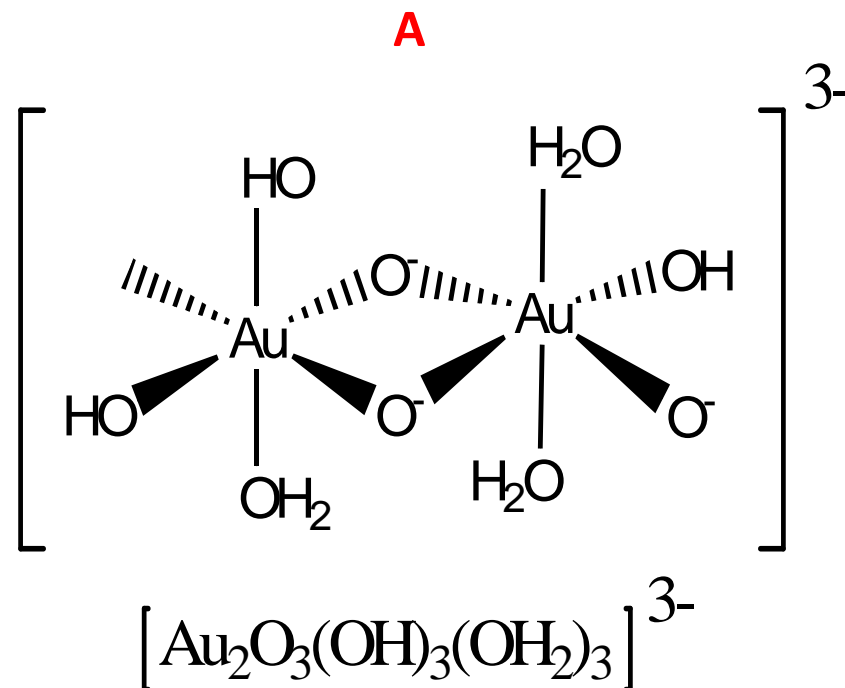
L.D. BURKE, M.E. LYONS and D.P. WHELAN

Chemistry Department, University College, Cork (Ireland)
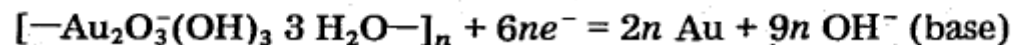
It is obvious that with the type of complex shown in scheme A across proton transfer processes can lead to alteration of the type of ligand at quite a number of coordination sites, and consequently the configuration illustrated in scheme A is only one of several possible for this species. The basic unit of the hydrous film is therefore assumed to be dimeric comprising of two edge sharing octahedral; oxygen bridging between dimers is assumed to produce relatively stable, probably nonlinear polymer chains (alternatively it may be taken as evidence that the degree of crosslinking is low)- hence the open structure of these hydrated films. The negative charge on the dimer units is assumed to be balanced by electrostatically bound cationic species such as H_3O^+ and Na^+.

Proposed structure of hydrous Au(III) repeat unit

A

$$\left[Au_2O_3(OH)_3(OH_2)_3 \right]^{3-}$$

$$[-Au_2O_3^-(OH)_3\ 3\ H_2O-]_n + 9n\ H^+ + 6ne^- = 2n\ Au + 9n\ H_2O \quad (acid)$$

or

$$[-Au_2O_3^-(OH)_3\ 3\ H_2O-]_n + 6ne^- = 2n\ Au + 9n\ OH^- \quad (base)$$

Hydrous oxide peaks

THE FORMATION AND STABILITY OF HYDROUS OXIDE FILMS ON IRON UNDER POTENTIAL CYCLING CONDITIONS IN AQUEOUS SOLUTION AT HIGH pH
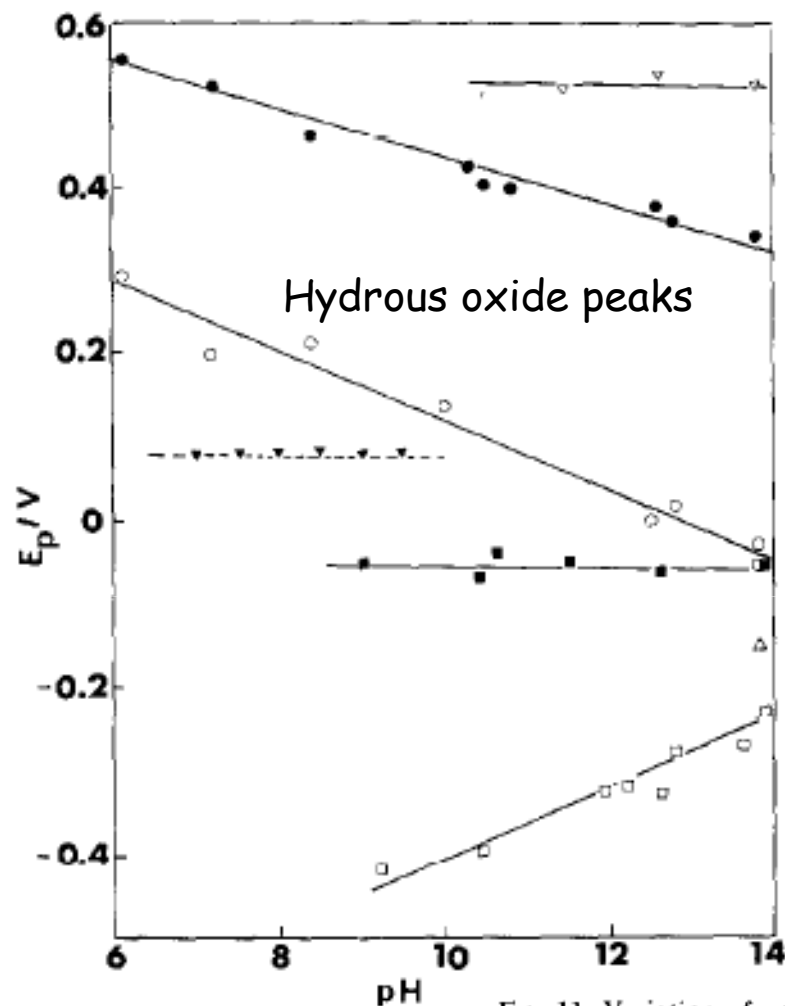
LAURENCE D. BURKE

Chemistry Department, University College, Cork (Ireland)

MICHAEL E.G. LYONS

University of Dublin, Chemistry Department, Trinity College, Dublin 2 (Ireland)
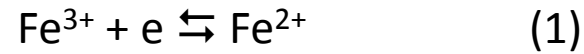
Later more developed analysis of pH shift & hydrolysis effects.

SN shift = 30 mV/dec (wrt RHE)
N shift = zero shift (wrt RHE)

Fig. 11. Variation of voltammetric peak potentials (E_p) for multicycled oxide covered and bright iron electrodes with solution pH. Oxide growth conditions: -0.5 to 1.25 V, 0.35 V s^{-1}, 30 cycles, 1.0 mol dm^{-3} NaOH, 25°C. Solution pH varied using a variety of phosphate (0.2 mol dm^{-3} H$_3$PO$_4$ + NaOH) and borate (0.1 mol dm^{-3} Na$_2$B$_4$O$_7$·10 H$_2$O + 0.9 mol Na$_2$SO$_4$ + NaOH) buffer solutions. ($\triangle$) peak A$_1$; ($\blacksquare$) A$_2$; ($\bullet$) A$_3$; ($\triangledown$) A$_4$; ($\square$) C$_1$; ($\bigcirc$) C$_2$. The potential–pH response of peaks C$_1$, C$_2$, A$_2$, A$_3$ was obtained using multicycled oxide covered electrodes, whereas the response for peaks A$_1$ and A$_4$ was obtained for the bright metal. Also included is the pH response of the passivation potential ($\blacktriangledown$) obtained from slow (10 mV s^{-1}) potentiodynamic measurements on a bright metal electrode.

The approach presented for Au has application in the related but more complex Fe(II)/Fe(III) redox transition in hydrated iron oxide films. If the Fe metal is regarded as relatively inert then the electrode during the course of the Fe(II)/Fe(III) transition (peak A_3) may be regarded as displaying behaviour analogous to that exhibited by a conventional redox electrode such as Pt/Fe^{2+},Fe^{3+} - the Fe(II) and Fe(III) species existing at equilibrium in the hydrous oxyhydroxide film, rather than in the bulk solution. Hence the gel like hydrous oxide layer is analogous to a standard redox electrode in contact with an aqueous solution containing the electro-active ions.
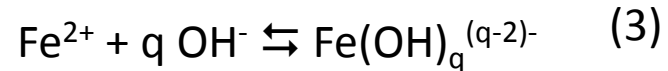
The basic electrode reaction is given by:

$$Fe^{3+} + e \rightleftarrows Fe^{2+} \qquad (1)$$

The corresponding Nernst equation is:

$$E = E^0 - \frac{RT}{F} \ln \frac{a_{Fe^{2+}}}{a_{Fe^{3+}}} \qquad (2)$$

For the ions in the hydrous regions of the film the activity values may be expressed in terms of the stability constants K_2 and K_3 of the hydroxyl species. The latter quantities are obtained by reference to the expressions:

$$Fe^{2+} + q\ OH^- \rightleftarrows Fe(OH)_q^{(q-2)-} \qquad (3)$$

$$Fe^{3+} + r\ OH^- \rightleftarrows Fe(OH)_r^{(r-3)-} \qquad (4)$$

Hence the stability constants are given by:

$$K_2 = \frac{a_{Fe(OH)_q}^{(q-2)-}}{a_{Fe^{2+}} a_{OH^-}^q} \qquad K_3 = \frac{a_{Fe(OH)_r}^{(r-3)-}}{a_{Fe^{3+}} a_{OH^-}^r} \qquad (5)$$

Substitution for the iron (II/III) ion activities using eqn. 5 into the Nernst equation eqn.2 yields on simplification that

$$E = E^0 - \frac{2.303RT}{F}\log\left\{\frac{a_{Fe(OH)_q}^{(q-2)-}}{a_{Fe(OH)_r}^{(q-3)-}}\frac{K_3}{K_2}\right\} - \frac{2.303RT}{F}\log a_{OH^-}^{(r-q)} \quad (6)$$

Noting that

$$a_{OH^-} = K_W / a_{H_3O^+} \quad (7)$$

then eqn.6 becomes:

$$E = E^0 - \frac{2.303RT}{F}\log\left\{\frac{a_{Fe(OH)_q}^{(q-2)-}}{a_{Fe(OH)_r}^{(q-3)-}}\frac{K_3}{K_2}\frac{1}{K_W^{(r-q)}}\right\} - \frac{2.303RT}{F}(r-q)\,pH \quad (7)$$
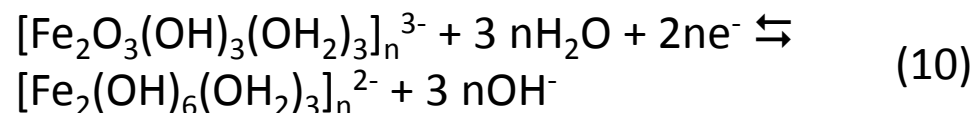
If the activities of the surface species are assumed to be pH independent (this means effectively that the hydrous film does not alter in composition with change in pH) then at 298 K one has:

$$\frac{dE}{dpH} = -\frac{2.303RT}{F}(r-q) = -0.059(r-q)\,V\,/\,pH \quad (8)$$

Experimentally, one finds that dE/d pH $\approx$ 0.088 V and so we assign 0.059 (r-q) = 0.088 and hence determine that r-q $\approx$ 3/2 . This suggests that the charge storage reaction for the iron oxide film should be written as

$$Fe(OH)_r^{(r-3)-} + e^- \leftrightarrows Fe(OH)_q^{(q-2)-} + (3/2) \, OH^- \quad (9)$$
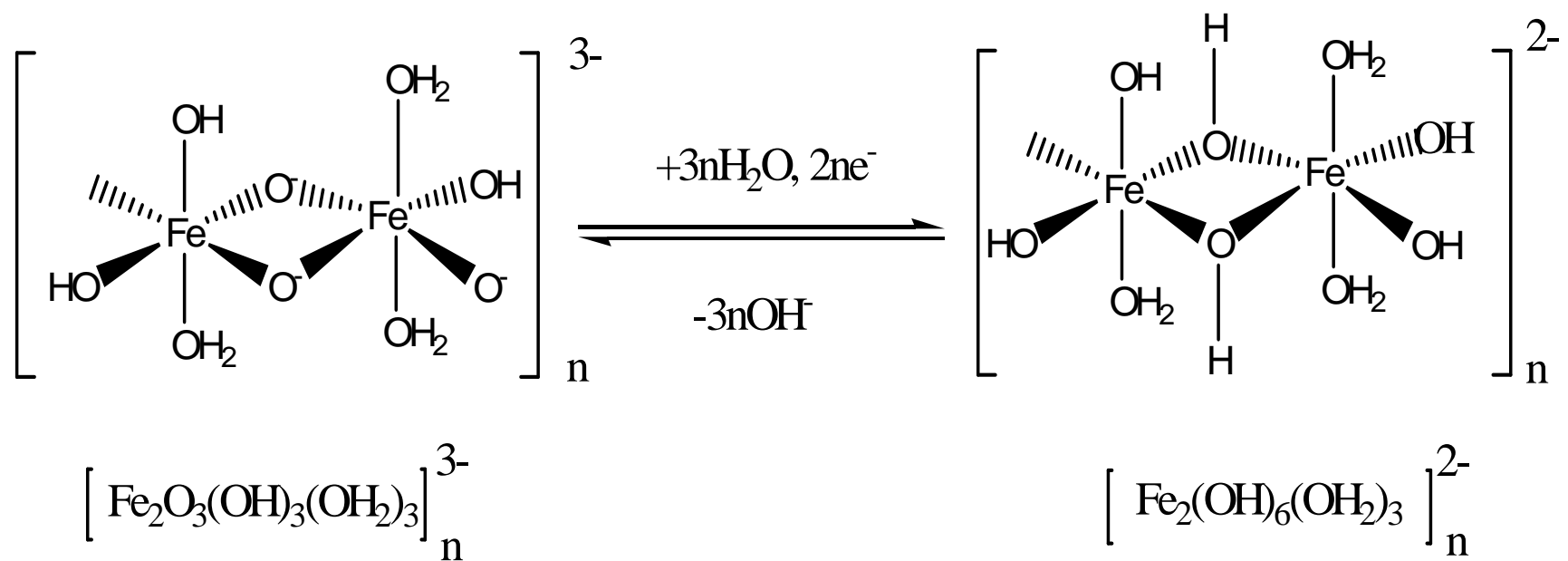
Now comes the important approximation. Since values for r and q cannot be determined explicitly by the present calculation, the assumption must be made that the hydroxyl complex of Fe(III) is similar to that previously proposed for Au(III). The composition of the **oxidized state** is therefore written as $Fe_2(OH)_q^{3-}$ or indeed $[Fe_2O_3(OH)_3(OH_2)_3]^{3-}$. On this basis the net charge storage reaction may be written as:

$$[Fe_2O_3(OH)_3(OH_2)_3]_n^{3-} + 3 \, nH_2O + 2ne^- \leftrightarrows$$
$$[Fe_2(OH)_6(OH_2)_3]_n^{2-} + 3 \, nOH^- \quad (10)$$
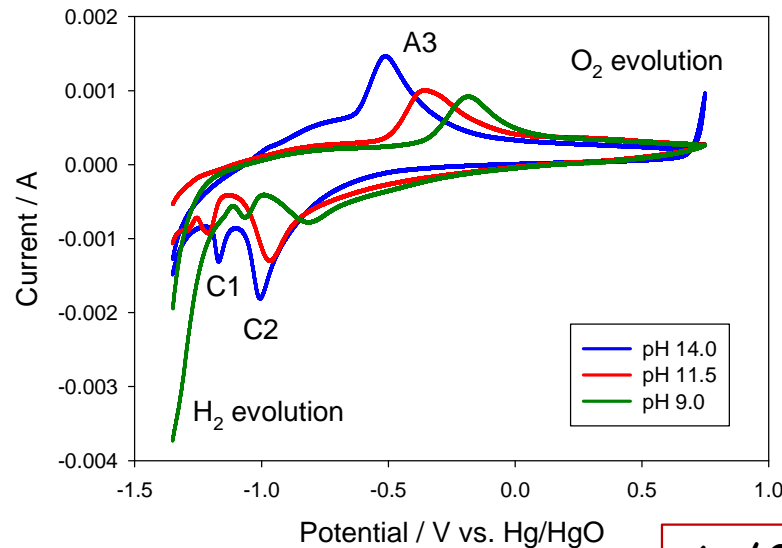
The oxidized and reduced forms may be represented in structural terms in scheme B.

Although the structures proposed here have not been derived in a rigorous manner, they provide a reasonable interpretation of the behaviour of the hydrous layer- even apart from the unusual pH effects.

$$\left[Fe_2O_3(OH)_3(OH_2)_3 \right]_n^{3-}$$

$$+3nH_2O,\ 2ne^-$$

$$-3nOH^-$$

$$\left[Fe_2(OH)_6(OH_2)_3 \right]_n^{2-}$$
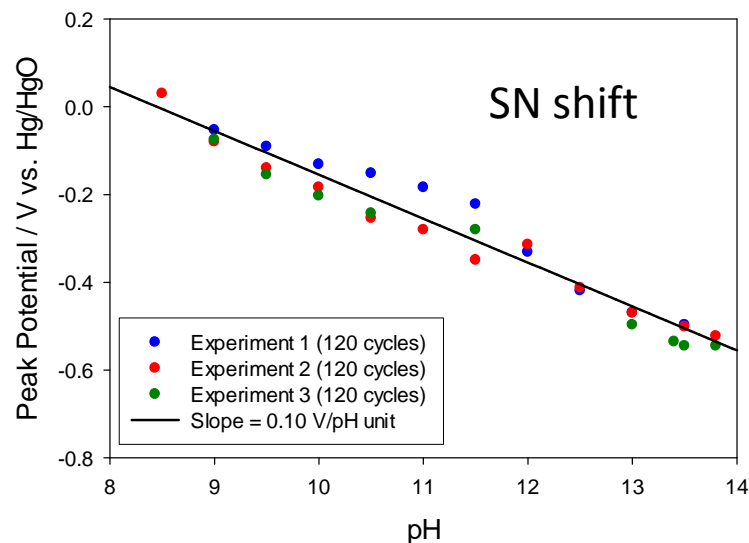
B

Redox switching chemistry: hydrous oxide Layer, Mixed conduction mechanism: ion/electron transfer.
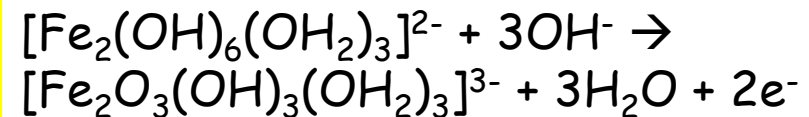

A_3/C_2

Redox switching involves topotactic charge storage reactions in open hydrous oxide layer which Behaves as ion exchange membrane.
Hydrated counter/co-ions (M^+, H^+, OH^- assumed present in pores and channels of film to balance negative charge on polymer chain.
Equivalent circuit model: dual/multi- rail Transmission Line as done for ECP films..

Fe(II)   Fe(II) Reduced form transparent

$$[Fe_2(OH)_6(OH_2)_3]^{2-} + 3OH^- \rightarrow$$
$$[Fe_2O_3(OH)_3(OH_2)_3]^{3-} + 3H_2O + 2e^-$$

Fe(III)   Fe(III) Oxidized form yellow-green
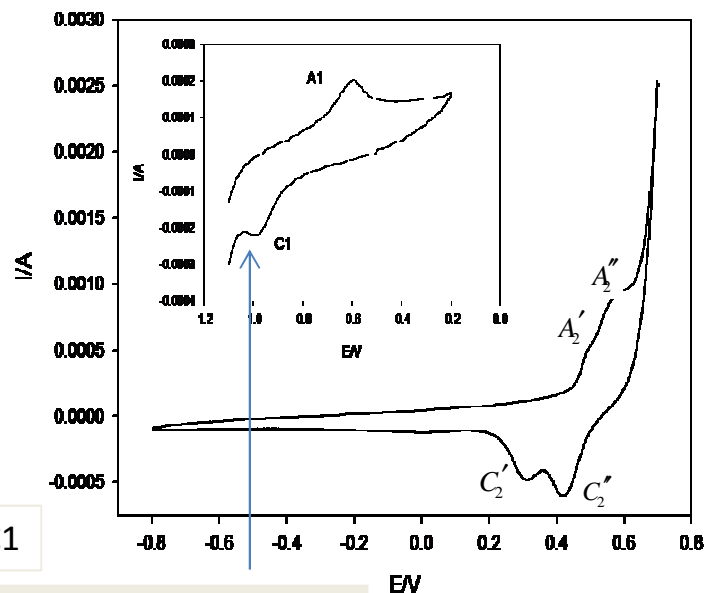
Super-Nernstian Redox Potential vs pH shift related to hydrolysis effects in hydrous layer yielding anionic oxide structures.

L.D. Burke, M.E.G. Lyons, E.J.M.O'Sullivan, D.P. Whelan J. Electroanal. Chem., 122 (1981) 403.
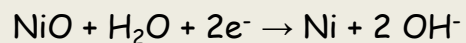
M. E. G. Lyons, R. L. Doyle, *Phys. Chem. Chem. Phys.* **2011**, *13*, 21530.

Surface redox chemistry of Ni electrodes in Aqueous base solution.
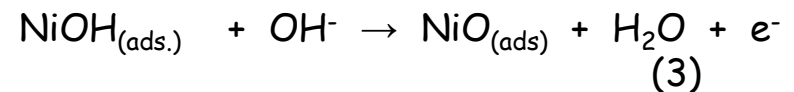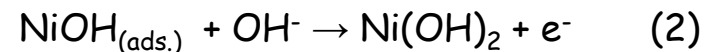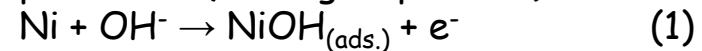
It is almost universally agreed that the lower anodic peak observed in the potential region between -0.6 V and – 0.8 V (vs Hg/HgO) is principally associated with the oxidation of metallic Ni(0) to Ni(II) species. There has been historically some disagreement about the nature of the Ni(II) oxide species formed at this potential with, for example, Makrides proposing the production of NiO and $Ni(OH)_2$, while Okuyama suggested that the oxide film in this potential region was non-stoichiometric, consisting of NiO and Ni_3O_4.
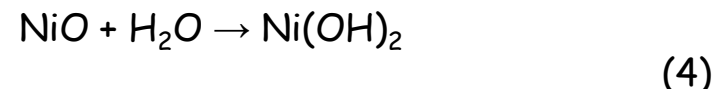
By analogy with the situation found at low potentials for Fe in base we can visualize the following sequence of reactions at low potentials (leading to peak A1) :

$$Ni + OH^- \rightarrow NiOH_{(ads.)} + e^- \qquad (1)$$

$$NiOH_{(ads.)} + OH^- \rightarrow Ni(OH)_2 + e^- \qquad (2)$$

$$NiOH_{(ads.)} + OH^- \rightarrow NiO_{(ads)} + H_2O + e^- \qquad (3)$$
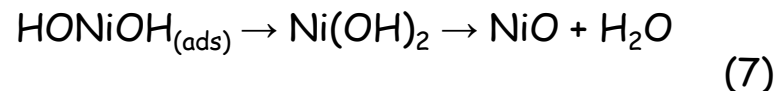
The overall interfacial reaction resulting in Ni(II) film formation may be more complex than that outlined above due to a variety of other possible reactions. For instance hydroxylation reactions such as:

$$NiO + H_2O \rightarrow Ni(OH)_2$$
$$\qquad (4)$$

will result in the conversion of oxy to hydroxy species in the outer region of the surface layer.

Peak C1

$NiO + H_2O + 2e^- \rightarrow Ni + 2\ OH^-$
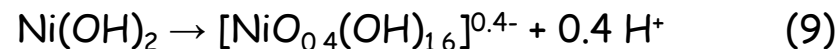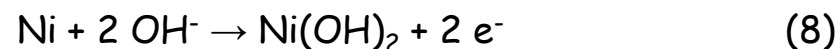
Uncycled Ni electrode 1M base, 50 mV/s

Place exchange processes can result in an increase in the thickness of the surface layer. The latter type of growth process has been proposed to involve a rapid place exchange step followed by a rate determining Temkin discharge of OH^- ions onto sites in which a surface iron atom is already attached to a hydroxyl group displaced into the first layer beneath the surface, viz:

$$NiOH_{(ads)} \rightarrow HONi \quad (fast) \qquad (5)$$

$$HONi + OH^- \rightarrow HONiOH_{(ads)} \quad (slow\ rds) \quad (6)$$

$$HONiOH_{(ads)} \rightarrow Ni(OH)_2 \rightarrow NiO + H_2O \qquad (7)$$

One should note that with a non noble metal such as Nickel or iron, the aforementioned surface processes are likely to be accompanied by film thickening (i.e. place exchange reactions)even at quite low potentials.
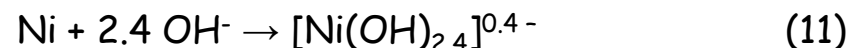
More recently the complex nature of the film even at these low potentials has been emphasised. Based on the variation of the voltammetric peak potential with changes in pH in alkaline solution (typically the redox potential for the anodic reaction decreases by ca. 13 mV per unit change in pH with respect to a pH independent reference electrode), Burke and Twomey proposed that both oxidation and hydrolysis processes were operative in this region, leading to the formation of a species with anionic character which was tentatively assigned, for purposes of rationalization, the formula $Ni(OH)_{2.4}^{0.4-}$. The reaction sequence proposed by the latter workers was:

$$Ni + 2\ OH^- \rightarrow Ni(OH)_2 + 2\ e^- \qquad (8)$$

$$Ni(OH)_2 \rightarrow [NiO_{0.4}(OH)_{1.6}]^{0.4-} + 0.4\ H^+ \qquad (9)$$

Note that eqn.9 may be represented as a hydroxide ion adsorption step since the reaction occurs in alkaline solution:

$$Ni(OH)_2 + 0.4\ OH^- \rightarrow Ni(OH)_{2.4}^{0.4-} \qquad (10)$$

Hence in very simple terms the net anodic reaction corresponding to peak A_1 can be represented as:

$$Ni + 2.4\ OH^- \rightarrow [Ni(OH)_{2.4}]^{0.4-} \qquad (11)$$

Hydrous oxide growth via CPM : Multicycled Ni electrode, 1.0 M NaOH.
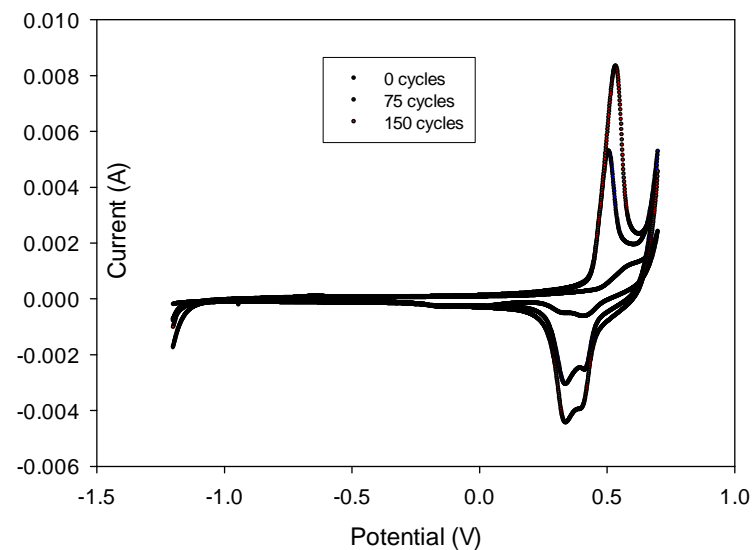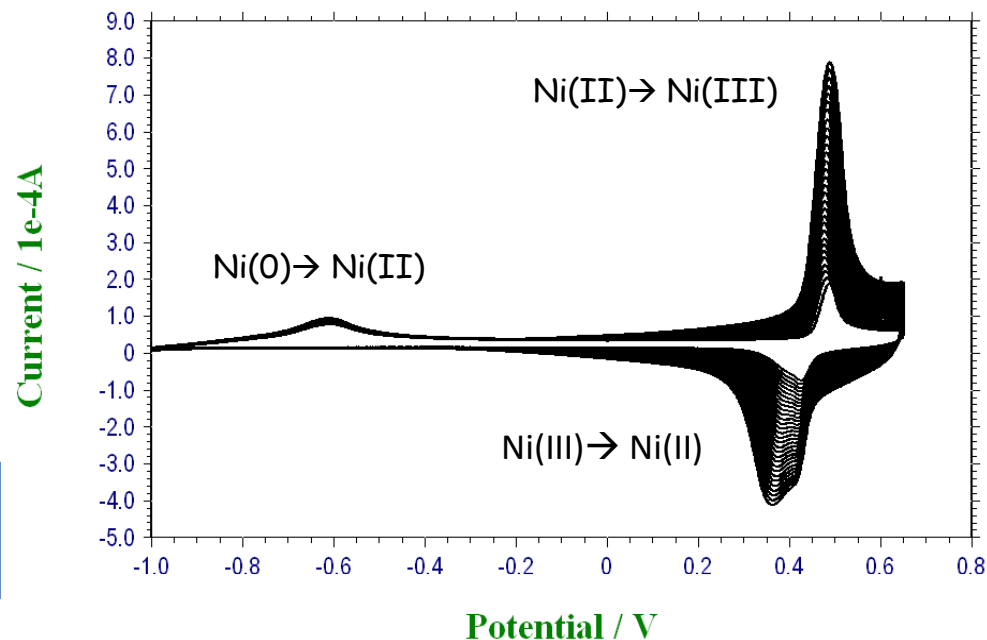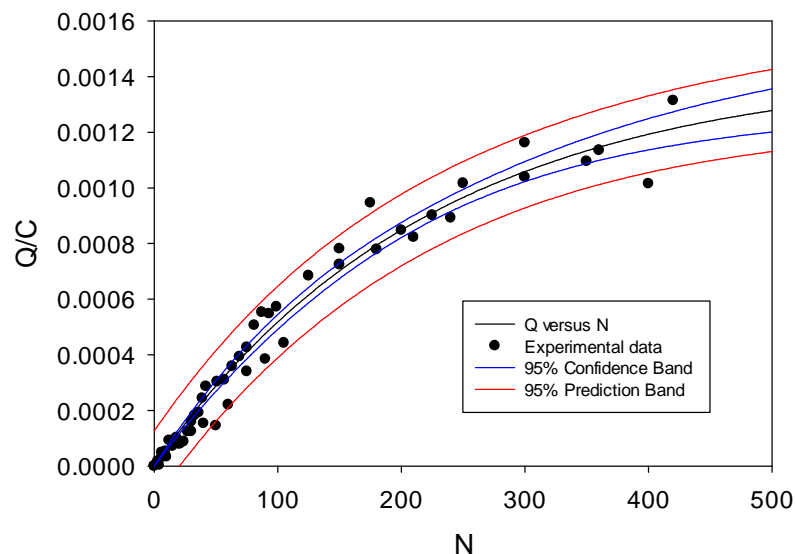
Typical voltammetric response recorded for a hydrous $Ni(OH)_2$ thin film growth on Ni support electrode grown in aqueous 1.0 M NaOH for N = 30 cycles at 150 mV/s between limits -1.45-0.65 V vs Hg/HgO.
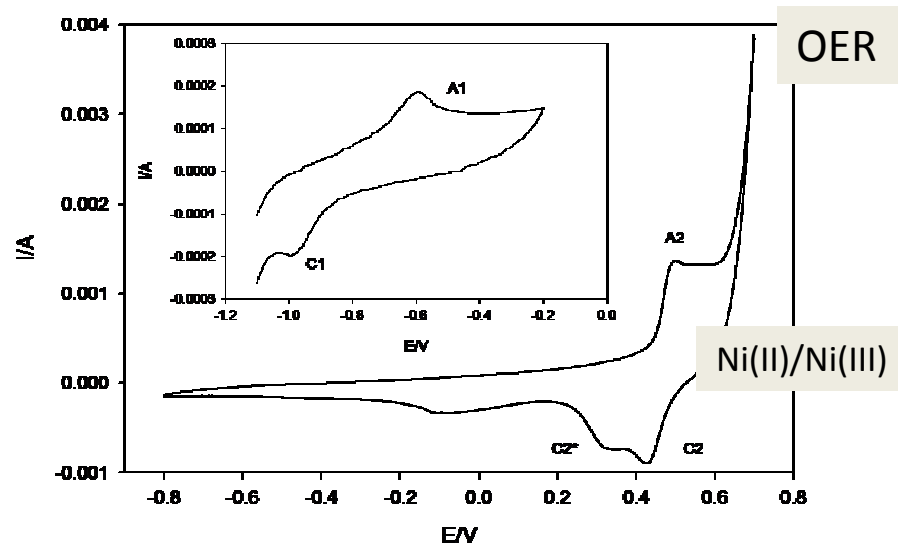
$Q=a(1-\exp(-bN))$
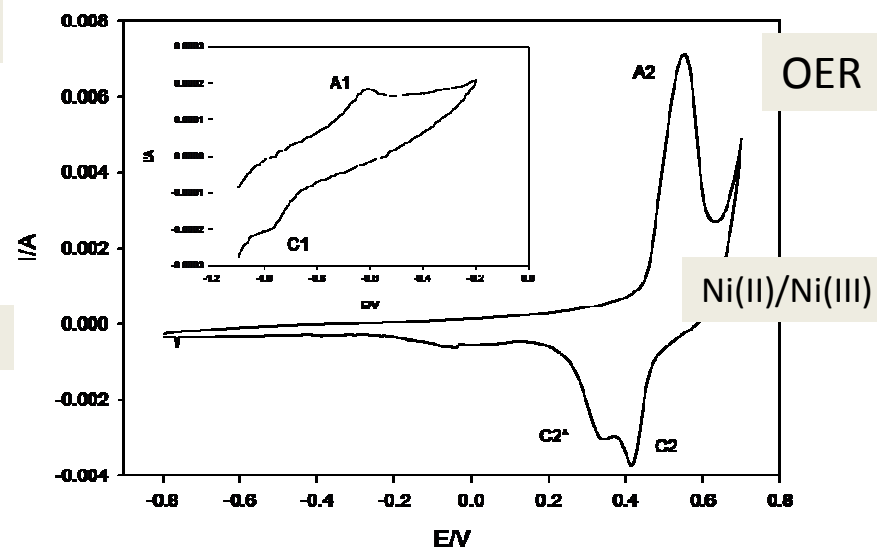
R = 0.9869, R² = 0.9739
a = $0.0014 \pm 7.43 \times 10^{-5} C$
b = 0.045 ± 0.0004 cycle^{-1}

Typical cyclic voltammetric response recorded for multi-cycled (N = 30 cycles) Ni electrode in 1.0 M NaOH. Sweep rate, 50 mV/s. Inset shows the peak set labeled A_1 and C_1 recorded at low potentials prior to the onset of active hydrogen evolution at ca. – 1.08 V (vs Hg/HgO).

Typical cyclic voltammetric response recorded for multi-cycled (N = 300 cycles) Ni electrode in 1.0 M NaOH. Sweep rate, 50 mV/s. Inset shows the peak set labeled A_1 and C_1 recorded at low potentials prior to the onset of active hydrogen evolution at ca. – 1.08 V (vs Hg/HgO).
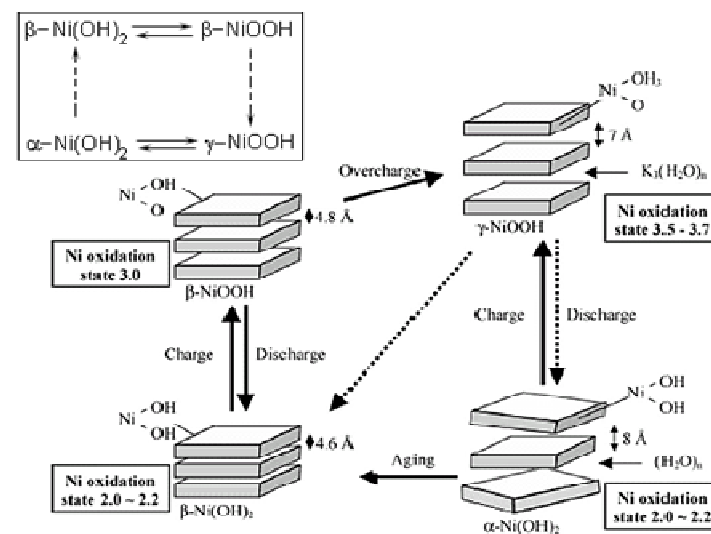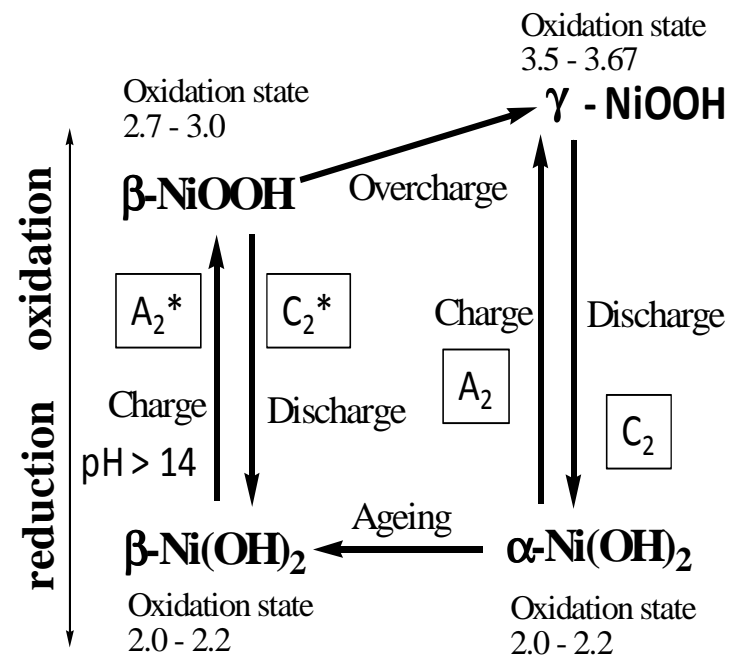
Lyons, Russell, O'Brien, Doyle, Godwin, Brandon, Int. J. Electrochem. Sci, 2012.

Nickel foil electrodes grown with electrochemically cycled nickel oxyhydroxide Films in 1 M NaOH .

The upper peaks observed in the potential region 0.3 to 0.6 V (vs Hg/HgO) are greatly enhanced when the Ni support electrode is subjected to a repetitive potential sweep. These are labeled the main charge storage or redox switching peaks. However only peak A_2 and the cathodic doublet peaks C_2 and C_2* may be observed when the electrode surface is coated with a thick hydrous oxide layer.

The interfacial redox chemistry of the multicycled nickel oxide electrode in aqueous alkaline solution can be readily understood in terms of the Bode scheme of squares .
Here the redox switching behaviour of electrochemically generated nickel oxide films was rationalized in terms of four phases as outlined across.
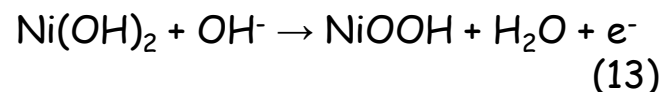
The discharged or reduced $Ni(OH)_2$ material can exist either as a largely anhydrous phase designated as $\beta - Ni(OH)_2$ (denoted β-Ni(II)) or as a hydrated phase denoted as α-$Ni(OH)_2$ (in short represented as α-Ni(II)). Oxidation of the β-Ni(II) material is envisaged to produce a phase referred to as β-NiOOH or β-Ni(III). In contrast oxidation of the α-Ni(II) material produces γ-Ni(III) or γ-NiOOH. Hence one expects two distinct redox transitions : β(II)/β(III) and α(II)/γ(III). The corresponding redox peaks are designated A_2^*/C_2^* and A_2/C_2 respectively. Burke and Twomey designated the latter peak sets as A_A/C_A and A_H/C_H respectively. We note from the Bode schemethat upon ageing, especially in more concentrated alkali solution, the α-$Ni(OH)_2$ can dehydrate and re-crystallize as β-$Ni(OH)_2$. Furthermore, upon overcharge (which occurs at more elevated potentials) β-NiOOH can convert to γ-NiOOH. The non-stoichiometric nature of both the discharged and charged material is indicated by the average oxidation state of Ni in each phase as indicated in the structural representation of the various phases presented in the Bode scheme
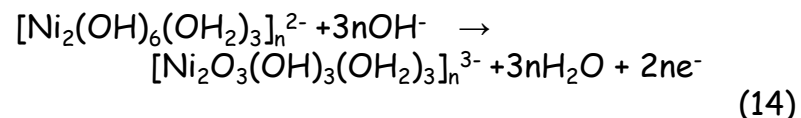
It is important to note that while there is a general acceptance for the general features of the Bode scheme, one must understand that it is inappropriate to think about the formation of a compound or a phase with definite stoichiometry during the chemically complex $Ni(OH)_2$/NiOOH transformation. Instead the four phases mentioned in the Bode scheme should be considered as the limiting forms of the divalent and trivalent materials – the actual composition of the oxide at a given potential depending on a range of factors including its history, method of preparation, degree of hydration, defect concentration etc.

In simple terms peaks A_2^*/C_2^*, can be attributed to the following Ni(II)/Ni(III) redox transformation:

$$Ni(OH)_2 + OH^- \rightarrow NiOOH + H_2O + e^-$$
$$(13)$$
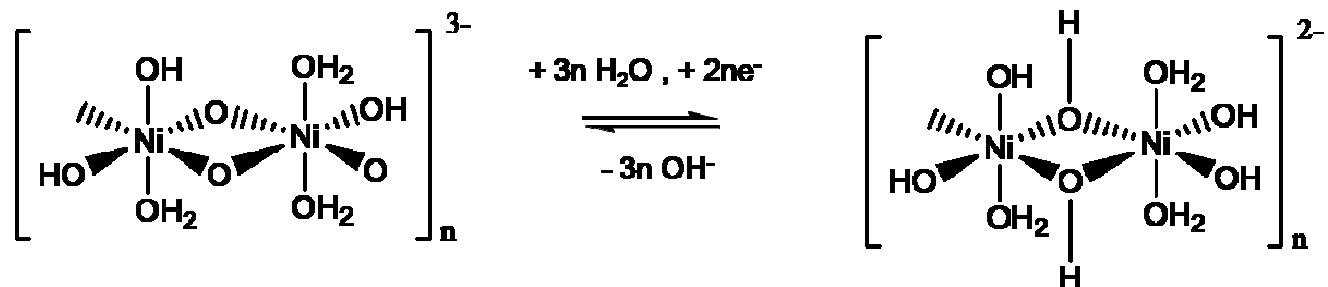
As noted previously for Iron, the potential for an ideal oxide electrode system in aqueous solution at 25°C, decreases with increasing pH by ca. 59 mV/pH unit, with respect to a pH independent reference electrode such as the NHE or the saturated calomel electrode (SCE). Such a shift in potential with pH, is referred to as a Nernstian shift, since it is predicted by the Nernst equation. It should be noted that if the reference electrode is pH dependent, such as the reversible hydrogen electrode (RHE) or the Hg/HgO electrode, no potential pH shift will be observed, since the potential of this type of electrode also alters by ca. 59 mV per unit change in pH at 25°C. Furthermore, Burke and Lyons have discussed super-Nernstian shifts that have been observed for various hydrous oxide systems – in these cases the potential/pH shift differs from the expected 0.059V/pH unit at 25^{0}C.
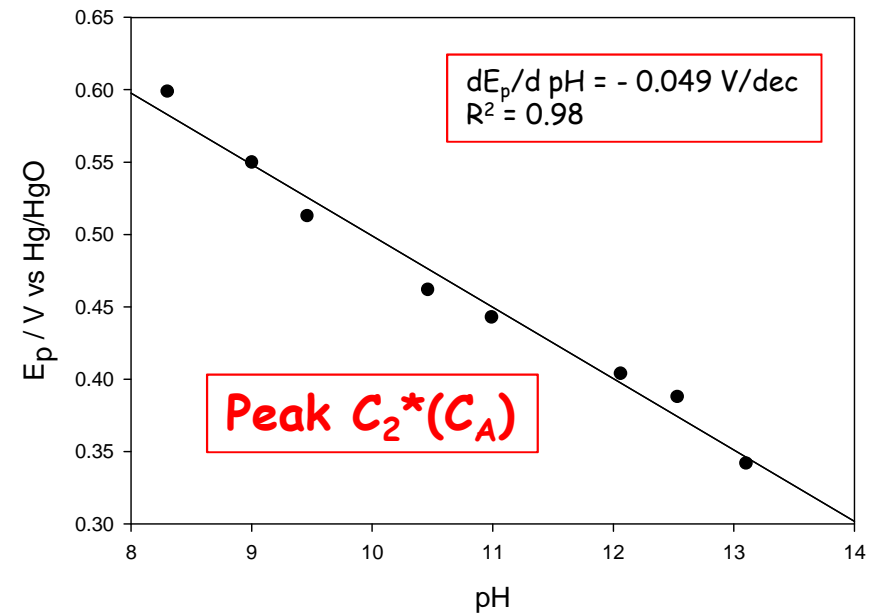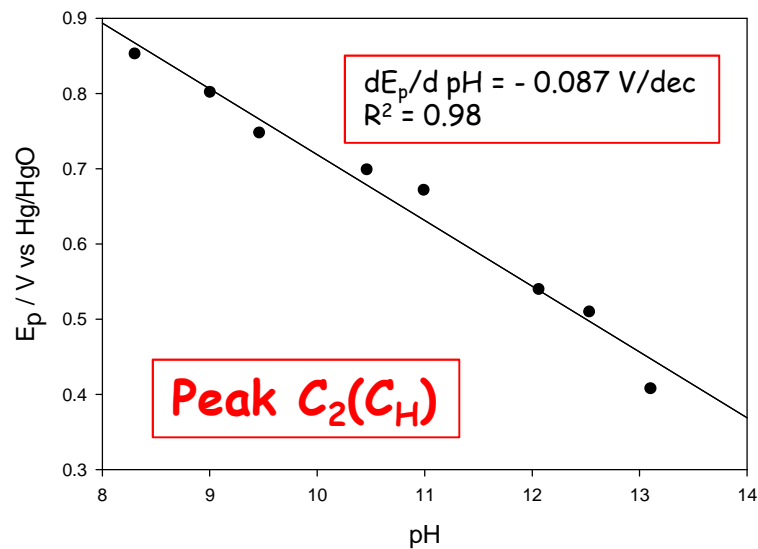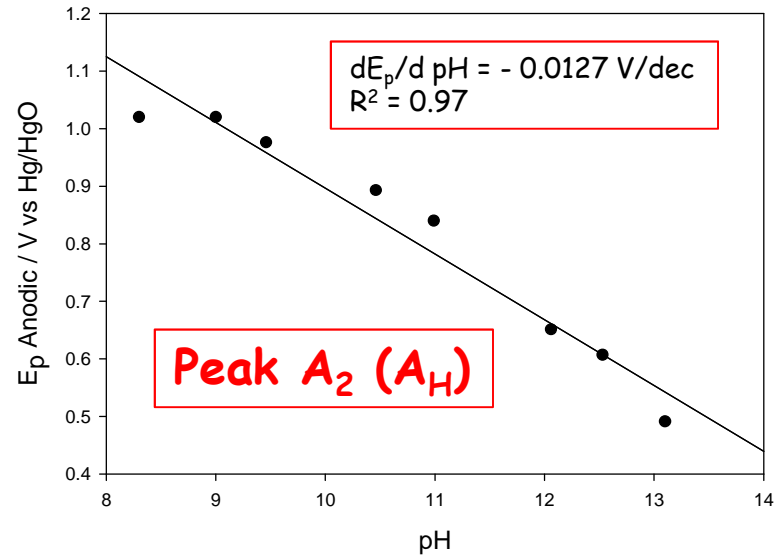
Thus, a zero potential shift (with respect to a pH dependent reference electrode) implies that both the reactants and the product possess the same net charge. A positive potential shift with pH, is indicative of an oxidised state that is more positive than the reduced state, whereas the converse is true in the case of an observed negative potential/pH shift.

However, it was shown that the anhydrous $A_2*/C*_2$ peaks exhibit a regular Nernstian shift whereas the hydrous counterparts A_2/C_2 exhibit the characteristic of a hydrous or hyper-extended oxide [38], i.e. a super-nernstian potential-pH shift, which typically has the value of dE/dpH = -2.303(3RT/2F) = -0.088V/pH unit at T = 298 K. Accordingly, by analogy with a scheme produced by Burke and Whelan for redox switching of iridium oxide films, it has been proposed that the main redox switching reaction may be written as:

$[Ni_2(OH)_6(OH_2)_3]_n^{2-}$ +3nOH$^-$ $\rightarrow$
$\qquad$ $[Ni_2O_3(OH)_3(OH_2)_3]_n^{3-}$ +3nH$_2$O + 2ne$^-$

$$(14)$$

corresponding to an Ni(II)/Ni(III) redox transition in a polymeric microdispersed hydrous oxide layer. This redox switching reaction is illustrated schematically below.
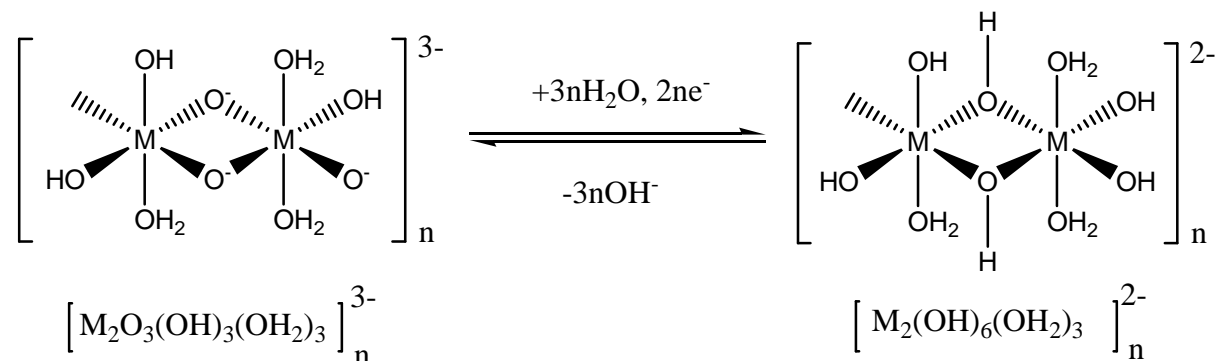
Multicycled Ni wire electrode (N = 120 cycles)
Coated with nickel oxyhydroxide film grown in 1 M
NaOH and redox behaviour examined in solutions
Of varying pH.

$dE_p/d\,pH = -\,0.0127$ V/dec
$R^2 = 0.97$

Peak A_2 (A_H)

$dE_p/d\,pH = -\,0.049$ V/dec
$R^2 = 0.98$

Peak C_2*(C_A)

$dE_p/d\,pH = -\,0.087$ V/dec
$R^2 = 0.98$

Peak C_2(C_H)

Ian Godwin 2013

$$M^{II}(OH)_r^{(r-3)-} + e^- \leftrightarrows M^{III}(OH)_q^{(q-2)-} + (3/2)\, OH^-$$
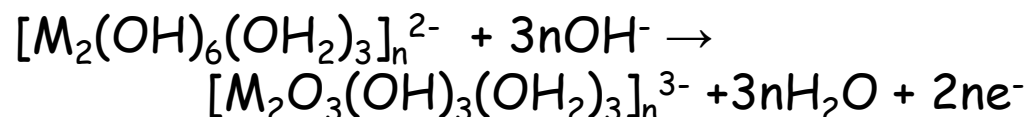
$$dE/dpH = -0.090\ V = -0.06\,(r-q)\ V \qquad r-q \approx 1.5$$

$$\left[M_2O_3(OH)_3(OH_2)_3 \right]_n^{3-} \qquad\qquad \left[M_2(OH)_6(OH_2)_3 \right]_n^{2-}$$

M = Fe, Ni

$$[M_2(OH)_6(OH_2)_3]_n^{2-} + 3nOH^- \rightarrow$$
$$[M_2O_3(OH)_3(OH_2)_3]_n^{3-} + 3nH_2O + 2ne^-$$
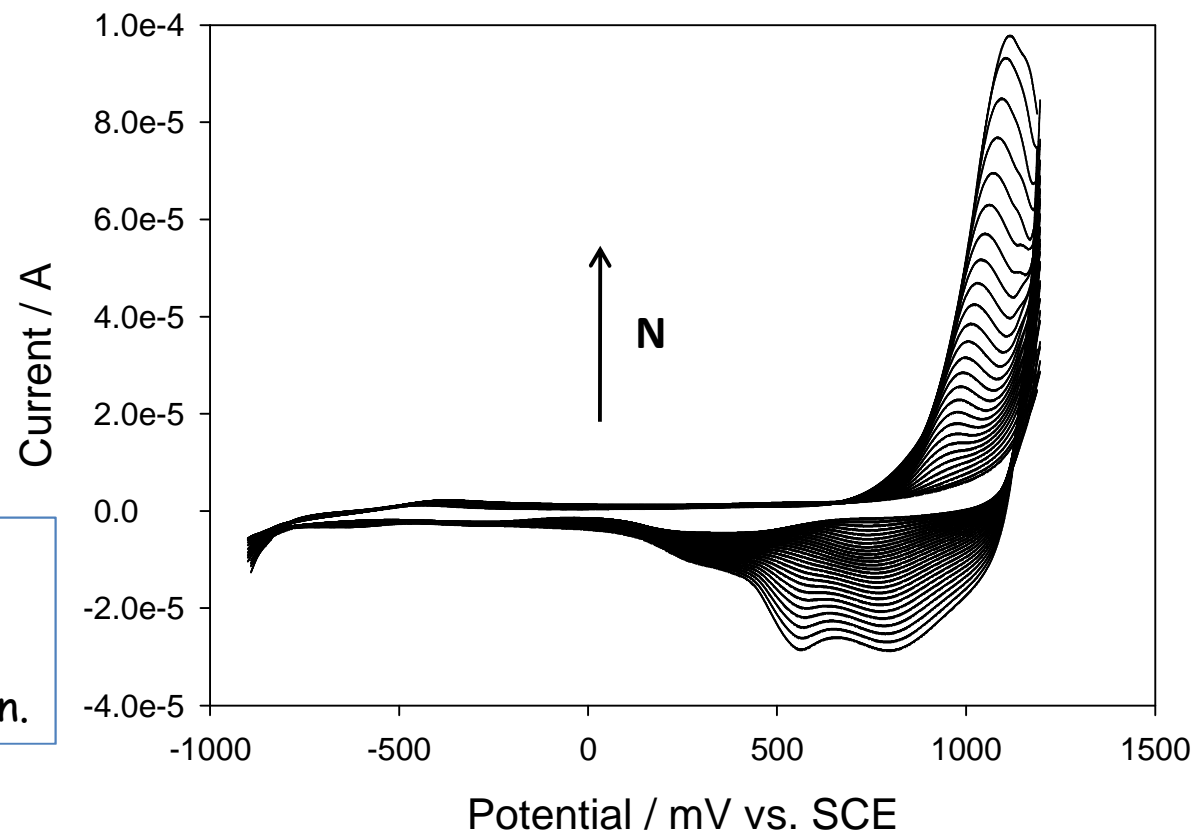
Assume that oxidized form of hydrous metal oxide has same composition as oxidized form of hydrous gold oxide.

Redox switching in hydrous oxide layer involves a rapid topotactic reaction involving hydroxide ion ingress and solvent egress
at the oxide/solution interface, and electron injection at the metal/oxide interface.
Also involves motion of charge compensating cations through film.
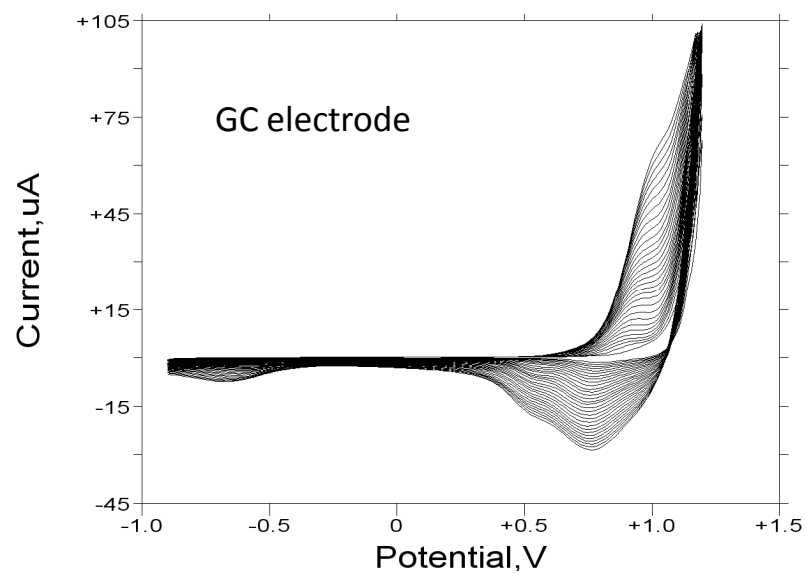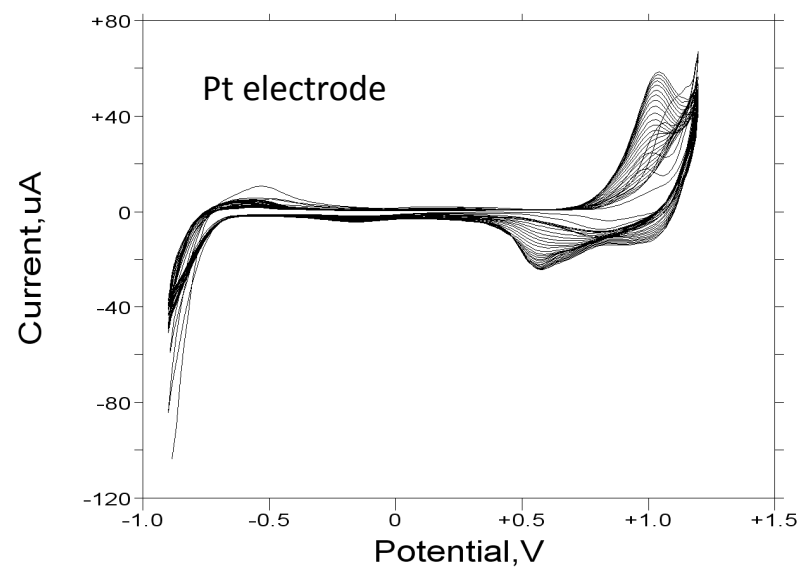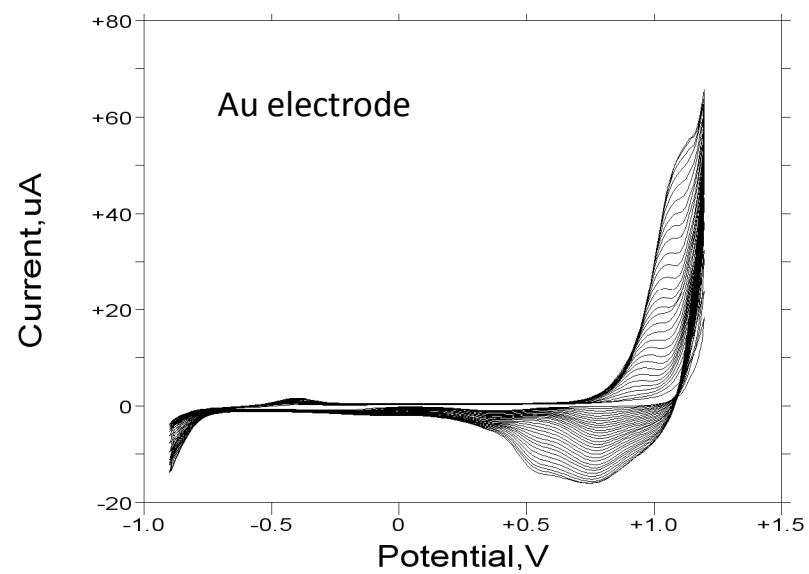
Electro-precipitated Nickel Oxy-hydroxide films : Au support.
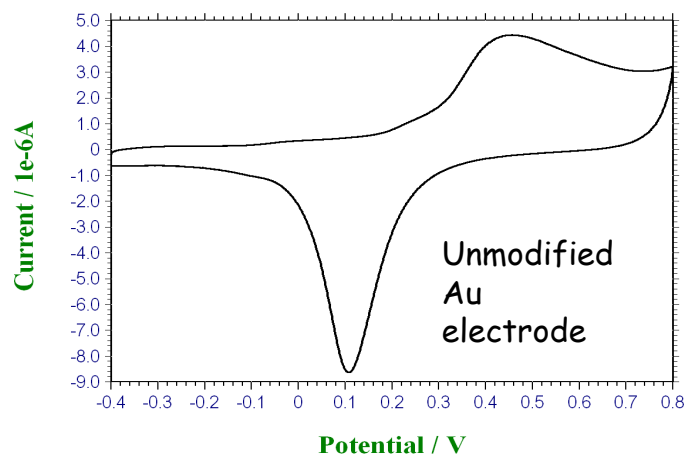
CPM technique is
Also useful for
Oxide formation
Via electro-precipitation.
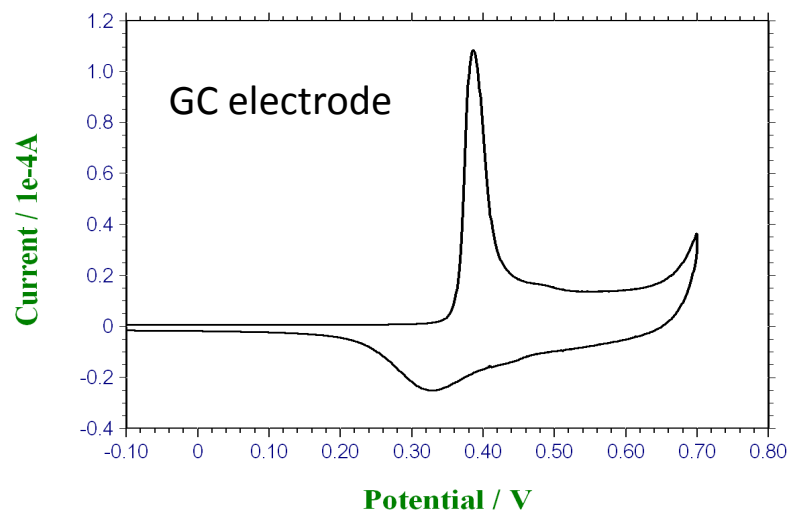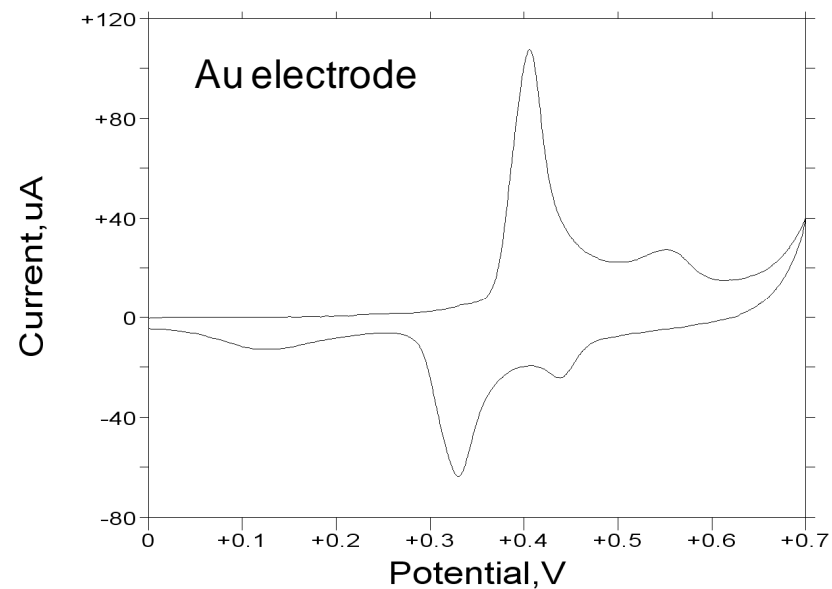
Electro-deposition solution: aqueous solution of 0.1 M $NiSO_4$, 0.1 M sodium acetate, 1 mM KOH .
Electro-deposition method: Cyclic Potential Multicycling (CPM) ;Gold substrate, 30 cycles between -0.9 V & 1.2 V vs. SCE at 50 mV/s.

Au electrode

Pt electrode
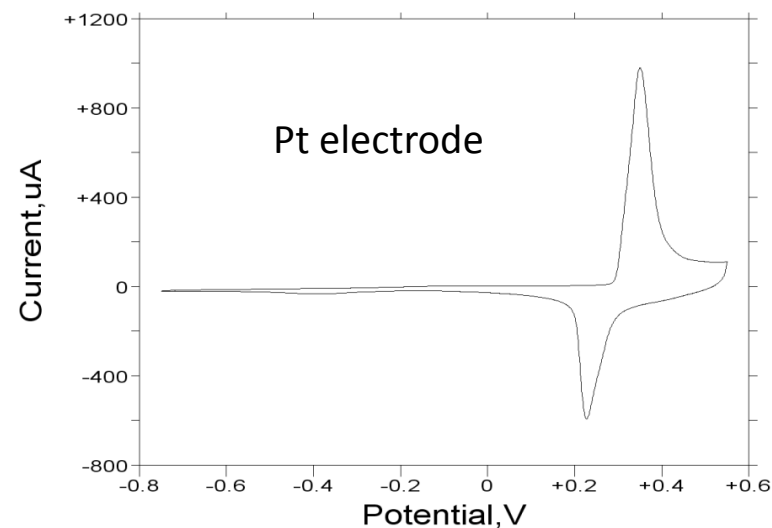
GC electrode

Cyclic voltammogram recorded for a polycrystalline gold electrode modified with a thin nickel hydroxide film (30 growth cycles) in 1.0 M NaOH. Sweep rate, 40 mV/s. Potentials are quoted with respect to Hg/HgO reference electrode (1 M OH⁻)

Cyclic voltammogram recorded for a glassy carbon electrode modified with a thin nickel hydroxide film (30 growth cycles) in 1.0 M NaOH. Sweep rate, 40 mV/s. Potentials are quoted with respect to Hg/HgO reference electrode (1 M OH⁻).
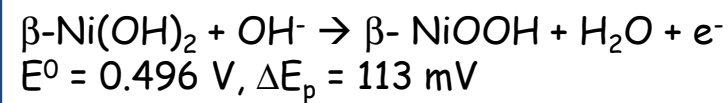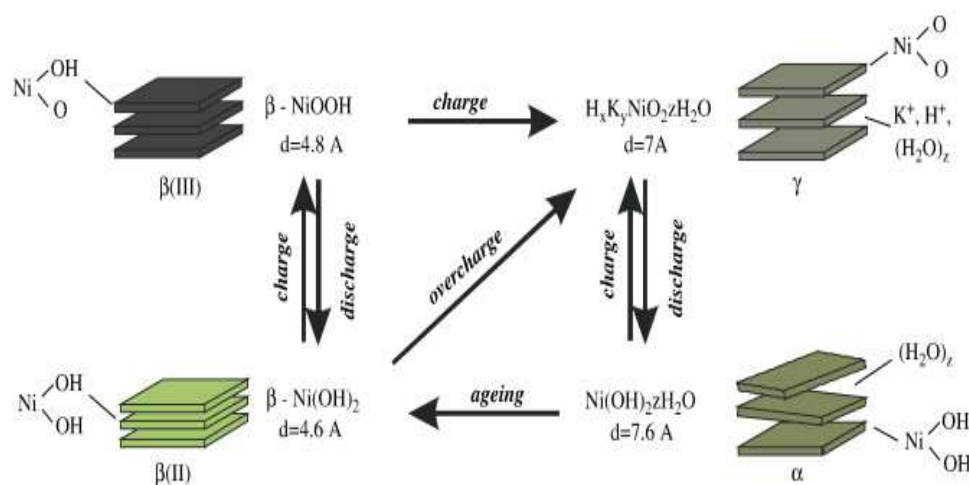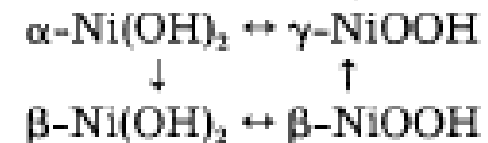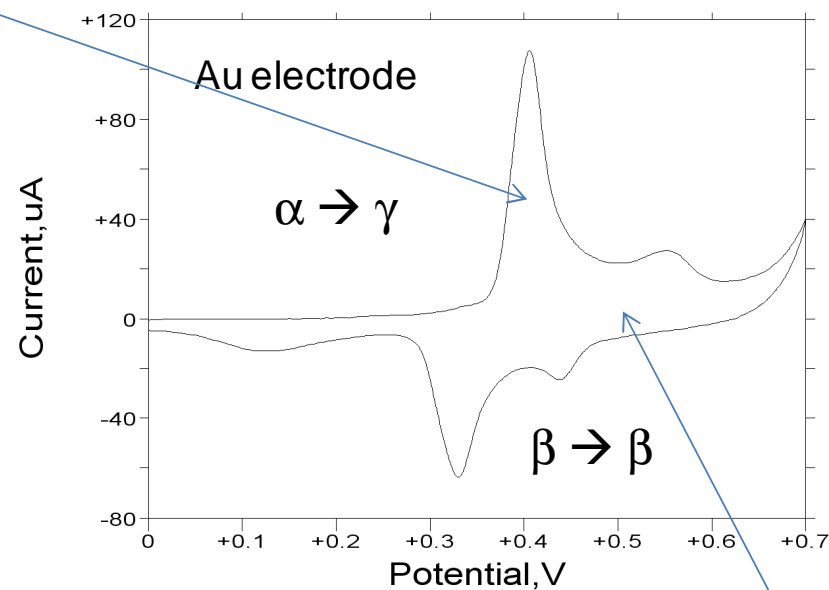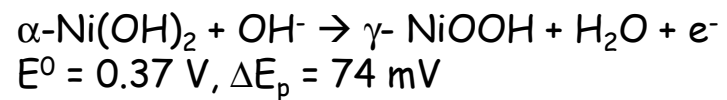
Cyclic voltammogram recorded for a Pt electrode modified with a thin nickel hydroxide film (30 growth cycles) in 1.0 M NaOH. Sweep rate, 40 mV/s. Potentials are quoted with respect to Hg/HgO reference electrode (1 M OH⁻).

Electro-precipitated Ni(OH)$_2$

α-Ni(OH)$_2$ + OH$^-$ → γ- NiOOH + H$_2$O + e$^-$
E^0 = 0.37 V, ΔE$_p$ = 74 mV

α-Ni(OH)$_2$ ↔ γ-NiOOH
↓ ↑
β-Ni(OH)$_2$ ↔ β-NiOOH

β-Ni(OH)$_2$ + OH$^-$ → β- NiOOH + H$_2$O + e$^-$
E^0 = 0.496 V, ΔE$_p$ = 113 mV
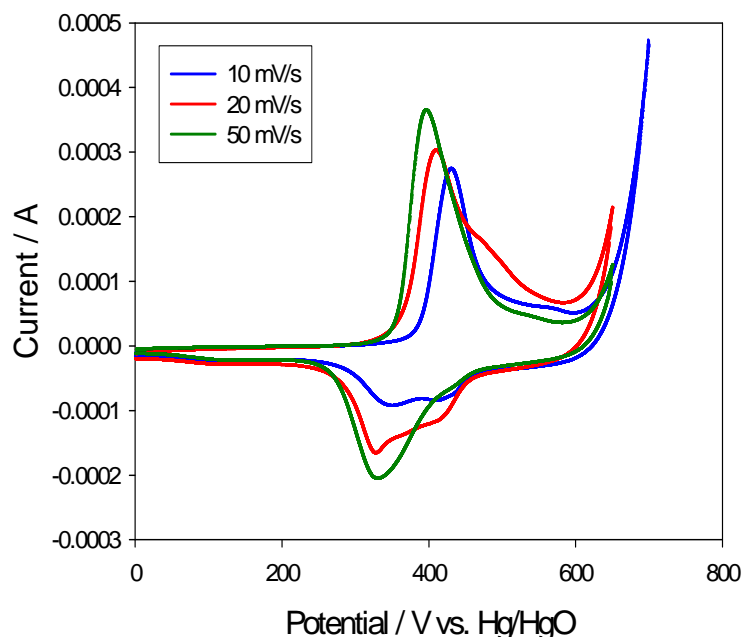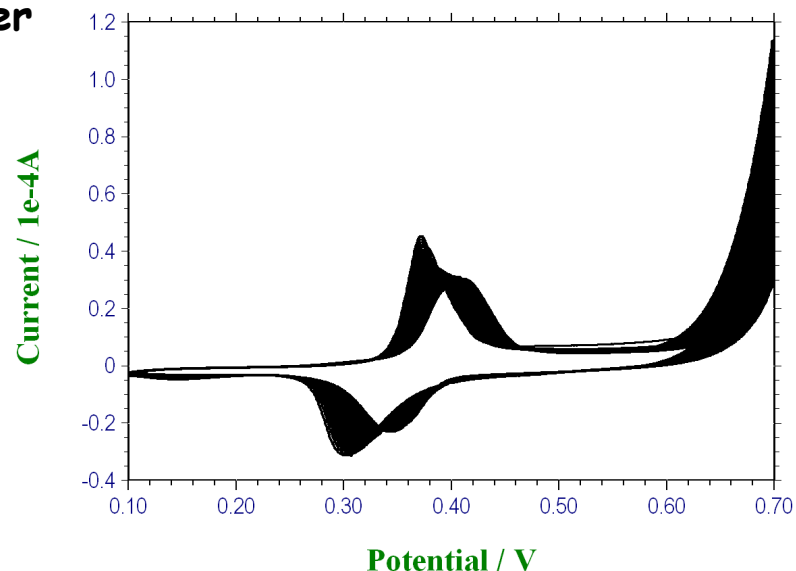
Bode Square Scheme

Temporal effects on Nickel oxyhydroxide layer redox chemistry.

Typical voltammetric response recorded for an electroprecipitated nickel oxide film deposited on a polycrystalline gold substrate subjected to slow multicycling (sweep rate 10 mV/s) between 0.1 and 0.7 V (vs Hg/HgO) in 5.0 M NaOH.
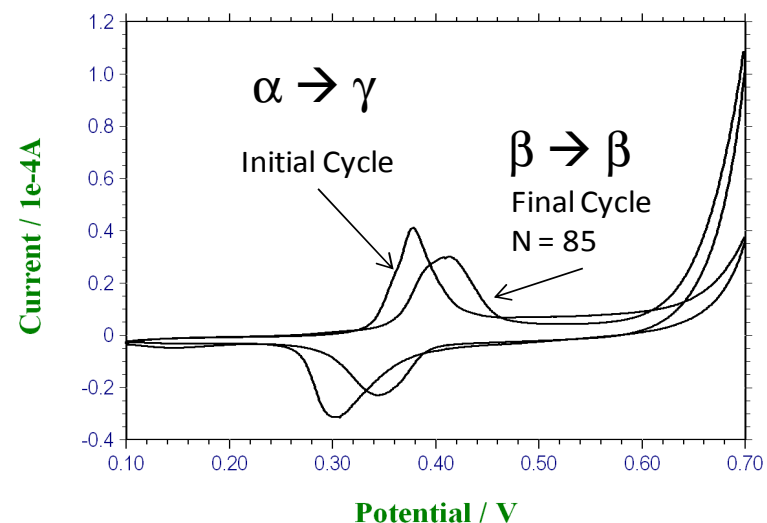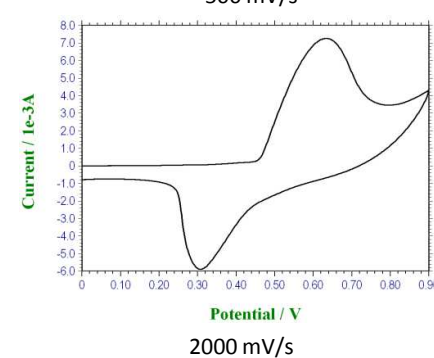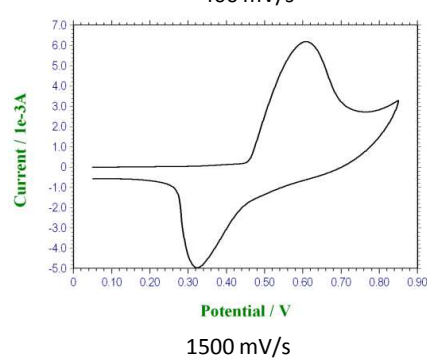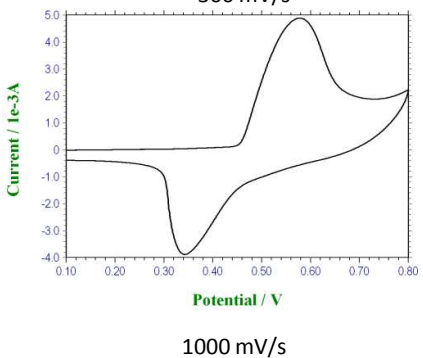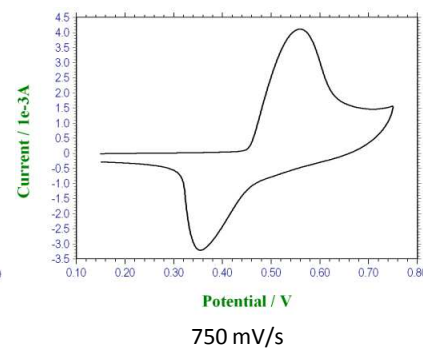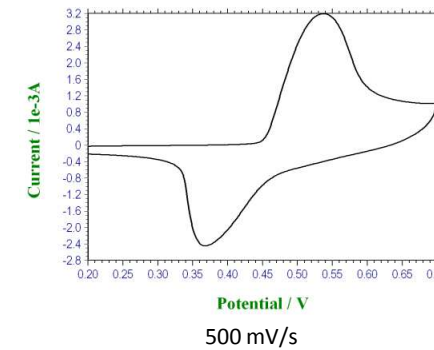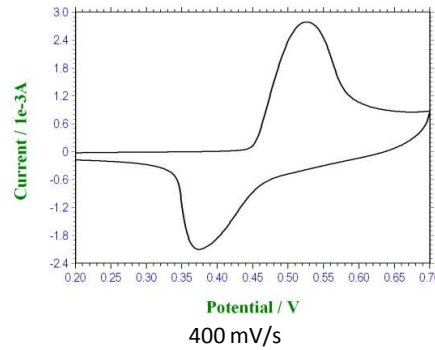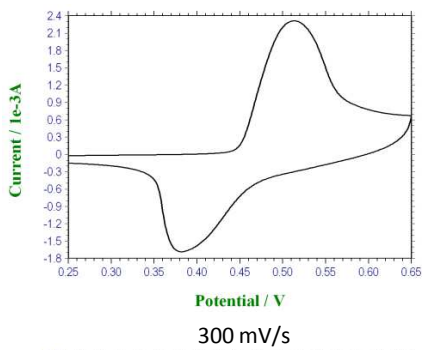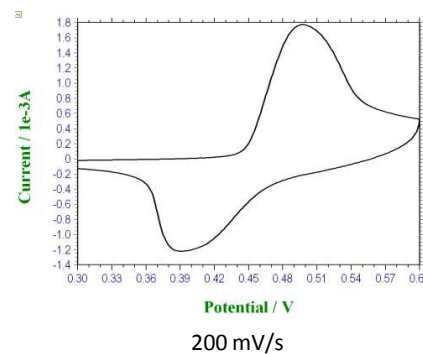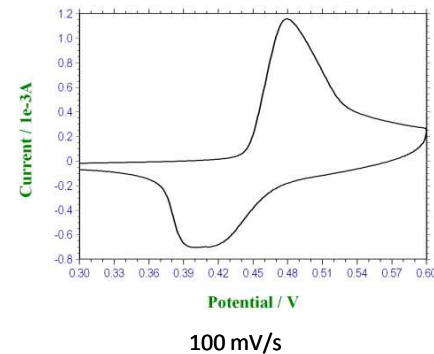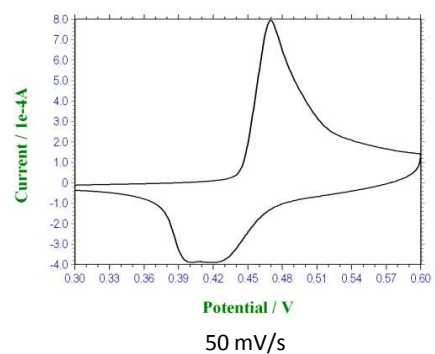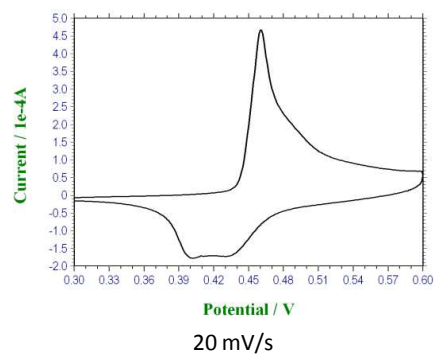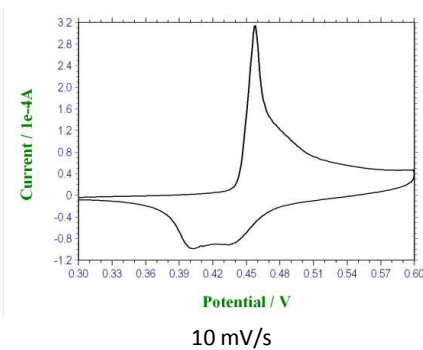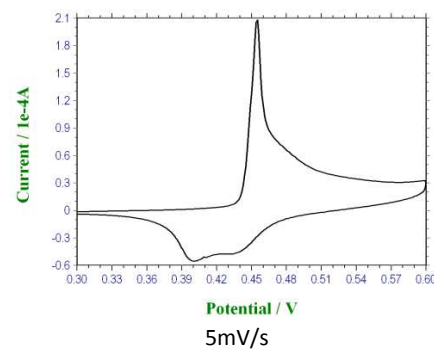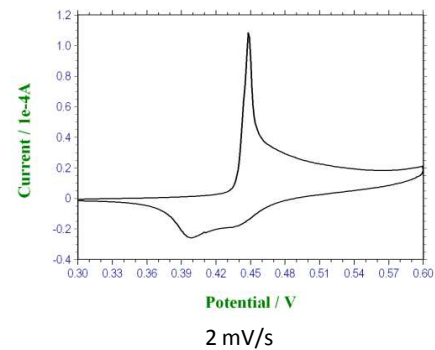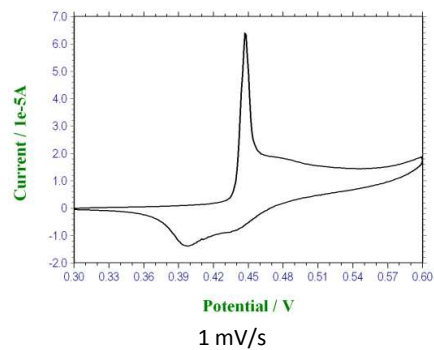
Effect of growth scan rate: Each film was deposited from the same solution , and using the same number of growth cycles (30 cycles).

Typical voltammetric response recorded for an electroprecipitated nickel oxide film deposited on a polycrystalline gold substrate subjected to slow multicycling (sweep rate 10 mV/s) between 0.1 and 0.7 V (vs Hg/HgO) in 5.0 M NaOH. The initial and final response profiles are presented.

1 mV/s

2 mV/s

5mV/s

10 mV/s

20 mV/s

50 mV/s

100 mV/s

200 mV/s

300 mV/s

400 mV/s

500 mV/s

750 mV/s

1000 mV/s

1500 mV/s

2000 mV/s
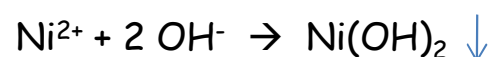
Sweep rate :
CV response

Deposition from $Ni(NO_3)_2$:

$NO_3^- + 7H_2O + 8e^- \rightarrow NH_3 + 10\ OH^-$ (extra OH^- generated from ammonia/ammonium ion equilibrium, $NH_3 + H_2O \rightarrow NH_4+ + OH^-$)
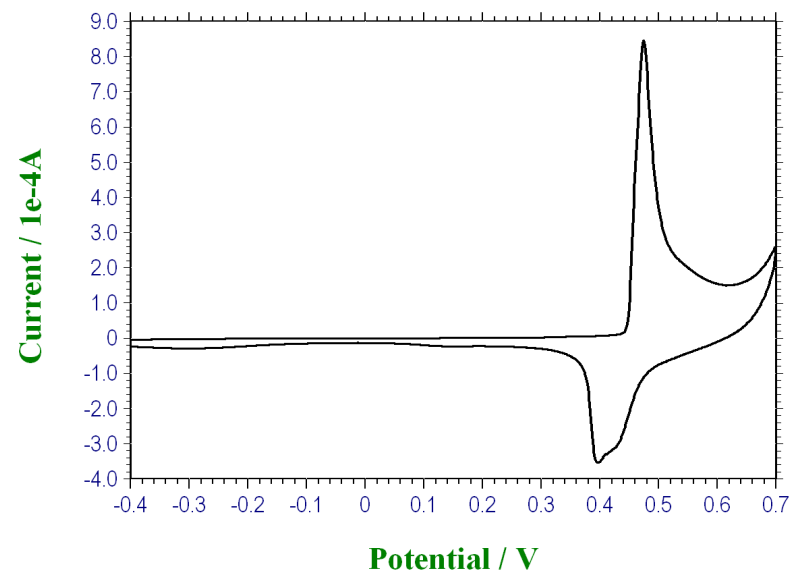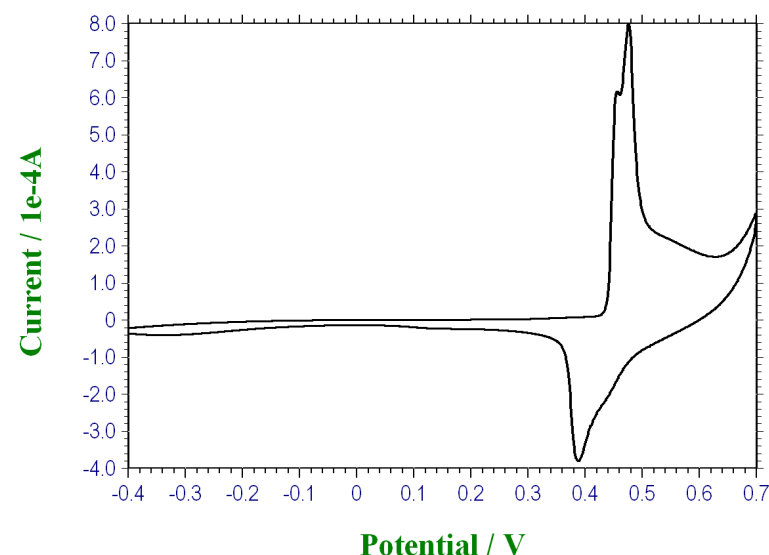
Production of OH^- increases the surface pH of the electrode resulting in precipitation of $Ni(OH)_2$

$Ni^{2+} + 2\ OH^- \rightarrow Ni(OH)_2 \downarrow$

CV in 1M NaOH at v= 40mV s^{-1} : Ni deposited on Au electrode at -1.5V vs Ag/AgCl for 300s in 0.1 M $Ni(NO_3)_2$/0.075M KNO_3

CV in 1M NaOH at v= 40mV s$^{-1.}$ but after additional multicycling for 30 cycles between -1.45 V to 0.65 V vs Hg/HgO @ 150 mV s^{-1}

Fine details of voltammetric response in aqueous base depends on pretreatment history.
Note sharp onset of redox switching: Ni(II)/Ni(III).
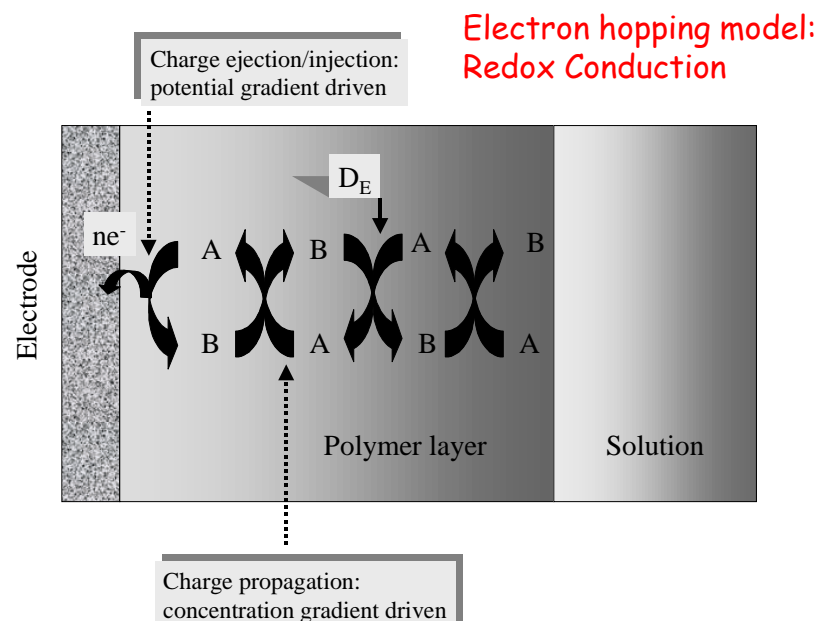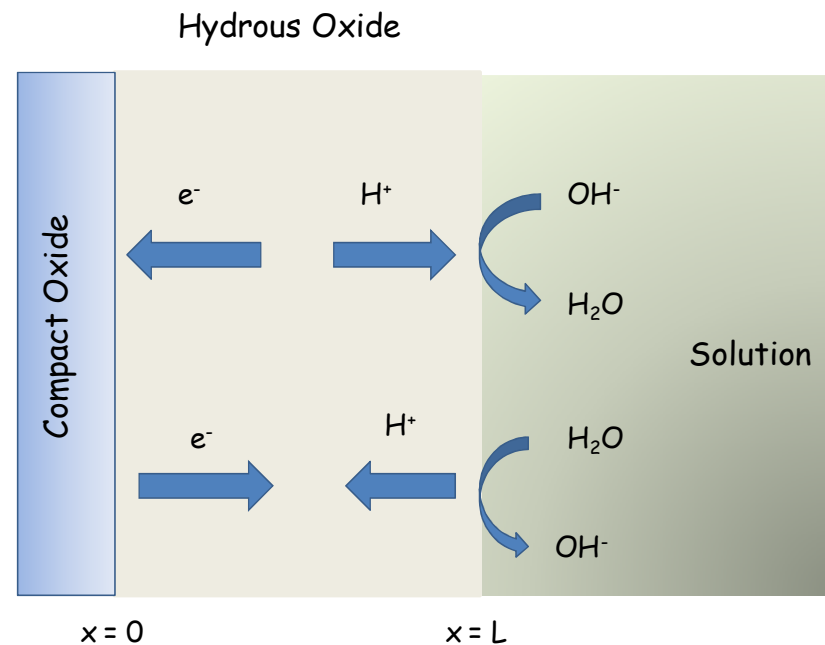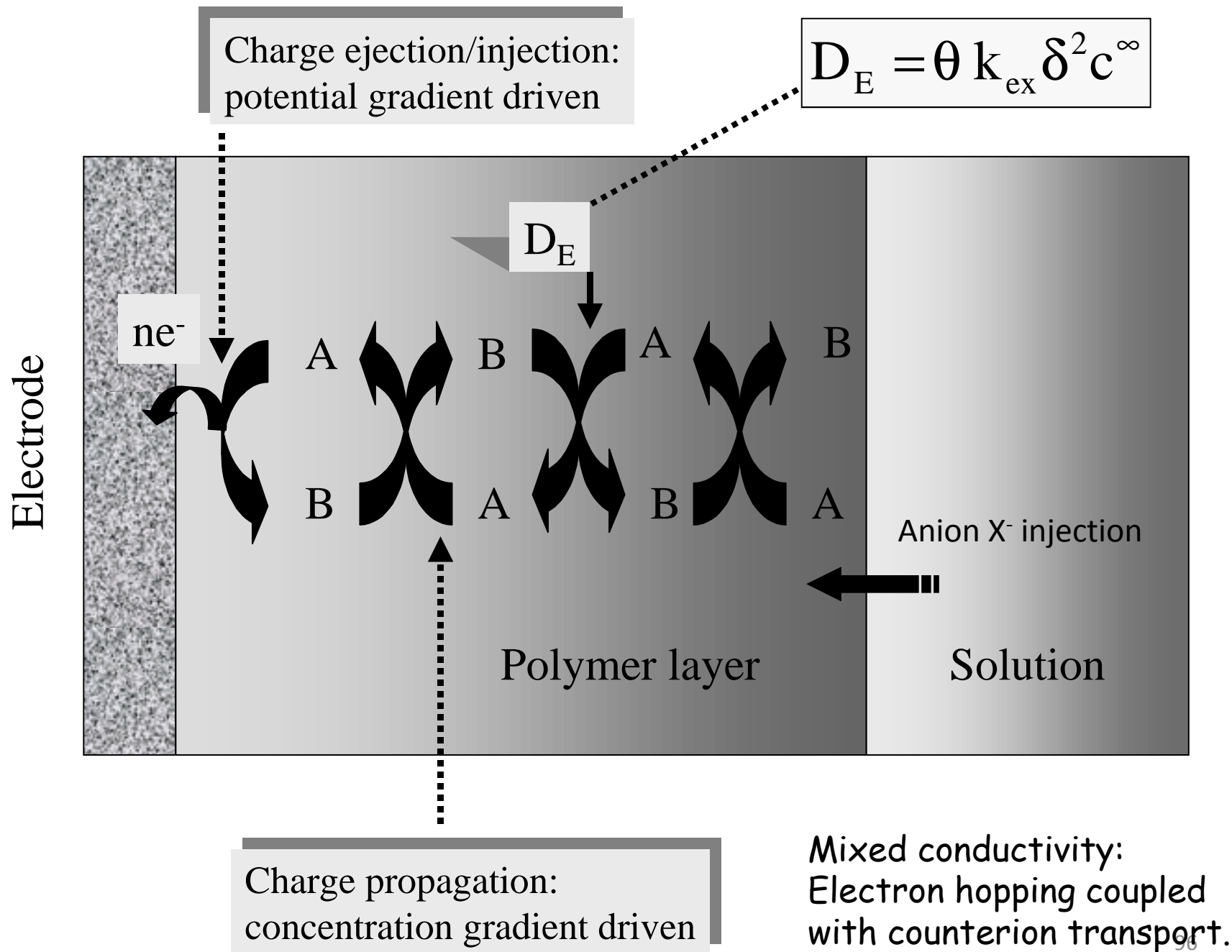
Redox switching in hydrous oxide layer

The redox switching reaction (associated with the main charge storage voltammetric peaks seen in Fe and Ni involving M(II)/M(III) transition) reflects the change in oxidation state of the film as a result of a potential perturbation. Redox centres immediately adjacent to the support electrode are directly affected by the electrode potential, whereas charge is further propagated along the oxy-iron polymer strands in the hydrous layer via a sequence of electron self exchange reactions between neighbouring oxy-metal sites.
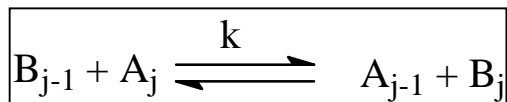
This process is envisaged to be analogous to redox conduction exhibited by electroactive polymer films. In the simplest terms this electron "hopping" may be modelled in terms of a diffusional process, and so the charge percolation rate may be quantified in terms of a *charge transport diffusion coefficient, D_{CT}.* In the case of hydrous iron oxide, the latter may reflect either the electron hopping rate or the diffusion of of OH^- (or equivalently H_3O^+) ions via a rapid Grotthus type mechanism. The charge transport diffusion coefficient may be quantitatively estimated using cyclic voltammetry.

Porous film model : Transmission Line

Hydrous Oxide

Compact Oxide

e^- H^+ OH^-

H_2O

Solution

e^- H^+ H_2O

OH^-

$x = 0$ $x = L$

Electron hopping model: Redox Conduction

Charge ejection/injection: potential gradient driven

D_E

Electrode

ne^- A B A B

B A B A

Polymer layer Solution

Charge propagation: concentration gradient driven

Charge ejection/injection: potential gradient driven

$$D_E = \theta\, k_{ex}\, \delta^2 c^{\infty}$$

D_E

ne^-

Electrode

A B A B
B A B A

Polymer layer

Solution

Anion X^- injection

Charge propagation: concentration gradient driven

Mixed conductivity: Electron hopping coupled with counterion transport.

Diffusion model for electron hopping.

$$B_{j-1} + A_j \overset{k}{\underset{}{\rightleftharpoons}} A_{j-1} + B_j$$

$$f_E = k\delta\left(b_{j-1}a_j - a_{j-1}b_j\right)$$

$$b_j = b_{j-1} + \delta\,\frac{db_{j-1}}{dx}$$

$$a_j = a_{j-1} + \delta\,\frac{da_{j-1}}{dx}$$
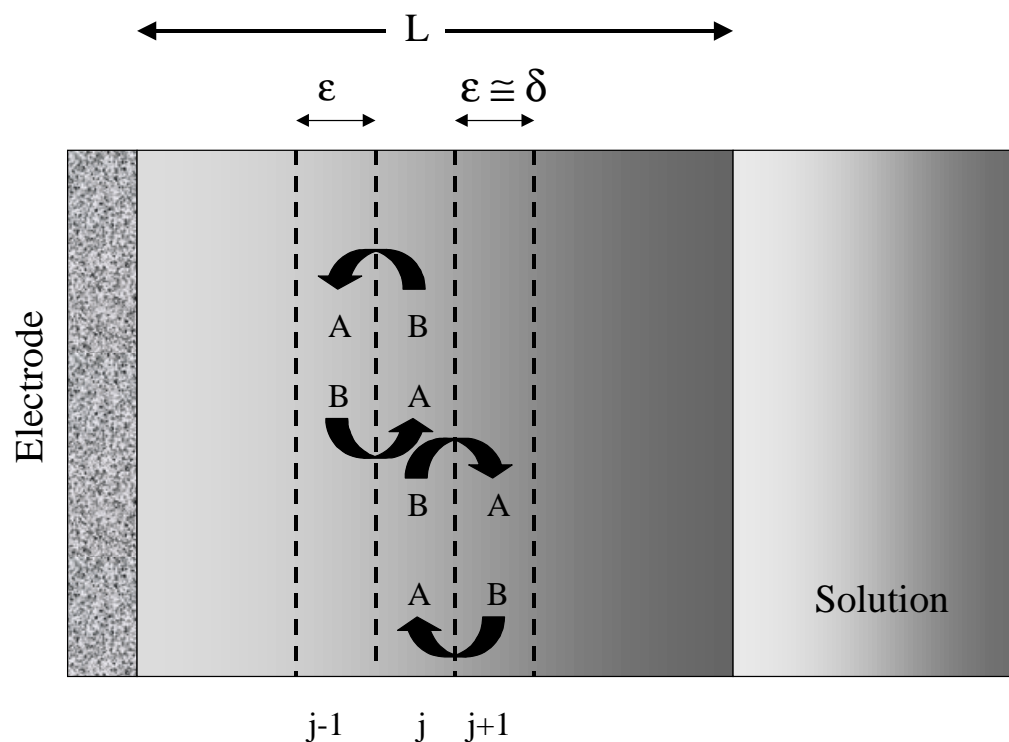
$$f_E = k\delta^2\left(b_{j-1}\frac{da_{j-1}}{dx} - a_{j-1}\frac{db_{j-1}}{dx}\right)$$

$$f_E = k\delta^2\left(b\frac{da}{dx} - a\frac{db}{dx}\right)$$

$$c^{\infty} = a + b$$

$$f_E = k\delta^2 c^{\infty}\left(\frac{b}{c^{\infty}}\frac{da}{dx} - \frac{a}{c^{\infty}}\frac{db}{dx}\right)$$

$$D_E = k\delta^2 c^{\infty}$$

Electrode

L

ε $\varepsilon \cong \delta$

A B

B A

B A

A B

Solution

j-1   j   j+1

Homogeneous polymer layer

$$\frac{\partial a}{\partial t} = -\frac{\partial b}{\partial t} = \frac{\partial f_E}{\partial x}$$

$$f_E = D_E\left(\frac{b}{c^{\infty}}\frac{da}{dx} - \frac{a}{c^{\infty}}\frac{db}{dx}\right) = D_E\frac{(a+b)}{c^{\infty}}\frac{da}{dx}$$

$$f_E = D_E\frac{da}{dx} = -D_E\frac{db}{dx}$$

$$\frac{\partial a}{\partial t} = D_E\frac{\partial^2 a}{\partial x^2}$$

$$\frac{\partial b}{\partial t} = D_E\frac{\partial^2 b}{\partial x^2}$$

Geometric hopping parameter

Bimolecular rate constant

- macroscopic charge propagation through polymer can be represented in terms of a diffusion process

- rate of electron hopping quantified via electron exchange rate constant k_{ex} or electron hopping diffusion coefficient D_E

- local potential gradients between redox sites produce a migration term in description of electron hopping flux

- D_E predicted to vary linearly with redox site concentration

- electron hopping can be further described using the Marcus theory of ET

- mechanism of electron hopping dependent on degree of local mobility of redox groups ; physical diffusion of redox groups also may be important

- electron hopping diffusion coefficients can be evaluated using transient or steady state electrochemical techniques

$$D_E = \theta_G \, k_{ex} \delta^2 c^\infty$$

Electron hopping distance

Total redox site concentration

$$D_E \cong 10^{-10} - 10^{-7} \, cm^2 s^{-1}$$
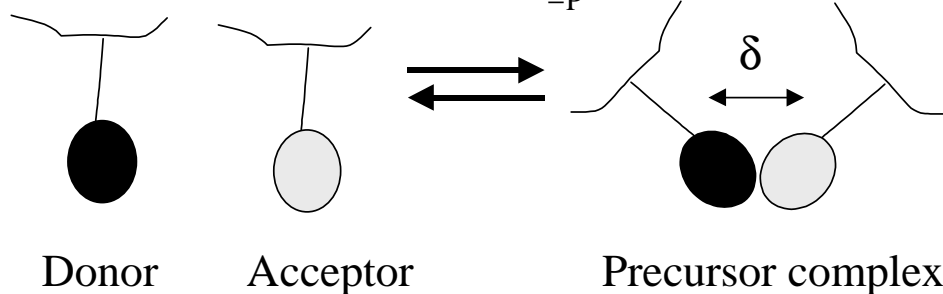
$$\theta_G = 1/6 \quad \text{3D hopping}$$
$$\theta_G = 1/4 \quad \text{2D hopping}$$

Precursor/successor complex model for nearest neighbour ET in redox polymer materials.

$$D_E = \theta \, k_{ex} \delta^2 c^\infty$$

$$K_P = \frac{k_P}{k_{-P}}$$

$$\theta = 1/6 \quad 3D \quad hopping$$

Donor   Acceptor

Precursor complex

$$k_{ex} = K_P k_E$$

k_E
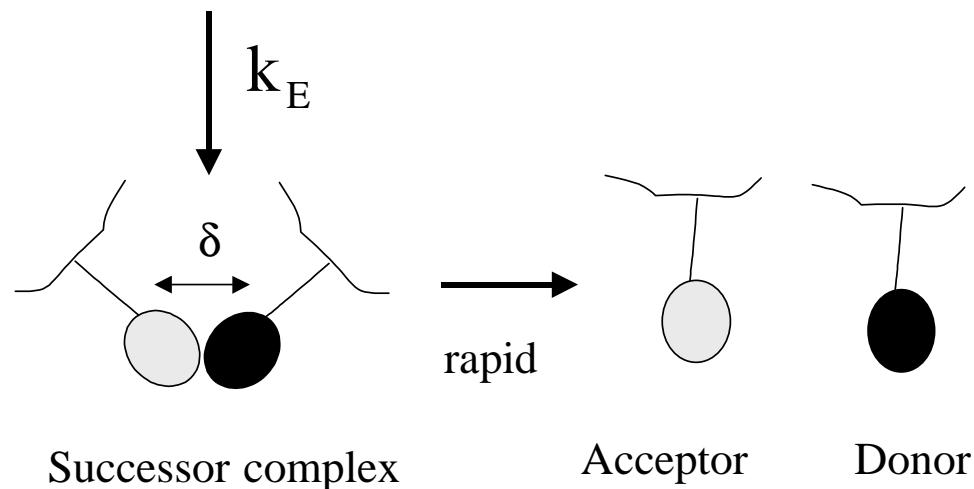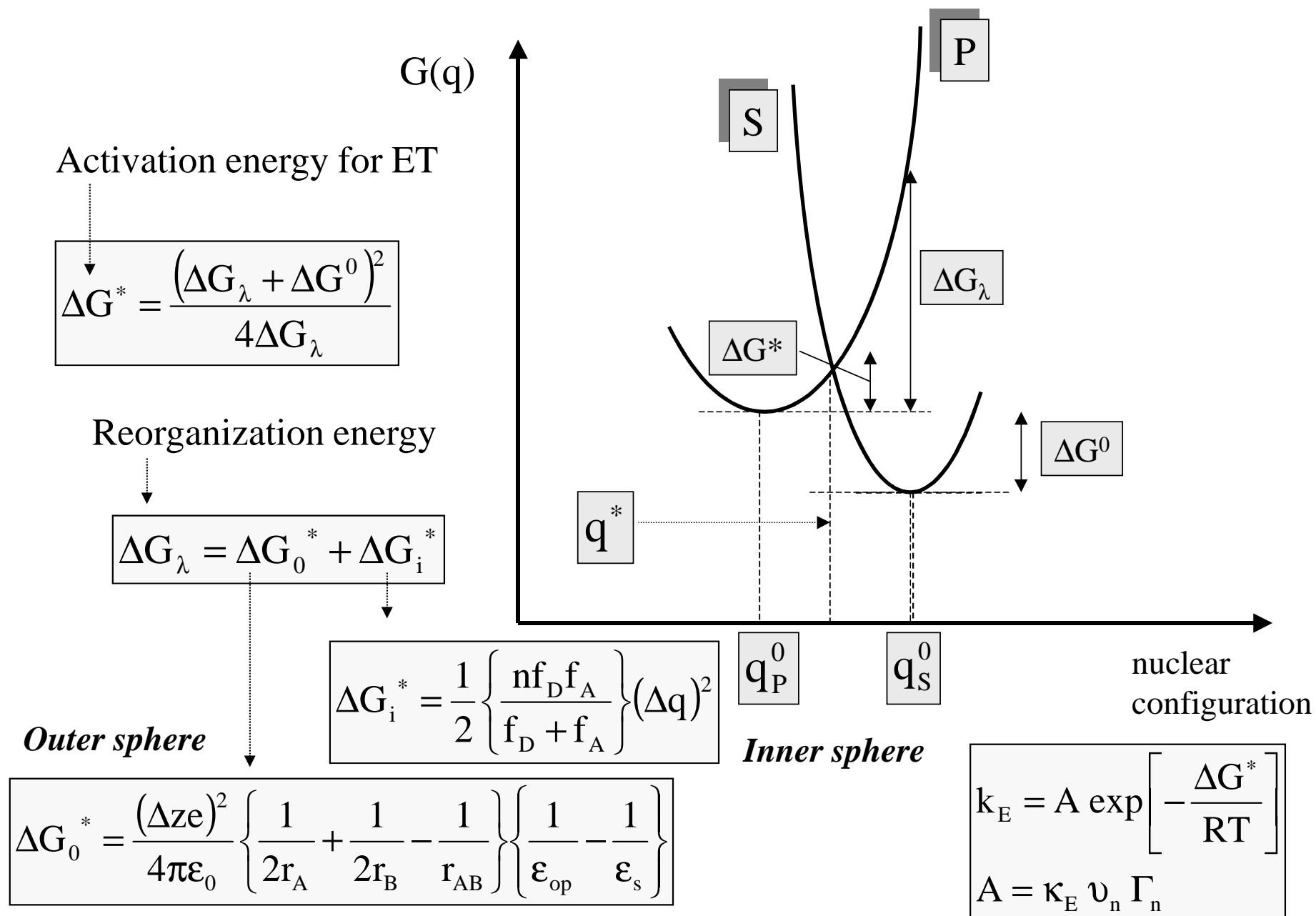
$$k_E = \kappa_E \, \upsilon_n \, \Gamma_n \, \exp\left[-\frac{\Delta G^*}{RT} \right]$$

Marcus Theory of ET.

δ

δ

rapid

Successor complex

Acceptor   Donor

99

Marcus Theory of ET

Activation energy for ET

$$\Delta G^* = \frac{\left(\Delta G_\lambda + \Delta G^0\right)^2}{4\Delta G_\lambda}$$

Reorganization energy

$$\Delta G_\lambda = \Delta G_0{}^* + \Delta G_i{}^*$$

$$\Delta G_i{}^* = \frac{1}{2}\left\{\frac{nf_D f_A}{f_D + f_A}\right\}(\Delta q)^2$$

Inner sphere

Outer sphere

$$\Delta G_0{}^* = \frac{(\Delta ze)^2}{4\pi\varepsilon_0}\left\{\frac{1}{2r_A} + \frac{1}{2r_B} - \frac{1}{r_{AB}}\right\}\left\{\frac{1}{\varepsilon_{op}} - \frac{1}{\varepsilon_s}\right\}$$

G(q)

S

P

ΔG_λ

ΔG^*

ΔG^0

q^*

q_P^0

q_S^0

nuclear configuration

$$k_E = A\exp\left[-\frac{\Delta G^*}{RT}\right]$$

$$A = \kappa_E\, \upsilon_n\, \Gamma_n$$

Aoki Model for redox conduction.

We utilise the mathematical formalism of Aoki and co-workers to derive an expression for D_{CT}. These workers solved the finite diffusion problem under conditions of a linear potential sweep. Transport information may be readily extracted from an analysis of the shape of the voltammetric response as a function of sweep rate. In particular, the peak current, i_p, representing the main redox switching process in the hydrated layer varies with sweep rate ν according to the Aoki equation provided that the M(II)/M(III) switching process is electrochemically reversible.

$$i_p = 0.446 nFA \left\{ \frac{\Gamma_\Sigma D_{CT}}{L^2} \right\} W^{1/2} \tanh Y$$

$$W = \frac{nFL^2\nu}{D_{CT}RT}, \quad Y = 0.56W^{1/2} + 0.05W$$

In the latter expressions, n, F, A and Γ_Σ denote respectively, the number of electrons transferred in the redox process, the Faraday constant, the geometric area of the electrode and the surface coverage of the active oxy-iron/nickel groups in the hydrous layer. The latter quantity is related to the charge capacity Q and the redox site concentration c_Σ via, $\Gamma_\Sigma = c_\Sigma L = Q/nFA$, where L denotes the layer thickness. The full Aoki equation may be solved numerically to obtain an estimate of the charge transfer diffusion frequency (units: s^{-1}) $f_D = D_{CT}/L^2$ or indeed the charge transfer diffusion coefficient D_{CT} (units: cm^2s^{-1}) provided the hydrous film thickness may be estimated.

Two limiting forms of the general Aoki expression may be identified. For low values of sweep rate corresponding to small W, we can set $\tanh Y \approx Y$ to obtain one limiting expression useful for thin hydrous oxide films.

$$i_p = \frac{n^2F^2A\Gamma\nu}{4RT}$$
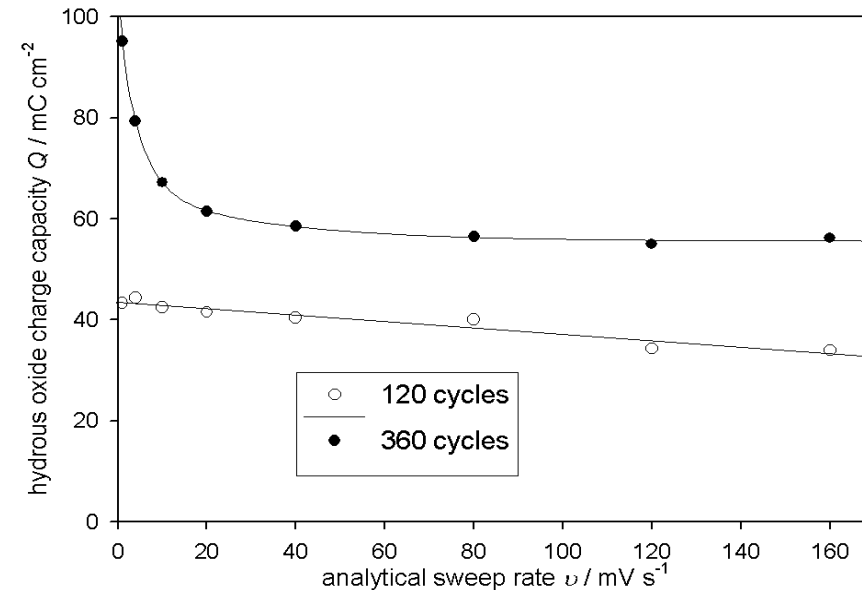
Alternatively at large sweep rates corresponding to large W values, we set $\tanh Y \approx 1$ and obtain a limiting expression useful for thicker hydrous oxide films. This is the Randles-Sevcik case.

$$i_p = 0.446 \left\{ \frac{(nF)^3}{RT} \right\}^{1/2} AD_{CT}^{1/2} c_\Sigma \nu^{1/2}$$
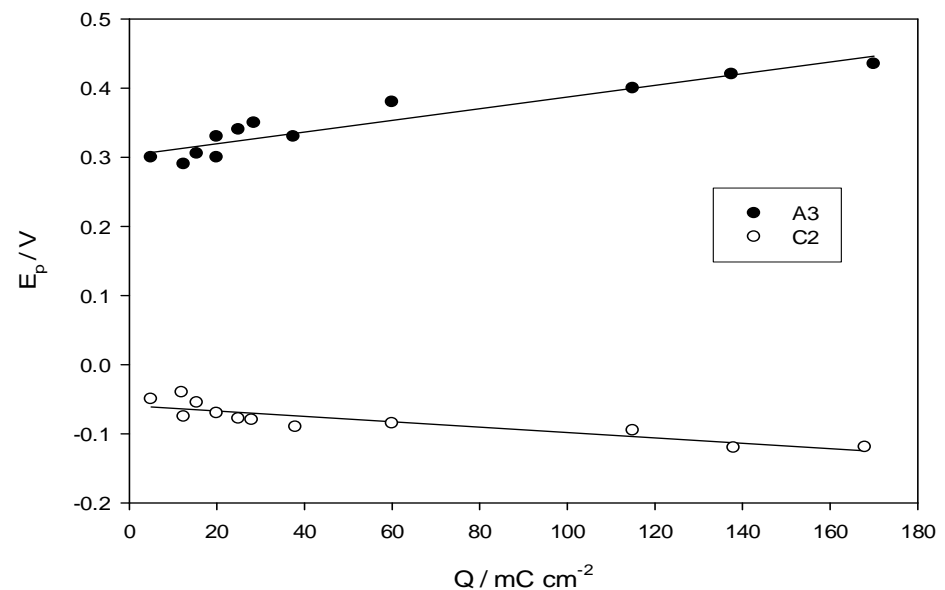
It should be noted that concentration polarization effects, due to incomplete titration of redox sites within the dispersed hydrated layer, are manifest at larger sweep rates. Diffusion coefficients may only be evaluated in this region. The $i_p/\nu^{1/2}$ proportionality can be most readily obtained at reasonable values of sweep rate for thick layers, whereas the i_p/ν proportionality (suggesting the operation of Nernstian equilibrium throughout the dispersed layer during redox switching) will be observed over an extended range of sweep rates with thin layers.

Variation of redox charge capacity with analytical sweep rate for an iron oxide film grown under potential cycling conditions for 120 cycles (open circle) and 360 cycles (filled circle) in 1.0 M NaOH at 298 K.

Marked increase in integrated charge capacity at low sweep rates indicative of slower redox electron hopping through thicker films since more oxymetal sites are being titrated over longer timescales (slower sweep rates).
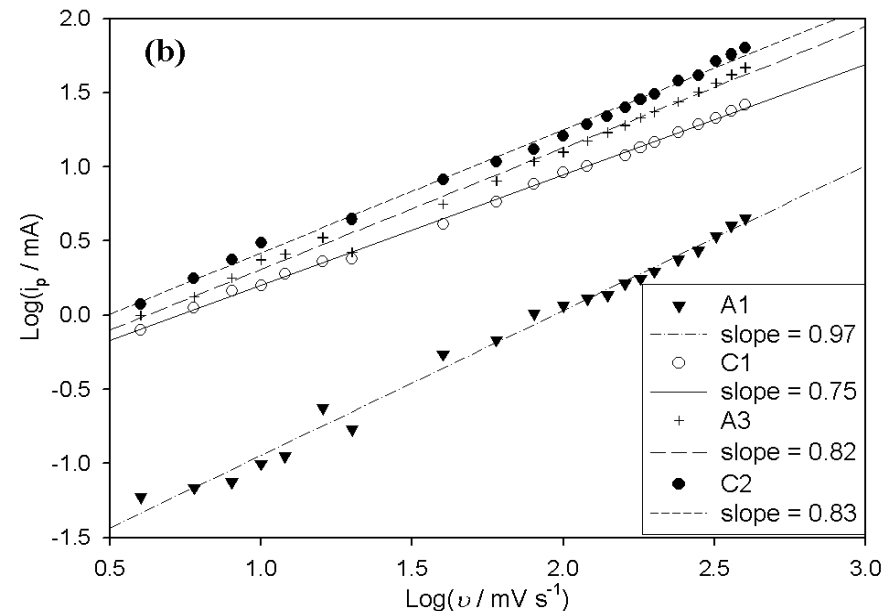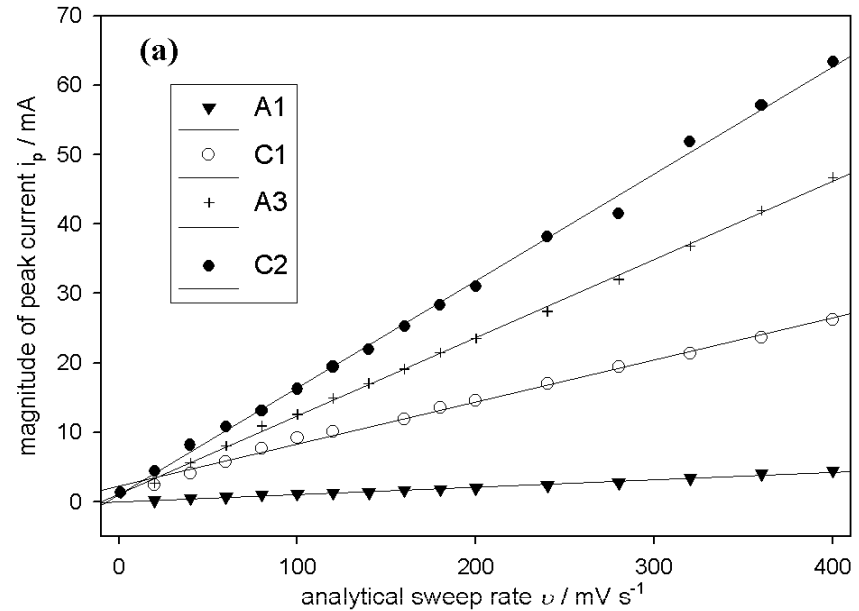
The variation in voltammetric peak potential with oxide charge capacity for a multicycled oxide electrode (ca. 30 growth cycles) is presented across for the main iron oxide charge storage peaks A_3 and C_2. The oxidation peak potential shifts to more positive values as the hydrous layer thickness increased whereas the reduction peak potential shifts to more negative values. The shift is linear with charge capacity in both cases. Hence the main Fe(II)/Fe(III) charge storage reaction becomes more irreversible with increasing hydrous layer thickness. This reflects a kinetic limitation to charge percolation through the hydrous layer as the hydrous film gets thicker.
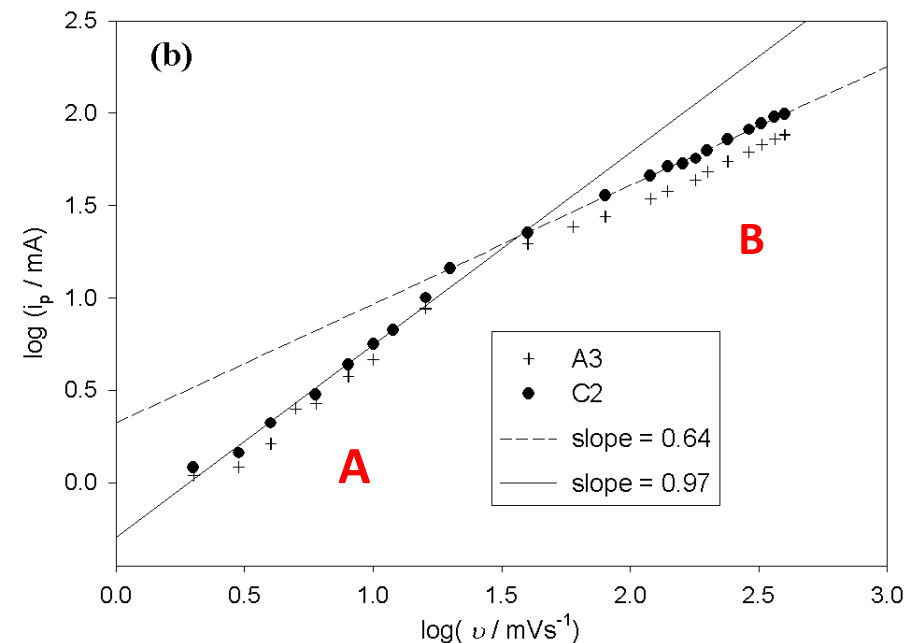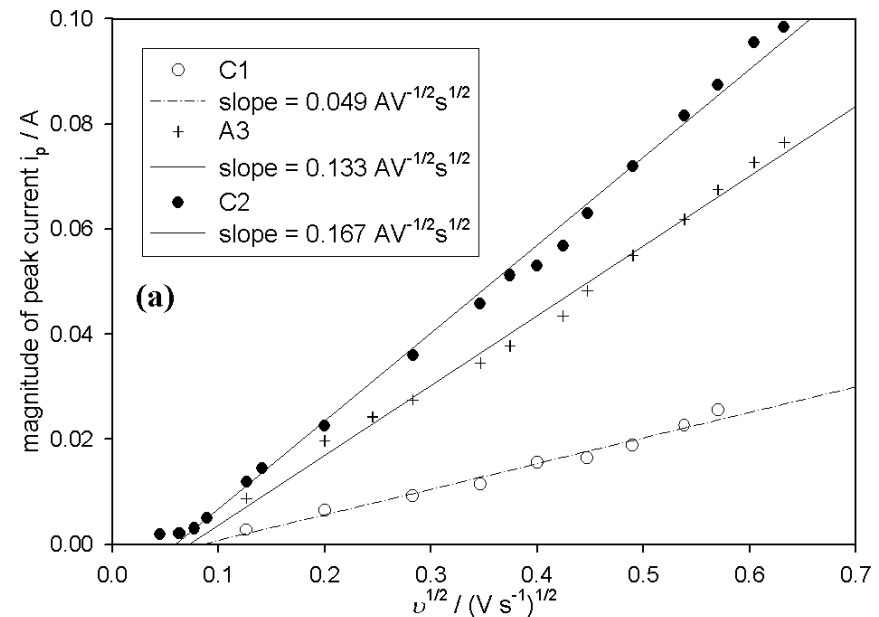
(a) Variation of voltammetric peak current with sweep rate for a multicycled iron electrode (30 cycles, – 1.425 to 0.325 V (vs Hg/HgO), 0.35 Vs^{-1}) in 1M NaOH at 25°C. (b) Log i_p/ log v plot of the data outlined in (a).

We note from the data for thin iron oxide films illustrated across in (a), that excellent linearity is observed between the peak current and scan rate, both for the hydrous oxide peaks A_3 and C_2, and for the compact oxide reduction peak C_1, over an extended scan rate window. This observation is confirmed in the double logarithmic analysis of the data illustrated in b across where the slopes of greater than 0.8 are noted for the A_3 and C_2 peaks.

(a) Variation of voltammetric peak current with sweep rate for a multicycled iron electrode (240 cycles, – 1.425 to 0.325 V (vs Hg/HgO), 0.35 Vs⁻¹) in 1M NaOH at 25°C. (b) Log i_p/ log v plot of the data outlined in (a).

In contrast data obtained for thicker iron oxide layers is outlined across. In this case we obtain good linearity (except at relatively low values of sweep rate) when i_p is plotted versus v as outlined in (a). The double logarithmic analysis of the data (b) is particularly interesting in that a dual slope behaviour is observed (gradient in region A: 0.97 ; gradient in region B : 0.64). The sweep rate at which concentration polarization effects become important may be readily discerned from the break point in this "dog's leg" curve. Transport information in the form of a D_{CT} value may be extracted from the data in region B.

(a) magnitude of peak current i_p / A vs $\upsilon^{1/2}$ / (V s⁻¹)^{1/2}

○ C1
slope = 0.049 AV^{-1/2}s^{1/2}
+ A3
slope = 0.133 AV^{-1/2}s^{1/2}
● C2
slope = 0.167 AV^{-1/2}s^{1/2}

(b) log (i_p / mA) vs log(υ / mVs⁻¹)

+ A3
● C2
slope = 0.64
slope = 0.97

A

B

The Randles-Sevcik plots yield gradients of 0.133 $AV^{-1/2}s^{1/2}$ and 0.167 $AV^{-1/2}s^{1/2}$ for the peaks A_3 and C_2 respectively. The concentration of redox sites in the oxide layer is effectively given by the expression $c_\Sigma = \rho/M$, where ρ denotes the density of the hydrous material and M represents the molar mass of the fundamental repeat unit of the hydrated oxy-iron polymer. For the anodic process (peak A_3) if the composition of the reduced state is assumed to be $[Fe_2(OH)_6(OH_2)_3]^{2-}$ with molar mass 267 g mol^{-1}, and if we assume that the density ρ is given by that for $Fe(OH)_2$ which is 3.4 g cm^{-3}, then given that n = 2 for the redox process), one can evaluate that D_{CT} = 1.88 × 10^{-10} cm^{2}s^{-1}. For the corresponding reduction process (peak C_2), where the oxidised repeat unit is assigned the composition $[Fe_2O_3(OH)_3(OH_2)_3]^{3-}$ we have M = 265 g mol^{-1}. It is known that the density of $Fe_2O_3.nH_2O$ is in the range 2.4 – 3.6 g cm^{-3} depending on the degree of hydration. We assume a mean value of ~ 3 g cm^{-3}. Hence again, for n = 2 one obtains from the Randles-Sevcik plot that D_{CT} = 3.77 × 10^{-10} cm^{2}s^{-1}. Hence the average charge transfer diffusion coefficient obtained from these voltammetric experiments conducted on thick oxide layers is 2.8 × 10^{-10} cm^{2}s^{-1}.
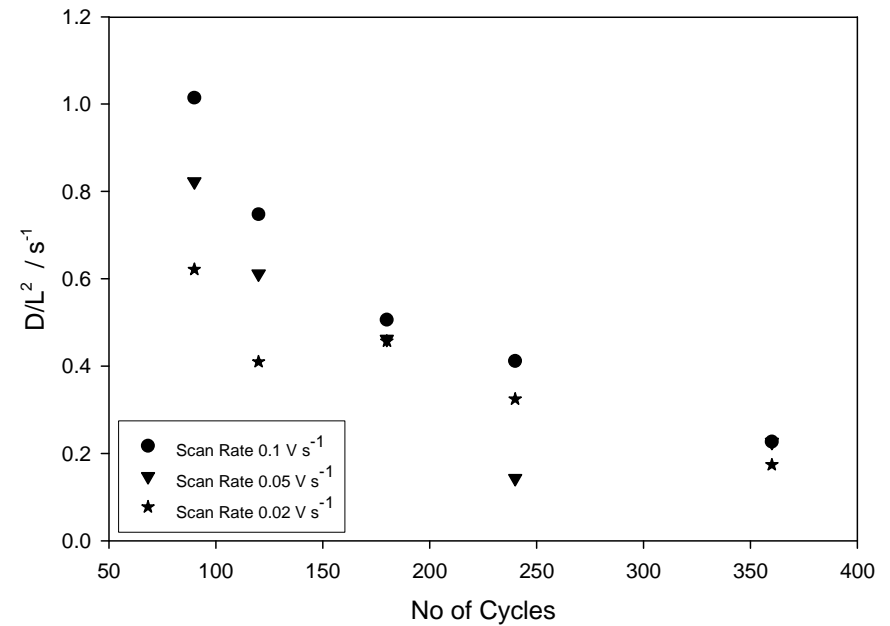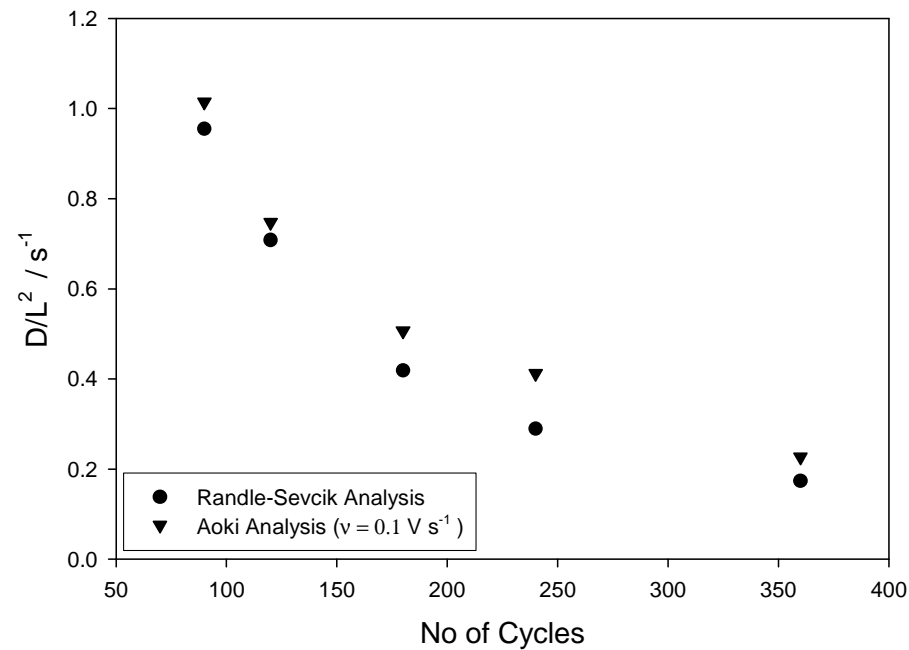
The latter value is not unreasonable compared with those obtained for electroactive polymer modified electrodes such as polyaniline (D_{CT} = 3 × 10^{-9} cm^{2}s^{-1}) and poly(pyrrole) (D_{CT} = 1× 10^{-8} cm^{2}s^{-1}) .The values obtained in the present work are somewhat lower than those obtained for other hydrated oxide materials such as hydrated iridium oxide in acid solution, where values of 1.5 × 10^{-9} cm^{2}s^{-1} and 1.0 × 10^{-7} cm^{2}s^{-1} were derived for the reduction and oxidation processes respectively . Unlike the iridium oxide case the charge transport diffusion coefficients for oxidation and reduction reported in this work do not differ appreciably.

In view of the assumptions made with regard to the density and surface area of the oxide, the value reported for D_{CT} is only approximate. Furthermore in view of the nature of the hydrous film, with charge percolation occurring through regions of varying oxide, solvent and electrolyte content, the value quoted must be regarded as a macroscopic average diffusion coefficient for transport through these various regions. It is also difficult to unambigiously identify the rate controlling transport process occurring within the layer during redox switching. The diffusion coefficient may correspond to ionic transport, electron self exchange between neighbouring sites, or the segmental motion of polymer chains antecedent to the latter processes. A definite assignment can only be obtained if the activation energy for charge percolation is determined.

Multicycled Ni oxyhydroxide films coated on No metal support in aqueous 1M NaOH.

Ian Godwin 2012
Nickel oxy-hydroxide films.

Comparison of theoretical models for the valuation of D/L^2
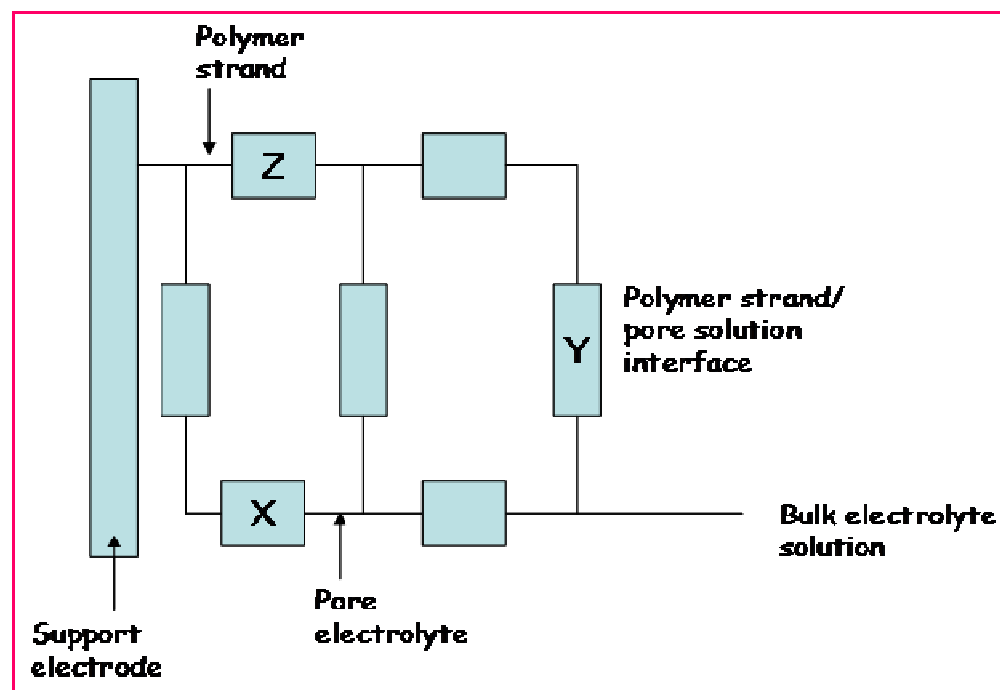
Richard Doyle 2012
Aoki Equation.
Fe oxy-hydroxide films.

# Growth cycles	D_{CT} / cm^2 s^{-1}
Uncycled	1.9×10^{-11}
30	3.3×10^{-11}
120	3.8×10^{-11}
300	3.0×10^{-11}

The Fe(II) →Fe(III) or Ni(II) → Ni(III) redox switching reaction is quite similar to that exhibited by **<u>conductive polymer materials</u>** such as poly(aniline), and other hydrous polymeric oxides such as iridium oxide, in that it involves the transport of both counterions and electrons and is therefore a mixed electronic/ionic conductor. The physical transport processes within the material may be described in terms of a dual rail electrical transmission line model of the type recently proposed for electronically conducting polymers and transition metal oxide materials (especially DSA type IrO_2 based thermal oxides) by Bisquert and co-workers and others The TL circuit consists of distributed impedances corresponding to charge transport along the polymer strand (Z), ion transport within the pore electrolyte (X) and an impedance representing the interface between the strand and the pore (Y). At the simplest level Z corresponds to the electronic resistance R_E, X to the ionic resistance R_I, and Y to a distributed capacitance C_Σ .
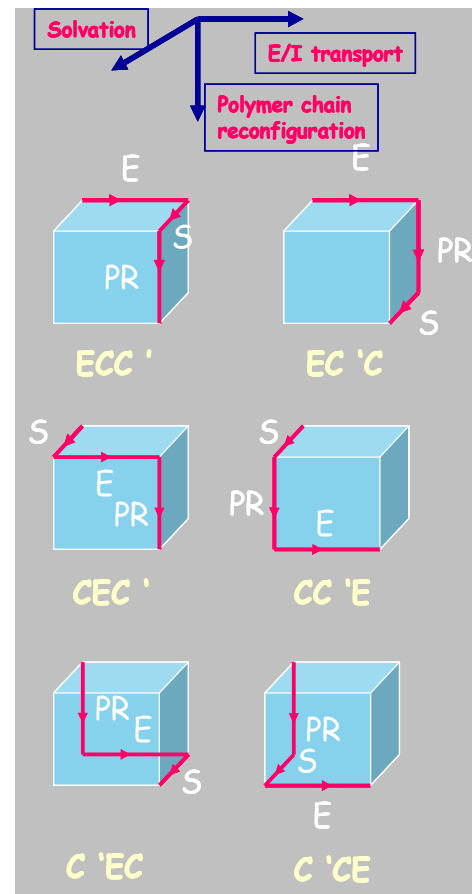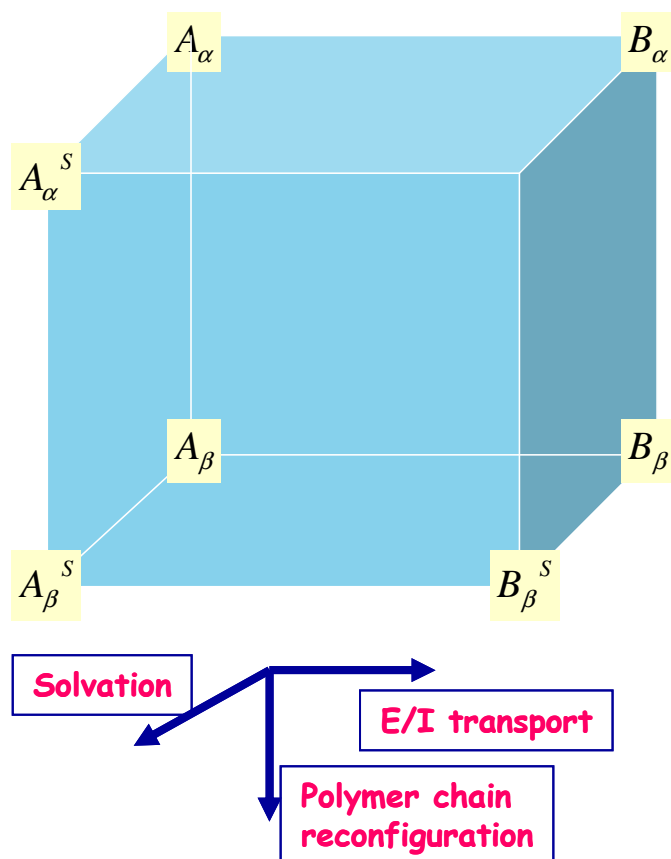
Dual Rail Transmission Line Model for Polymeric Oxy-hydroxide modified electrodes.

Redox Switching in Metal Oxide/ECP materials.

- Redox switching refers to a potential driven change in oxidation state of the sites within the polymer film.
- Usually accompanied by a change in layer conductivity.
- Oxidative (reductive) redox switching causes an increase (decrease) in oxidation state of redox sites on polymer chain.
- Electroneutrality requires a corresponding ingress (egress) of anions X^- from the solution into the polymer film or an egress (ingress) of cations C^+ from the polymer layer into the solution in order to ensure charge compensation.
- The observed redox switching rate depends on how quickly charge can be transferred through the polymer matrix.
- Volume, nature and morphology of electroactive polymer film can change during redox switching.
- Redox switching is a complex mechanism involving electron, ion, salt, and solvent transport. Polymer conformational changes may also occur (polymer chain relaxation). Any of these processes can be rate determining.

- Electrochemical techniques provide information only on the transport of charged species. Exclusive reliance on electrochemical techniques implies that the specific role of electroinactive species such as counterions, ion pairs and solvent molecules, cannot be directly deduced.
- Non electrochemical techniques such as FTIR, ellipsometry, Probe Beam deflection and , electrochemical quartz crystal microbalance can be used to obtain fuller information on the specifics of redox switching.
- Time scales for electron transfer, counterion transport (which is coupled to electron transfer via the electroneutrality condition), are in general quite different from the timescale involved in transferring such heavy species as a solvent, neutral molecule or a salt.
- Hence the question of whether an electroactive polymer film is at complete thermodynamic equilibrium when the activities of all mobile species must equal those of their counterparts in solution can be difficult to ascertain.

The Hillman-Bruckenstein scheme of cubes defining the possible rate controlling steps involved in redox switching of an electroactive polymer from a less solvated reduced α configuration to a more solvated oxidised β configuration.
Concept may well apply to hydrous metal oxyhydroxide polymeric films as well.

Redox Switching_ Rate determining steps:
• Coupled electron/ion transfer
•Solvent transfer
• Film structural change

Probe Beam Deflection

- Probe Beam Deflection (PBD) is based on the Mirage effect, and is a technique that measures the concentration gradient in front of an electrode by monitoring the refractive index gradient with a light beam.

- The redox switching process in an electroactive polymer film is accompanied by a counterion exchange with the bathing solution to maintain film electroneutrality.

- The ion concentration in the solution changes, creating a gradient of refractive index normal to the electrode surface.

- A beam travelling parallel to the surface suffers a deviation proportional to the concentration gradient, and so also proportional to the extent and direction of the ion flux.

- *Positive* beam deflection *away* from the electrode corresponds to insertion of ions into the film from the solution, while *negative* beam deflection *toward* the electrode implies the *release* of ions from the film to the solution.

- The mechanism of detection in PBD involves deflection (refraction) of the probe beam by the refractive index gradient.

- If a refractive index gradient is present in a transparent medium, different parts of a beam travelling perpendicular to the gradient would traverse zones of different refractive index. The speed of light would be different for each part of the beam and so the beam will deflect.

Interaction Path length

Beam deflection $\rightarrow$

$$\theta(x,t) = \frac{\ell}{n}\frac{\partial n}{\partial c}\left(\frac{\partial c(x,t)}{\partial x}\right)$$

Bulk refractive index
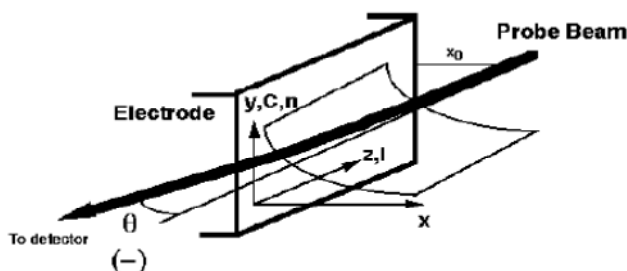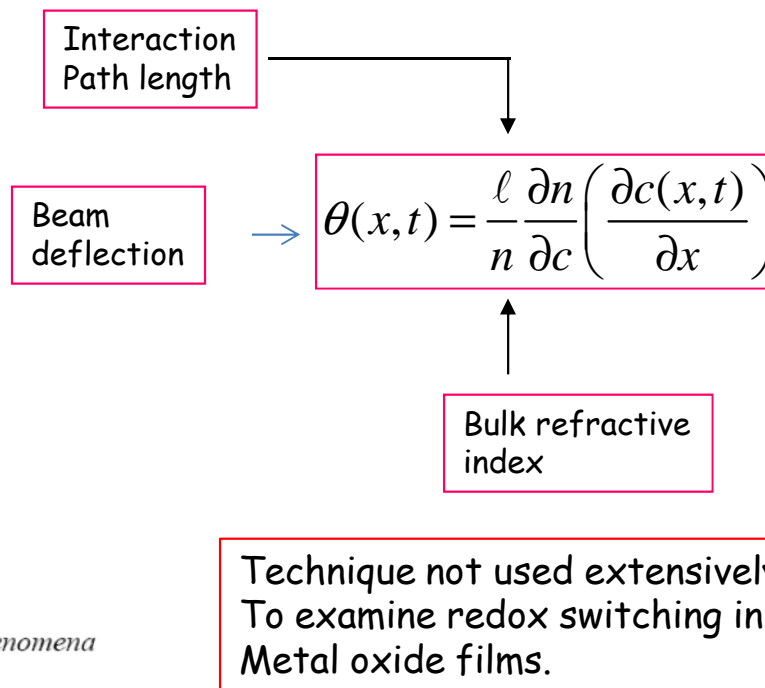
Figure 1: Probe Beam Deflection. Scheme of the deflection phenomena

Technique not used extensively To examine redox switching in Metal oxide films.

110

Probe Beam Deflection.

- The PBD method detects ion transport across the oxide polymer/solution interface. The technique probes concentration gradients near the electrode surface.

- The sign of the laser beam deflection indicates whether an interfacial redox reaction is accompanied by a net ion flux away from the electrode surface or towards the electrode surface.

- Cation expulsion from the film during redox switching gives rise to an increase in concentration at the polymer/solution interface. The concentration gradient is negative so the laser beam path is deflected in a negative manner toward the electrode. The voltammetric current is positive (oxidation). Negative beam deflection accompanied by positive (oxidation) current indicates cation expulsion.

- A positive beam deflection away from the electrode (reflecting a positive interfacial concentration gradient) combined with a positive voltammetric current indicates anion insertion into the film.

- Furthermore, a negative beam deflection combined with a negative (reduction) current indicates anion expulsion from the layer, a positive deflection combined with a negative current indicates cation insertion.
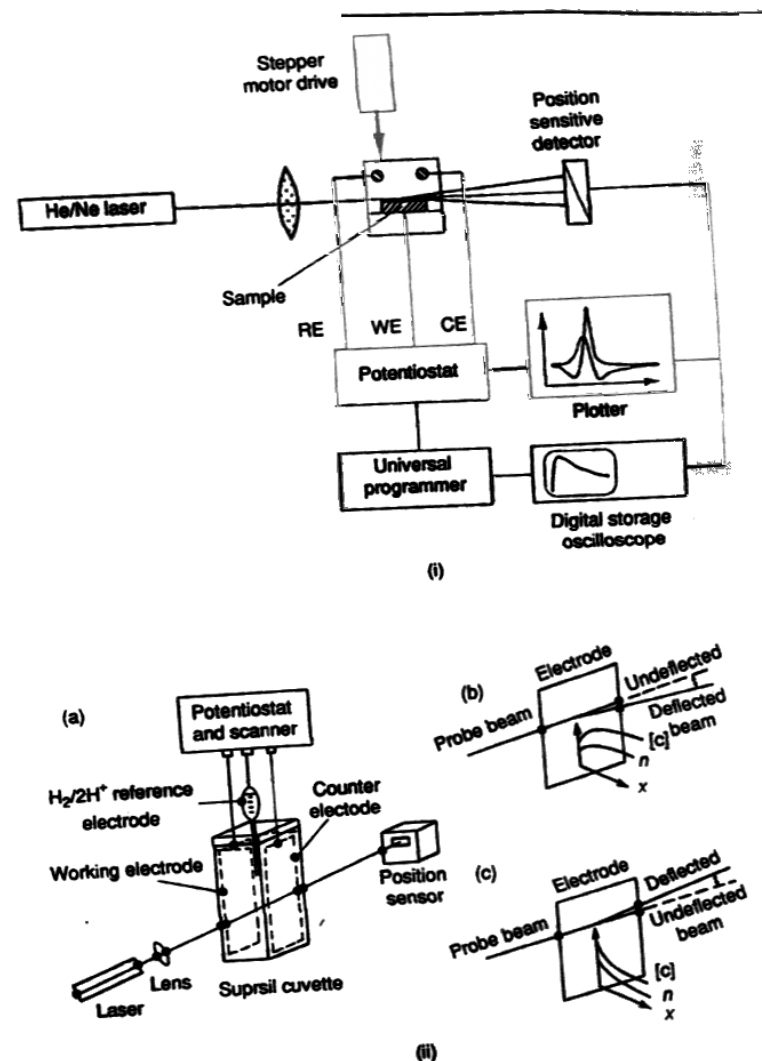

Figure 15 (i) General experimental arrangement for probe beam deflection measurements.[429] (ii) (a) Electrochemical cell arrangement for the recording of a cyclic deflectogram,[428] (b) Positive deflection of the probe beam resulting when the concentration gradient is positive. (c) Negative deflection obtained when the concentration gradient adjacent to the electrode is negative.

# PBD Studies PVF Chemically Modified Electrode.
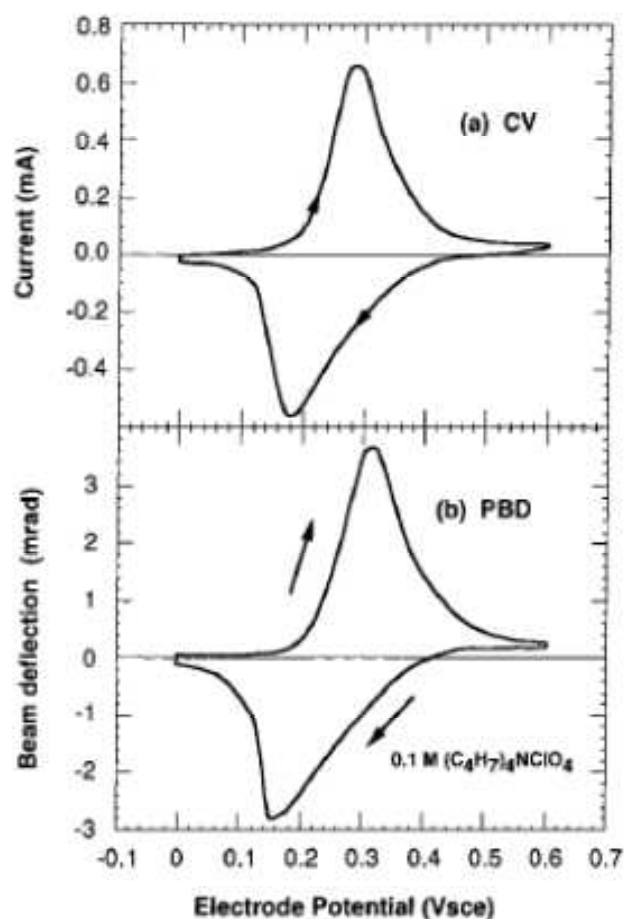
Figure 1. (a) Cyclic voltammogram and (b) cyclic deflectogram of a PVF film in 0.1 M tetrabutylammonium solution in acetonitrile. $v = 50$ mV/s. $A = 1$ cm^2. $\Gamma = 5.5 \times 10^{-8}$ mol cm^{-2}.

$$PVF \xrightarrow{-e^- + ClO_4^-} PVF^+(ClO_4^-) \qquad (I)$$
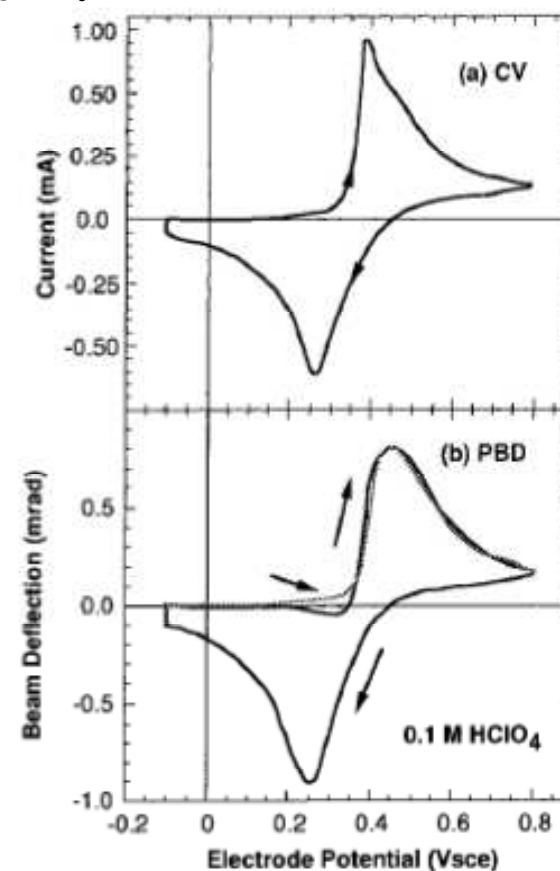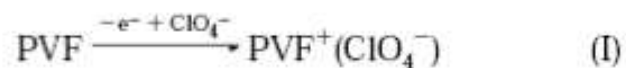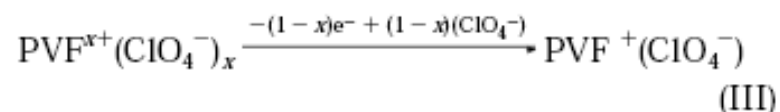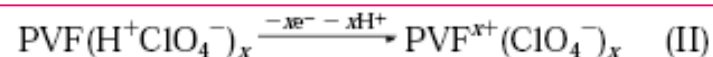
Figure 3. (a) Cyclic voltammogram and (b) cyclic deflectogram of a PVF film in 0.1 M HClO$_4$ solution. $v = 50$ mV/s. $A = 1$ cm^2. $\Gamma = 7.7 \times 10^{-8}$ mol cm^{-2}. The dashed line shows the current convoluted using a beam–electrode distance of 75 μm and a diffusion coefficient of 3.45×10^{-5} cm^2/s.

$$PVF(H^+ClO_4^-)_x \xrightarrow{-xe^- - xH^+} PVF^{x+}(ClO_4^-)_x \qquad (II)$$

$$PVF^{x+}(ClO_4^-)_x \xrightarrow{-(1-x)e^- + (1-x)(ClO_4^-)} PVF^+(ClO_4^-) \qquad (III)$$

Barbero et al. Langmuir, 2002, 18, 2756-2764.

Electropolymerization of poly(aniline).
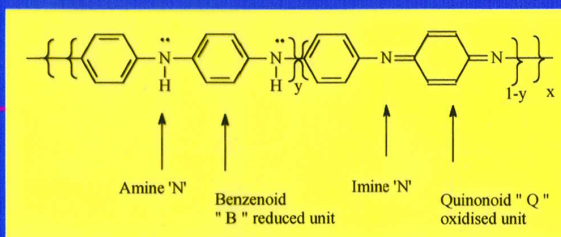
- Polyaniline (PANi) is best made in thin film form via electropolymerization at either a Pt or GC electrode via a potential cycling method. Typical conditions are 0.5M aniline monomer in 1M HCl at 50 mVs^{-1}.
- The potential is cycled between -300 mV to ca. 900 mV for a fixed number of cycles to form a uniform layer of polymer.
- The polymerization occurs most efficiently in solutions of low pH (especially in strongly acidic media).
- The electropolymerization mechanism is similar to that proposed for polypyrrole.


Poly(aniline) PAN.

$0 < y < 1$
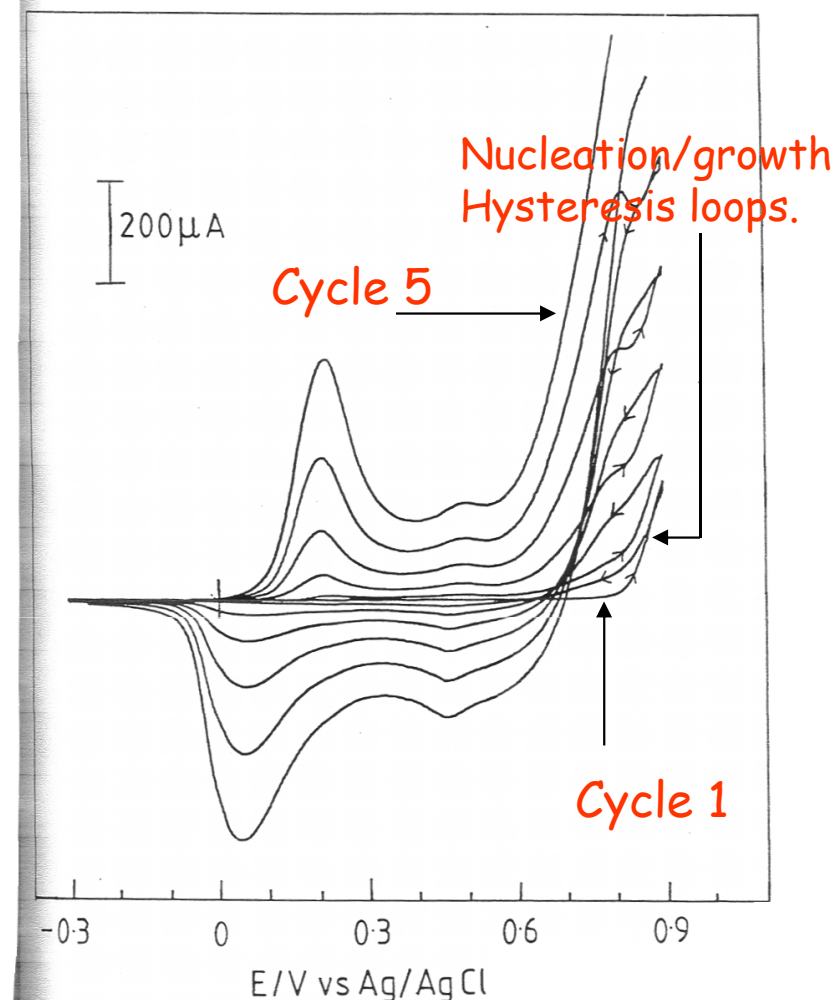
3 main oxidation states

Have various degrees of protonation depending on solution pH.

Amine 'N'
Benzenoid "B" reduced unit
Imine 'N'
Quinonoid "Q" oxidised unit

y	1	0.5	0
Name	Leuco-emeraldine all B units	emeraldine 3:1 B/Q ratio	per nigraniline 1:1 B/Q ratio
Description	Completely reduced	Intermediate	Completely Oxidised
Conductivity	Insulator	Conductor	Insulator

Nucleation/growth Hysteresis loops.

Cycle 5

200µA

Cycle 1

E / V vs Ag/AgCl

Anodic

cycle 17

cycle i

E_2

E_i

Cathodic

curve crossing
due to nucleation/
growth of
polymer phase

6mA
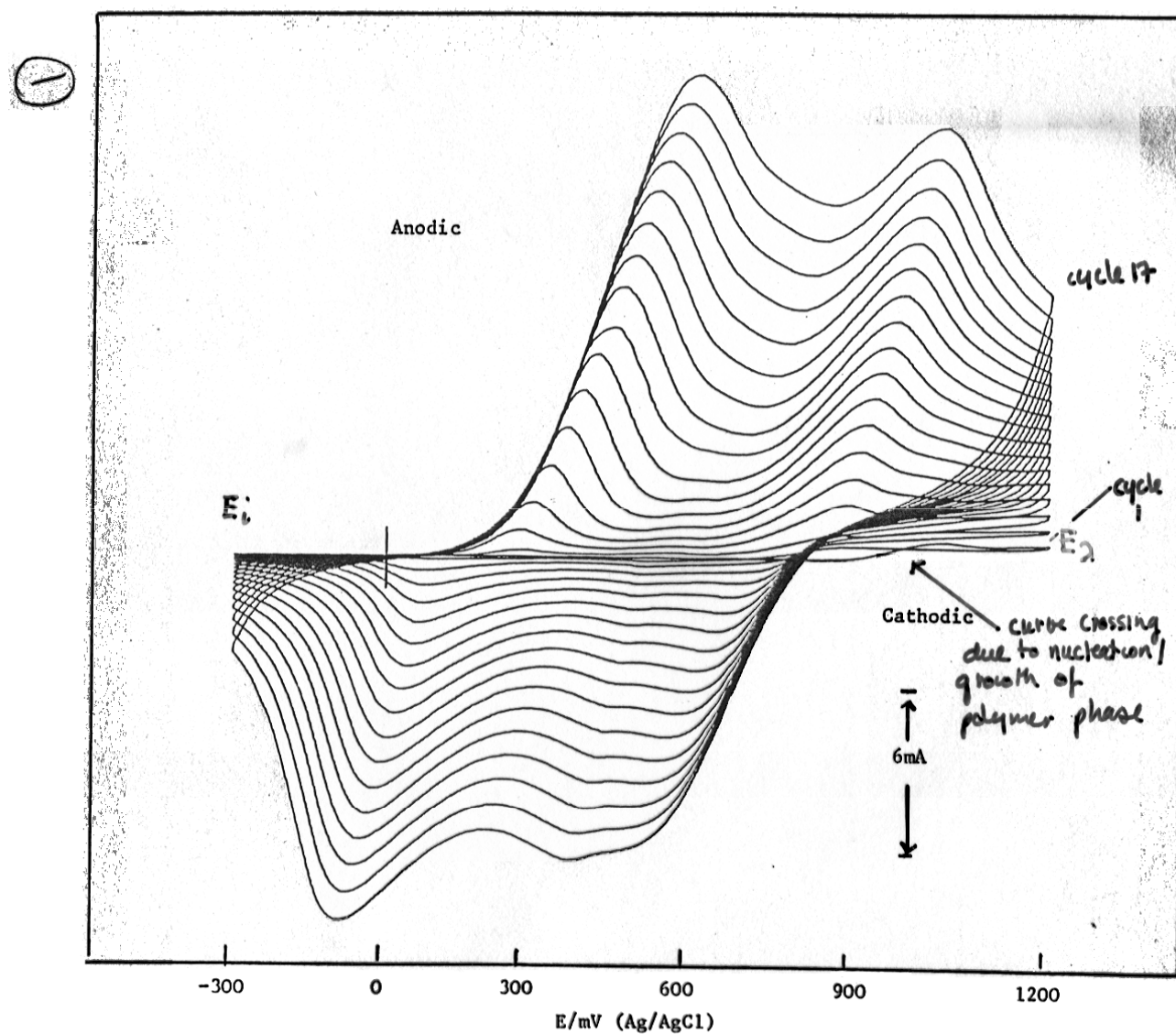
Figure 14

In situ electro-
deposition from a
dilute aniline
solution onto a
glassy carbon substrate.
Sweep rate, 50 mV s^{-1},
T = 298 K.

(0.55 M aniline
in 1.0 M HCl)

E/mV (Ag/AgCl)

-300   0   300   600   900   1200

pH effect on redox switching stoichiometry.
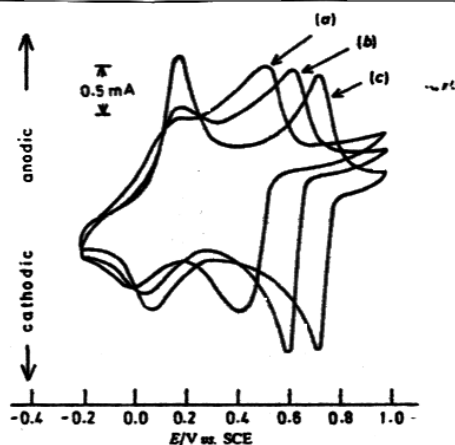
Fig. 2. Cyclic voltammograms of chemically synthesized emeraldine hydrochloride in electrolytes of (a) pH 2.0, (b) pH 1.0 and (c) pH −0.2 (1.0 mol dm⁻³ HCl).


dE/d pH = 120 mV/pH Unit
2H⁺, 1e⁻ process.
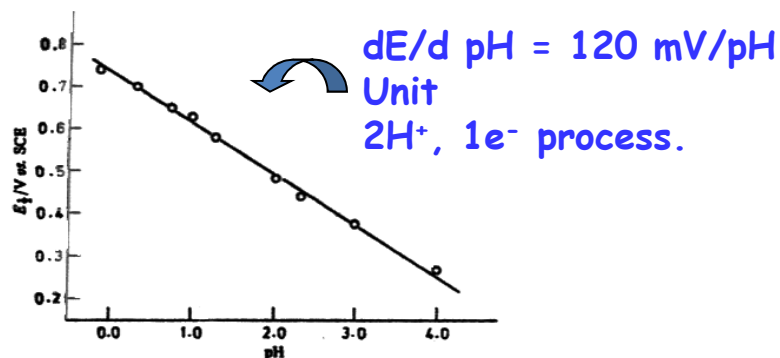
Fig. 3. Relationship between $E_{\frac{1}{2}}$ of the second redox process between pH −0.20 (1.0 mol dm⁻³ HCl) and pH 4.0. Slope = −120 mV per pH unit.

**Redox Process II**

pH>2
dE/dpH = 0.
No proton transfer.
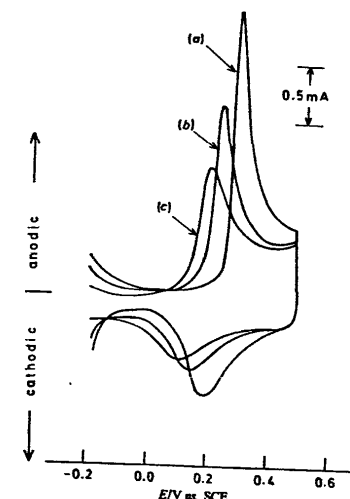
Fig. 4. Cyclic voltammograms (50 mV s⁻¹) of the first redox process of chemically synthesized emeraldine hydrochloride in electrolytes of (a) pH −2.12 (6.0 mol dm⁻³ HCl), (b) pH −1.05 (3.0 mol dm⁻³ HCl) and (c) pH −0.2 (1.0 mol dm⁻³ HCl).


Strong acid
dE/d pH = − 59mV/pH unit.
Equal numbers of electrons and protons transferred.
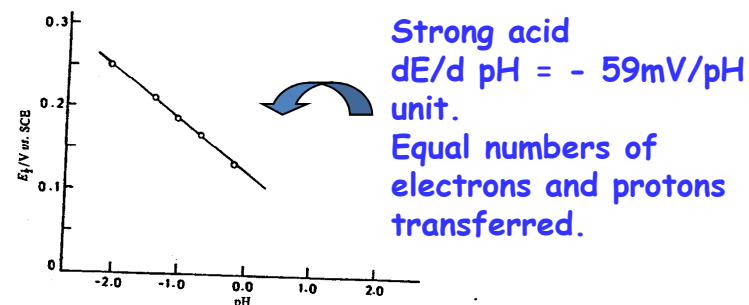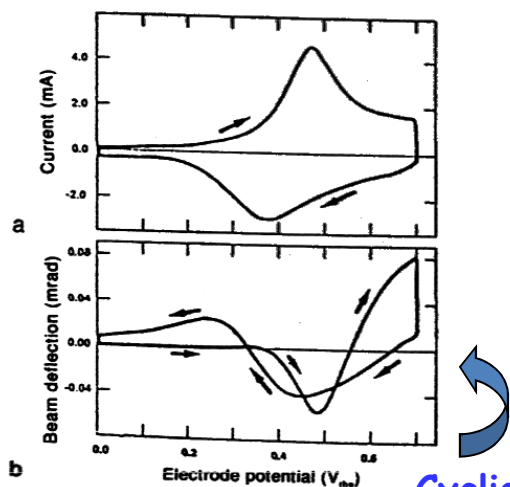
Fig. 5. Relationship between $E_{\frac{1}{2}}$ for the first redox process between pH −2.12 (6.0 mol dm⁻³ HCl) and pH 2.0. Slope = −58 mV per pH unit.

Redox Process I

115
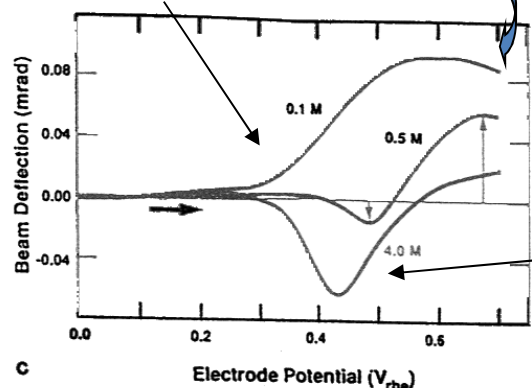
PANi redox switching : PBD experiments.

PBD experiments on PANi in HCl solution show that the PBD signal exhibits both negative and positive deflections during the oxidative potential sweep.
Hence both proton expulsion and anion insertion occur during polymer oxidation. Proton release preceeds anion ingress during the oxidative sweep.
Subsequently there is consecutive anion ejection and proton insertion during the reverse reductive sweep.
Cyclic deflectograms recorded during layer oxidation, as a function of acid concentration indicate a more enhanced negative deflection as the acid concentration increases. Positive deflections also noted at higher oxidation potentials.
Proton expulsion is the dominant mode for electroneutrality preservation in concentrated acid media, but anion insertion also occurs at more positive potentials.

Cyclic deflecto-grams

Positive deflection

Negative deflection

FIGURE 1.40. Probe Beam Deflection (PBD) used to examine the redox chemistry of poly(aniline) modified electrodes. Cyclic voltammogram (a) and corresponding cyclic deflectogram (b) recorded for a poly(aniline) film electrodeposited on an Au support electrode in 1 M HCl. Sweep rate, 50 mV s^{-1}; surface coverage, 1.4×10^{-8} mol cm^{-2}. (c) Forward scan of the cyclic deflectogram obtained for poly(aniline) films in contact with various HCl solutions. Concentrations of supporting electrolyte are indicated in the figure. Sweep rate, 50 mV s^{-1}. Upward- and downward-pointing arrows indicate positive and negative deflections of the laser beam, respectively. (Adapted from Ref. 158.)


FIGURE 1.41. Redox chemistry of poly(aniline) and correlation with PBD data illustrated in Fig. 1.40.

Little evidence of solvent transport during redox switching.

Significant amount of charge passed before onset of mass increase. Proton expulsion during oxidation.

Increase in mass during film oxidation. Oxidation accompanied by hydrated anion insertion.

C

A

B

+

FREQUENCY

F

-0.2   0   0.2   0.4   0.6

E   VS   SCE
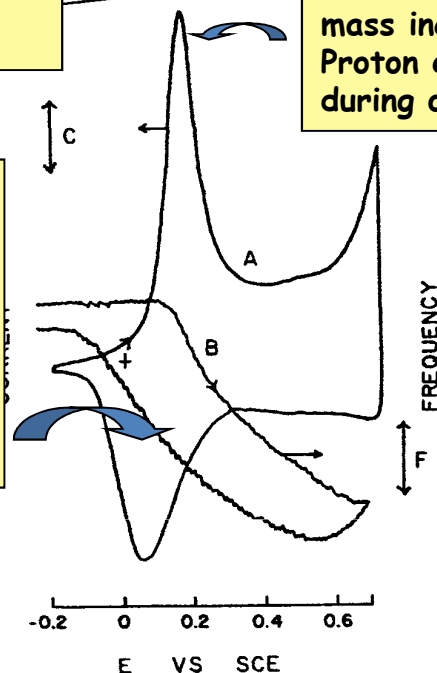
Figure 1. CV/QCM steady state scan from –0.2 to 0.75 V in 0.1 M aniline, 1.0 M H$_2$SO$_4$. Scan rate, 100 mV/s. $C = 100 \mu A$, $F = 20$ Hz. (A) Cyclic voltammetric response. (B) QCM frequency response. Curve B is offset 40 mV to the left with respect to curve A.

Hillman Logic Diagram for Redox Switching Diagnostics.

EQCN very useful for ECP films. Needs to be examined more for TM oxide layers, especially use of Hillman Logic Diagram.

Q vs. E   Y   ΔM vs. E   Y   'equilibrium'

N   N

ΔM vs. Q   Y   rate-limiting electron/ion motion (x)

N

rate-limiting heavy neutral species relaxation (y, z)
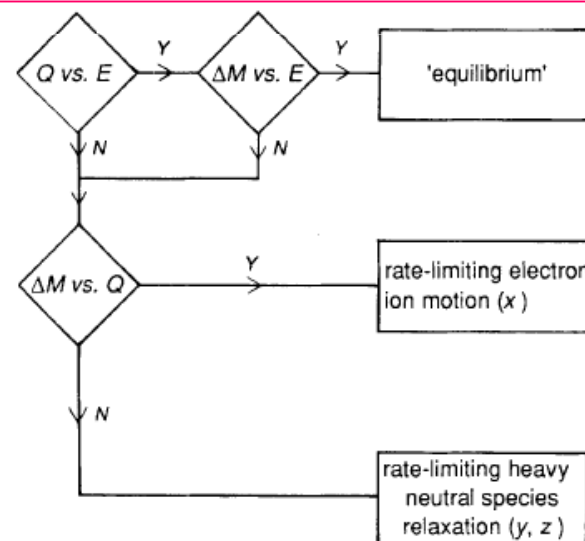
Fig. 3 Logic diagram for determining rate limiting step during redox switching of an electroactive polymer film. The diagram shows the three principal possibilities, 'equilibrium', rate-limiting transfer of charged species and rate-limiting motion of heavy neutral species. The path in the diagram can depend on the direction of electron transfer